Scanning Microscopy

Volume 9 | Number 1 Article 1

3-29-1995

Swift Heavy Ion Induced Electron Emission from Solids

Hermann Rothard
Centre Interdisciplinaire de Recherches, Caen Cedex

Scanning Microscopy, Vol. 9, No. 1, 1995 (Pages 1-42) 0891-7035/95$5.00+.25
Scanning Microscopy International, Chicago (AMF O'Hare), IL 60666 USA

SWIFT HEAVY ION INDUCED ELECTRON EMISSION FROM SOLIDS

Hermann Rothard*

Centre Interdisciplinaire de Recherches avec les Ions Lourds CIRIL (Laboratoire Mixte CEA-CNRS UMR C0011)
B.P. 5133, rue Claude Bloch, F-14040 Caen Cedex, France

(Received for publication April 16, 1994, and in revised form March 29, 1995)

Abstract

Quite a number of experiments have been performed on electron emission from solids induced by slow (projectile velocity $v_P < 1$ atomic unit) or medium velocity heavy ions (projectile energy $E_P < 1$ MeV/u). Only a few experiments have been made with fast heavy ions (projectile atomic number $Z_P > 8$, $E_P > 2$ MeV/u) concerning either electron emission yields γ, or double differential electron energy spectra $d^2n(\Theta)/dEd\Omega$ as a function of the observation angle Θ. We present the results obtained so far on electron emission induced by fast ($E_P > 2$ MeV/u) heavy ions ($Z_P \geq 6$). Topics discussed include experimental results for electron yields, -energy and -angular distributions and channelling phenomena as well as the theoretical approaches. We also present new results from recent studies on the evolution of electron yields and doubly differential electron spectra with target thickness for Ar (13.6 MeV/u) obtained at GANIL (the french heavy ion accelerator "Grand Accélérateur National d'Ions Lourds").

Key Words: Electron emission, swift heavy ion, solids, yield, spectra and angular distributions, stopping power, ionization and excitation, plasmons and wake, channelling, Auger-, convoy- and delta electrons, electron transport in condensed matter, surface phenomena.

*Address for correspondence:
Hermann Rothard
CIRIL
B.P. 5133
rue Claude Bloch
F-14040 Caen Cedex
France

Telephone number: (+33) 31 45 47 91
(+33) 31 45 46 01
FAX number: (+33) 31 45 47 14
E-mail: ROTHARD@GANAC4.IN2P3.FR

Contents

Table of Symbols

D	particle fluence (particles/cm^2)
d	thickness (foils, surface layer)
BE	binary encounter
b_{min}	minimum impact parameter
$C_{B,F,T}$	normalized ratio of electron yields and dE/dx (cf. eq. 29)
CE	convoy electron
CM	cascade multiplication (of SE)
d_{eq}	charge equilibrium thickness
dE/dx	energy loss per unit path length
e	charge of a proton
E	electron energy
<E>	mean energy transferred in an ionization event
E_B	binding energy of an electron
E_{BE}	kinetic energy of BE electrons
Eco	cut-off energy in MC simulations
E_{eq}	kinetic energy of electrons with $v_e=v_p$
E_F	Fermi energy
E_{FA}	final energy of electrons from multiple collision sequences (Fermi acceleration)
E_g	band gap
E_L	kinetic energy of loss electrons
E_P	projectile kinetic energy
EE	electron emission
$F(E,\Omega)$	internal flux of electrons (as a function of energy and direction)
$F(E_0,\Theta_0)$	internal flux of electrons with energy E_0 in directon Θ_0
F(q,x)	depth dependent charge state distribution
F_0	fraction of neutrals (q=0)
$f(x,\lambda_\delta)$	fast electron transport function (eq. 14)
g(x-z)	energy dissipation function (eq. 15)
I	mean ionization potential
I_{FC}	Faraday cup current
$I_{PI}{}^P$	electron flux from projectile ionization
$I_{PI}{}^T$	electron flux from target ionization
$I_n(E,\Omega)$	nth generation of the double differential electron energy and angular distribution
L	stopping number
m_e	electron mass
$M(E,\Theta,E_0,\Theta_0)$	scattering probability (cf. eq. 9)
MC	Monte Carlo (simulation)
ML	monolayer
N(E)	angle-integrated energy distribution
N(R)	radial electron distribution
$N(\Theta)$	energy-integrated angular distribution
n	electron emission cross section
n(x,y,z)	spatial distribution of electrons
n_e	density of a free electron gas
n_s	number of slow electrons from PI
n_δ	number of slow electrons liberated in secondary ionization by fast electrons
P	surface transmission probability
P_n	probability that n electrons are emitted (or exited projectile state population probability, quantum number n)
p	pressure
$P_{B,F}(x)$	slow electron attenuation function
PI	primary ionization
PP	polypropylene
q	charge of incoming ions
<q>	mean charge
q*(x)	depth dependent effective ion charge
q_{eff}	effective charge
$q_f{}^{c,r}$	final ion charge under channeling (c) or random impact (r) conditions
q_{ZBL}	q_{eff} used in stopping power tabulations
R	ratio of electron spectra (or radial distance from the ion track)
$R_{F,B}(d)$	target thickness dependent ratio of electron yields (F=forward, B=backward)
S(E)	low energy electron stopping power
S_e	electronic stopping power
SE	secondary electron
U_0	magnitude of the surface potential barrier (or target/Faraday cup/grid potential)
U_{rep}	repeller potential (Faraday cup)
U1s	K shell ionization energy
v_{Bohr}	atomic unit of velocity
v_e	electron velocity
v_P	projectile velocity
v_s	electronic shock wave group velocity
v_{BE}	velocity of BE electrons
v_0	atomic unit of velocity
Y_{CE}	convoy electron yield
x	depth
Z_P	projectile atomic number
Z_T	target atomic number
$\hbar\omega_P$	plasmon frequency
β_δ	fraction of energy loss leading to fast δ-electron liberation
β_s	fraction of energy loss leading to liberation of PI of slow electrons in PI
δ	target tilt angle
γ	electron yield (mean numer of emitted electrons per projectile)
γ_T	total electron yield (foils, both surfaces)
γ_B	backward yield of slow electrons
γ_F	forward yield of slow electrons
γ_{SE}	slow electron yield (= $\gamma_B+\gamma_F$)
γ_δ	yield of fast electrons (= $\gamma_T-\gamma_{SE}$)
$\varepsilon(\omega,k)$	dielectric function
Φ	workfunction
ϕ_{TR}	track potential
φ	ion impact angle with respect to crystallographic axe or plane
φ_{crit}	critical angle for channeling
$\Lambda^*_{B,F,T}$	ratio of electron yields (backward, B, forward, F, total, T) and dE/dx
λ	de Broglie wave length
λ_{eq}	charge equilibration length

λ_δ	transport length of fast δ-electrons (in forward direction)
λ'_δ	transport length of fast δ-electrons (in backward direction)
$\lambda_\perp$	transport length of fast δ-electrons (perpendicular to the ion track)
λ_S	diffusion length of slow electrons
λ^{MC}	transport lengths of fast electrons from MC simulations (indices as above)
λ_L	mean electron loss length
Ω	solid angle
ρ	mass density
σ	cross section
$\sigma_{H,S,M,C}$	cross sections for ionization in hard (H) or soft collisions (S), quasi molecular (M), or capture to the continuum (C)
Θ	observation and emission angle (or surface coverage with adsorbates in ML)
Θ_{em}	mean shock electron emission angle

I. Introduction

a. Context

Electron liberation and emission plays an important role whenever ionizing radiation interacts with matter, because swift charged particles deposit energy mainly by electronic processes such as *excitation* and *ionization* of the target atoms. Positively charged projectiles may *capture* target electrons (to the ground- or an excited state). If the projectiles carry electrons, electron *loss* or projectile excitation may take place. Most of the projectile energy loss per unit path lengths dE/dx leads to ionization and thus to electron emission (EE). The term "swift" refers to particles with velocities comparable to or exceeding the velocity of the target electrons, $v_P > Z_T v_0$ (with the velocity measured in atomic units $v_0 = v_{Bohr} = 1$ a.u., and the target atomic number Z_T).

Electron emission from solid surfaces under ion impact has been discovered around 1900 (Villard 1899, Thomson 1904, Rutherford 1905, Füchtbauer 1906a,b). As pointed out by Hofer (1990), the first systematic studies were performed by Füchtbauer (1906a, 1906b, 1907). In his quite remarkable papers, Füchtbauer described most of the basic features concerning electron yields as well as energy- and angular distributions. The review by Sigmund and Tougaard (1981) and its "follow-up" (Sigmund, 1993) can serve as an excellent introduction to all of the basic aspects (and problems) of EE. Much important information on EE can be found in four recent books edited by Schou, Kruit and Newbury (1990), Höhler and Niekisch (1991a,b) and Baragiola (1993a).

In the following, we will only consider the process of so-called *kinetic electron emission* due to transfer of kinetic projectile energy. The so-called *potential electron emission* is dominant at low velocities and particularly important for slow, highly charged projectiles as thoroughly discussed in the recent review by Varga and Winter (1991). Kinetic electron emission has recently been discussed by Hasselkamp (1988,1991). He also gives an overview of applied aspects of EE in his 1991 paper. Information on kinetic electron emission from thin foils (Rothard, Groeneveld and Kemmler, 1991) can be found in the same volume. Theoretical aspects are thoroughly treated by Rösler and Brauer (1991) and Devooght et al. (1991) in Höhler and Niekisch (1991b) and by Rösler (1993). Other recent comprehensive reviews have been given by Hofer (1990), Brusilovsky (1990) and Baragiola (1993b). EE from thin carbon foils bombarded with high velocity (MeV/u) ions has been treated by Schiwietz (1993).

In order to understand EE induced by *heavy ions* (including other *composite*, *structured* projectiles like *molecules* and *clusters*), it is necessary to understand EE in simpler collision systems. A review on electron emission in *ion-atom* (and also ion-foil) collisions has been given by Toburen (1990), information on δ-electron emission in ion-atom collisions can be found in the papers by Kelbsch et al. (1992) and Shinpaugh et al. (1993). EE from solids induced by *single* particles such as *electrons* and *protons* has been reviewed by Schou (1988). Most of these reviews refer to experimental and theoretical studies which have been performed on EE induced by slow ($v_P < 1$ a.u.) or medium velocity ions (< 1 MeV/u). Studies in the energy range E_P = 2-10 MeV/u are sparse (Schiwietz 1993), and studies in the high energy region (10-100 MeV/u) and for relativistic projectiles (E_P >100 MeV/u) (Vane et al., 1993) can still be considered as "pioneering work".

It is particularly astonishing that no systematic data exist in the high energy range 10-100 MeV/u or above, even for ion-atom collisions (gaseous targets). Heavy ion beams in this particular energy range will be used in the very near future for cancer therapy (Kraft and Gademann, 1993), but also in other "high-tech" domains. As examples, we mention *nuclear power production* (plasma-wall interactions, stability of irradiated materials in reactors and nuclear waste containers, high energy density deposition for inertial confinement fusion), *semiconductor- and nanotechnology* (material modification by radiation, nuclear track formation, high energy implantation, surface treatment, influence of radiation on electronic devices, in particular in spacecraft, ...). An overview concerning basic aspects and applications of heavy ions can be found in the proceedings of the 1992 conference on swift heavy ions in matter (SHIM-92) edited by Angert, Armbruster and Jousset (1993). The role of electrons in track formation has been discussed by Groeneveld (1988, 1991), Johnson (1993) and Tombrello (1993).

Biological damage of tissue (as well as material modification in solids), can be induced by the primary ionization of the biological target molecules (or the target atoms or molecules in the solid) by the heavy ion itself, but also secondary ionization caused by the so-called δ-electrons emitted in the primary ionization

event. This explains the need of data about ionization cross sections and electron transport in condensed matter, which can be investigated by studying electron emission induced by a fast heavy projectile. Studies should cover "*simple*" targets such as rare gases and must then be extended to more *complex* targets (molecules, clusters). In parallel, as applications concern condensed matter, *solid* (or, if possible, liquid) targets should be used in order to account for *transport-* or "*collective*" effects.

In particular, the target thickness dependence of electron emission from thin foils makes it possible to study the evolution from primary ionization (with very thin foils assuring single collision conditions) to multiple collisions including electron transport and the evolution of the secondary electron cascade (Rothard, Groeneveld, Kemmler, 1991, Schiwietz, 1993). Experiments with thin foils allow to relate electron emission and final projectile charge states via coincidence techniques.

No systematic studies on EE have been published for heavy ions (of projectile nuclear charges $Z_P > 8$) at energies above 10 MeV/u (Rothard 1994), and a compilation of results on *EE by swift heavy ions* covering projectile energies above 1-2 MeV/u is still missing up to now, although a choice of experimental results on energy distributions from thin carbon foils and in particular, a review of theoretical aspects have been given by Schiwietz (1993). Therefore, in this paper, we will focus on the results obtained so far on electron emission by fast (> 2 MeV/u) heavy ($Z_P > 6$) ions.

Topics discussed include experimental studies of electron yields, -energy and -angular distributions and channelling phenomena as well as the theoretical approaches. For the reasons quoted above, we will in particular consider EE from thin solid foil targets and pre-equilibrium phenomena. We also present new results from studies on the evolution of electron yields and double differential electron spectra $d^2n(\Theta)/dEd\Omega$ with target thickness for Ar^{q+}(13.6 MeV/u) obtained at GANIL by Rothard et al. (1994, 1995). In order to point out what results or mechanisms are specific for swift heavy ions, we also refer to results obtained with protons or "light ions", gaseous targets, or at lower projectile velocities where it appears necessary and useful.

b. Basic Quantities and Observations

Concerning experimental studies on EE by swift heavy ions, one can distinguish between two different types of experiments: Studies of *electron emission yields* γ, and measurements of *double differential electron energy spectra* $d^2n(\Theta)/dEd\Omega$, or in other words, the mean number of electrons ejected per energy interval dE and solid angle $d\Omega$, as a function of the observation angle Θ. By integrating over electron energy, one obtains *angular distributions*

$$N(\Theta) = \int_0^\infty dE \; d^2n(\Theta)/(dEd\Omega) = dn/d\Omega \qquad (1)$$

and by integrating over the observation angle, one obtains the *energy distribution*

$$N(E) = \int_0^{4\pi} d\Omega \; d^2n(\Theta)/(dEd\Omega) = dn/dE \qquad (2)$$

Electron yields are related to the double differential spectra by

$$\gamma = \int_0^\infty dE \int_0^{4\pi} d\Omega \; d^2n(\Theta)/(dEd\Omega) \qquad (3)$$

In order to get familiarized with some basic features of the phenomenon of EE, let us start with a look at figs. 1 and 2. Fig. 1 shows total electron yields from carbon foils, defined as the mean number of electrons ejected per incoming projectile, as a function of the elec- tronic stopping power $S_e = -(dE/dx)$. The yield includes electron emission from the foil in forward as well as in backward direction. A rough proportionality of electron yields and stopping power (eq. 4) within a factor of 2 in a wide range of projectile velocities v_p (15 keV/u $\leq E_p/M_p \leq$ 46 MeV/u) and -atomic numbers Z_P ($1 \leq Z_P \leq 92$) over four decades of electron yield- and stopping power values can be stated. The mean value of the proportionality factor is $\Lambda_T = (0.31 \pm 0.14)$ Å/eV. Most of the theoretical approaches consider the yield γ to be proportional to the electronic stopping power S_e (or to the amount of energy deposited near the surface)

$$\gamma_T = \Lambda_T \; S_e \qquad (4)$$

We will come back to this point in chaps. II and III. In particular, *deviations* from this simple rule can tell us a lot about ion-solid interactions.

An example for an electron spectrum, given in the *top* curve as a function of the projectile velocity v_P, the upper horizontal scale, is shown in fig. 2. It has been recorded in the direction of a 1.2 MeV proton beam (Θ=0 deg., comp. fig. 3 for the geometry) traversing a carbon foil by Rothard et al. (1990b). The dominating structure is the low energy "true" secondary electron (SE) peak with an intensity maximum at (2.1±0.3) eV. This peak contains about 85% of all emitted electrons. Consequently, electron yield measurements mainly provide us with information about these low energy electrons (E << 100 eV), whereas electron spectra also yield information on high energy (often denoted as δ-) electrons (say, E > 100 eV). However, the low energy part of spectra contains important information about the SE cas- cade multiplication, projectile charge effects and collective excitation mechanisms (plasmons, IV.c).

At $v_e \approx 0.64\ v_P \approx 4.4\ v_0$ (E ≈ 265 eV), we find the carbon KLL Auger electron distribution. A further prominent peak appears at an electron velocity equal to the projectile velocity, $v_e \approx v_P$.

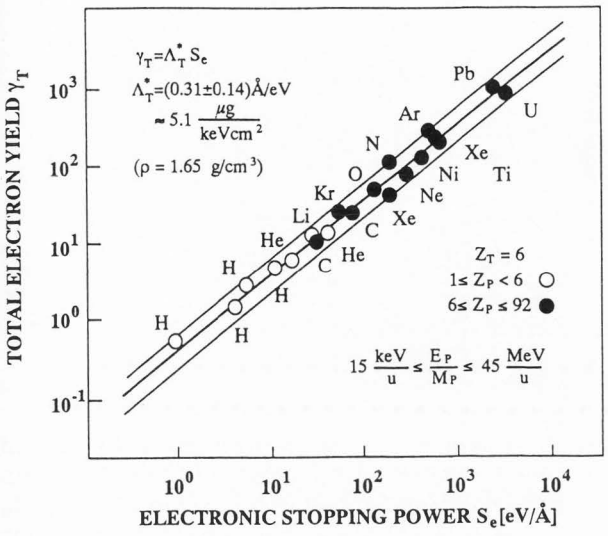

Fig. 1: Total electron yields γ_T from carbon foils (the mean number of electrons ejected per incoming projectile, including electron emission from the foil in forward as well as in backward direction) as a function of the electronic stopping power $S_e = -(dE/dx)$. A proportionality of electron yields and stopping power, $\gamma_T = \Lambda_T S_e$, within a factor of 2 in a wide range of projectile velocities v_p (15 keV/u $\le E_p/M_p \le 46$ MeV/u) and atomic numbers Z_P ($1 \le Z_P \le 92$) over four decades of electron yield and stopping power values is observed (from Rothard, Schou, Koschar and Groeneveld, 1992). The mean value of the proportionality factor is $\Lambda_T = (0.31 \pm 0.14)$ Å/eV assuming a carbon foil density of $\rho = 1.65$ g/cm^3.

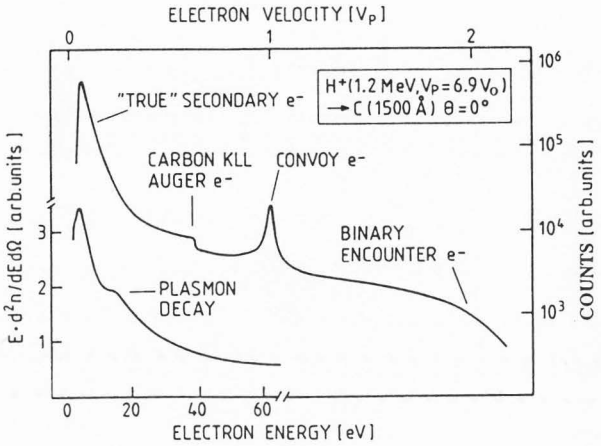

Fig. 2: Typical ion induced electron velocity spectrum, given in the top curve as a function of the elctron velocity (right-hand scale). It has been recorded in the direction of a 1.2 MeV proton beam (Θ=0 deg., comp. fig. 3 for the geometry) traversing a carbon foil. The bottom curve shows the low-energy part of the spectrum as a function of electron energy (left-hand scale), from Rothard et al. (1990c).

It belongs to the convoy electrons (Breinig et al., 1982) which can be used to study electron transport in solids.

As a consequence of elementary collision dynamics, the high energy binary encounter electron distribution from close collisions with maximum momentum transfer between the (heavy) projectile and a (light) target electron can be seen at twice the projectile velocity, $v_e \approx 2v_P$. In the case of "structured" or composite projectiles which carry electrons (or, if target electron capture occurs) broad structures due to projectile ionization can be observed around $v_e \approx v_p$ in the forward direction. Also, peaks from collisional loss of projectile electrons can be observed in backward direction. These electrons appearing at $v_e \approx -v_p$ in the laboratory frame, are produced in a similar way as the binary-encounter electrons from the target in forward direction at $v_e \approx -v_T$, the target velocity in the projectile frame.

At the bottom of fig. 2, we show the low-energy part of the spectrum $Ed^2n/dEd\Omega$ as a function of electron energy E. At an energy of $E < 20$ eV, a structure can be observed that is attributed to the decay of a collective excitation of the solid's electron plasma, the *plasmon* (Hasselkamp, 1988, 1991). In this process, the energy $\hbar\omega_p$ of a plasmon (for carbon: $\hbar\omega_p \approx 25$ eV) is transferred to a single electron. When escaping from the surface, the energy of these electrons is reduced by the effective surface potential given by the workfunction Φ (for carbon: $\Phi \approx 5$ eV). Eventually, they are observed at an energy of $E < \hbar\omega_p - \Phi$, i.e. at $E < 20$ eV in the case of carbon (Burkhard, Rothard and Groeneveld, 1988a). Collective excitation may also manifest itself as "shock electron emission" observable in angular distributions (Burkhard et al., 1987b) or as unexpected correlation of electron emission probabilities from forward and backward surfaces of thin foils (Yamazaki et al., 1993).

c. Experimental Methods

The geometry of a typical electron spectroscopy experiment is shown in fig. 3a. The ion beam traverses a target (either gaseous or solid) and is stopped in a Faraday cup for beam current measurement. If the target is a massive solid target (fig. 3c) the beam will be stopped in the target and accurate beam current measurement can be performed by biasing the target with a sufficiently high potential which inhibits the SE to leave the target. With gases or thin foils, it is possible to separate the final charge states q_f of the projectiles with electric or magnetic fields (fig. 3b). The charge state distribution can thus be measured with e.g. a position sensitive detector.

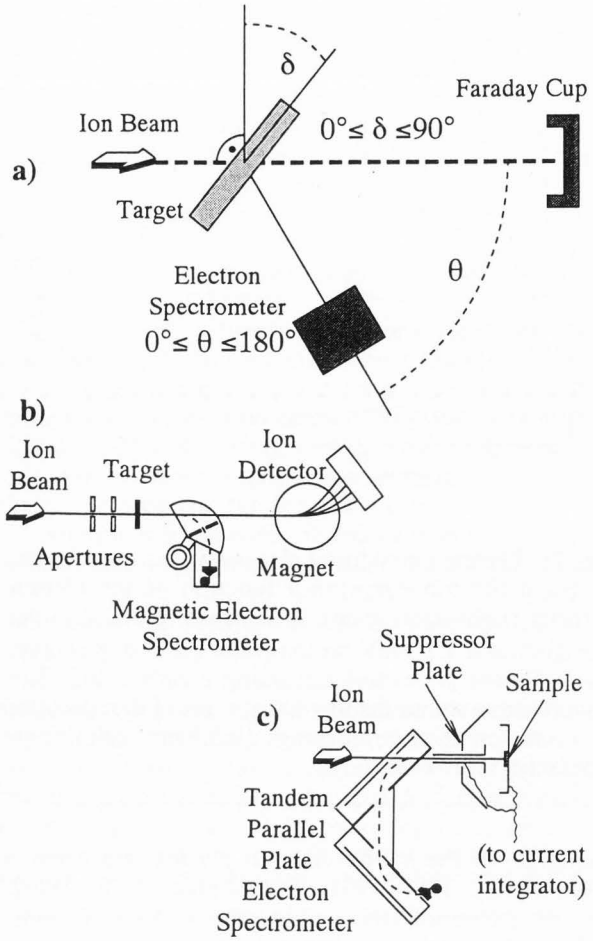

Fig. 3: a.) The geometry of a typical electron spectroscopy experiment: An ion beam traverses a gaseous or solid target under a certain angle (tilt angle δ, perpendicular impact for $\delta = 0$ deg.) and is stopped in a Faraday cup. The electron spectra can e.g. be measured under a certain observation angle Θ with **b.)** a magnetic spectrometer or **c.)** with electrostatic analyzers (Schneider et al. 1989, Kudo et al. 1991a). With gases or thin foils, it is possible to separate the final charge states q_f of the projectiles with electric or magnetic fields, and electron emission can be studied in coincidence with final projectile charge states (Kemmler et al., 1988).

With such a set up, electron emission can be studied in coincidence with final projectile charge states (Kemmler et al., 1988). Often, a perpendicular impact of the ions (tilt angle $\delta = 0$ deg.) is chosen. In many cases, and in particular in channelling experiments, it is interesting to tilt the target ($\delta \neq 0$ deg.). The extreme case of $\delta \rightarrow 90$ deg. is called "*grazing incidence*". In this report, we do not deal with electron emission under such conditions and refer the reader to papers by Winter et al.(1993) and Hasegawa et al. (1988).

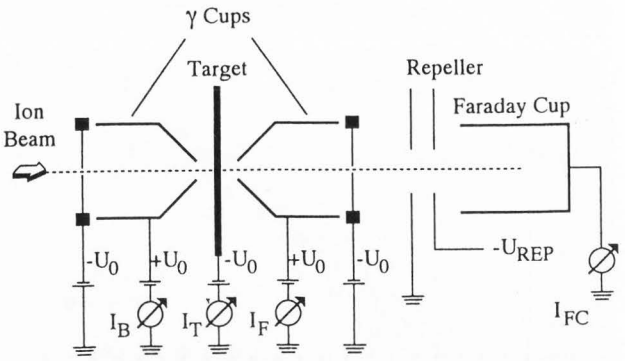

Fig. 4: Experimental setup for forward- and backward low energy electron yield determination by direct measurements of the current of low energy electrons, I_B and I_F, with two Faraday cups or electrodes on the beam entrance- (B) and exit (F) side of thin foils as described by e.g. Kroneberger et al. (1988) or Rothard et al. (1990a). The cups are held at a positive potential $+U_0$ (typically some tens or hundreds of volts), the target holder and grids in front of the cups are biased by a negative potential $-U_0$ in order to assure complete collection of all low energy electrons.

The electron spectra can e.g. be measured with a magnetic spectrometer (fig. 3b) or with electrostatic analyzers (fig. 3c) at a certain observation angle Θ. Different types of electrostatic analyzers are in use such as spherical sector-, cylindrical mirror-, toroidal-, or parallel plate spectrometers, the later ones often in a two stage (tandem) arrangement (fig. 3c) (Schneider et al., 1989, Kudo et al., 1991a). It is also possible to measure the electron energy by time-of-flight techniques at low energies (E = 0.1-300 eV). Electron counting is done with secondary electron multipliers (SEM) such as *channeltrons*. In order to measure a certain range of electron energies and/or angles simultaneously, *microchannel plates* (MCPs) are widely used.

Total yields γ_T can easily be obtained by measuring the ion induced target current I_T and the ion beam current I_{FC} with a Faraday cup equipped with a repeller (U_{REP} being in the order of several hundreds of Volts). The electron yields are given by the ratio of the two currents taking into account the mean final charge q_f and the incoming charge state q of the ions according to Schader et al. (1978). This method is similar to the "*quotient method without collector*" as described by Hasselkamp (1991). If electron fluxes are directly measured with Faraday cups or electrodes, the method is called "*quotient method with collector*". Both of this methods and the possible experimental errors associated with them have been discussed by Hasselkamp (1991).

An example for a typical set-up is shown in fig. 4: The forward- and backward electron yields (γ_B and γ_F) are obtained by directly measuring the current of low energy electrons, I_B and I_F, with two Faraday cups or electrodes on the beam entrance- (B) and exit (F) side of the thin foils as described by e.g. Kroneberger et al. (1988) or Rothard et al. (1990a). The cups are held at a positive potential U_0 (typically some tens or hundreds of volts). The target holder and, in our example shown in fig. 4, also grids in front of the cups, are biased by a negative potential in order to assure complete collection of all low energy electrons. However, electrons with energies exceeding about 100 eV in our case, which are emitted in extreme forward (0-15 deg.) or backward (165-180 deg.) direction can escape from the cups. Thus,

$$\gamma_\delta = \gamma_T - \gamma_{SE} \tag{5}$$

with

$$\gamma_{SE} = \gamma_B + \gamma_F \tag{6}$$

gives a qualitative information about high-energy (δ–) electrons (E > 100 eV), whereas γ_{SE} is a measure of low energy electron emission (often wrongly denoted as "secondary" electrons, SE) . Error bars for low energy electron yields are in the order of ± 6-8 %.

Furthermore, the *statistics* of EE has been investigated (Varga and Winter,1991, Kozochina, Leonas and Fine, 1993), but again, studies with swift and/or heavy ions are sparse (Clerc et al., 1973, Yamazaki et al. 1993, Azuma et al., 1993). In these experiments, one measures the probability P_n of emission of n=1,2,3,... electrons following the impact of a single particle. The electron yields are then given by

$$\gamma = \sum_{n=1}^{\infty} n\, P_n \tag{7}$$

with

$$\sum_{n=0}^{\infty} P_n = 1 \tag{8}$$

A problem associated with this method is that the probability distribution for P_n must be know for the calculation of P_0 and γ (Hasselkamp, 1991, Hofer, 1990). On the other hand, if the mean yields are determined from measurements of the total number of projectiles and emitted electrons simultaneously, the probability that no electron is emitted can be calculated from eqs. (7-8) (Kozochina, Leonas and Fine,1993). This is import for the application of EE in single particle counting with channeltrons and converter plates (Schütze and Bernhard, 1956, Hofer, 1990, Hasselkamp, 1991, Albert et al., 1992).

d. The Solid Surface

Most high energy experiments have been performed under standard vacuum conditions with poor surface control. This is to some extend justified if one is only interested in high energy electron emission where surface effects can be neglected. However, if one envisages to study low energy electron spectra, measurements must be performed in ultrahigh vacuum (UHV, $p < 10^{-7}$Pa) with controlled surface conditions. In this context, it is important to note that not only studies on clean, flat surfaces are of interest, but also (if not, in particular) studies on "technical", contaminated or rough surfaces. But even in this case, one must be able to characterize contamination and surface structure.

Since there are no studies yet with swift heavy ions, in the following, we present results obtained with MeV light ions. It is in particular interesting that even with MeV protons where *nuclear stopping* and *sputtering* are negligible, *surface erosion* due to *electronic processes* occurs (see below). Similar effects can be observed with swift heavy ions, too (LeBeyec, Della Negra and Thomas, 1989). The fact that heavy ions deposit enormous amounts of energy in electronic excitations in a small volume during a very short time period, however, makes it probable that interesting new effects will be observed with heavy ions thus opening a new field of future investigations.

The strong dependence of EE on surface contamination is demonstrated in fig. 5. Double differential electron spectra (not corrected for the transmission of the spectrometer) as a function of the electron velocity v_e from H^+ (1.2 MeV) penetration through a copper foil (d = 1500 Å) are shown in fig. 5b. The dash-dotted lines belong to spectra from untreated foils, and the solid lines to spectra from sputter-cleaned foil surfaces. The lower part of fig. 5b shows the ratio R = n(untreated surface)/n(sputter-cleaned surface) of the spectra. Here, intensity enhancements after cleaning can be observed as dips, intensity reductions as peaks. The distinct structures which can be observed in the spectra are labelled A-F. The thin foils produced by standard evaporation techniques are contaminated with about 2-3 monolayers (ML) of adsorbed hydrocarbons and water, which can be removed by sputter-cleaning with slow (keV/u) noble gas ions. The residual coverage Θ with carbon and oxygen was estimated to be lower than $\Theta(C) < 0.2$ ML and $\Theta(O) < 0.1$ ML (Burkhard et al., 1988b, Rothard et al., 1991).

The fast binary encounter electrons have a mean velocity of about 13.9 v_0 and in fig. 5b, we see the low energy tail (F) and not the peak itself. These high energy electrons mainly originate from a depth of several hundred Å and thus are only weakly affected by changes of the near surface layers (R = 1). Since the surface is cleaned from carbon adsorbates, much less carbon Auger electrons at E = 265 eV (D) can be observed, whereas the copper MVV Auger electrons at E = 63 eV (C) appear from the clean copper surface.

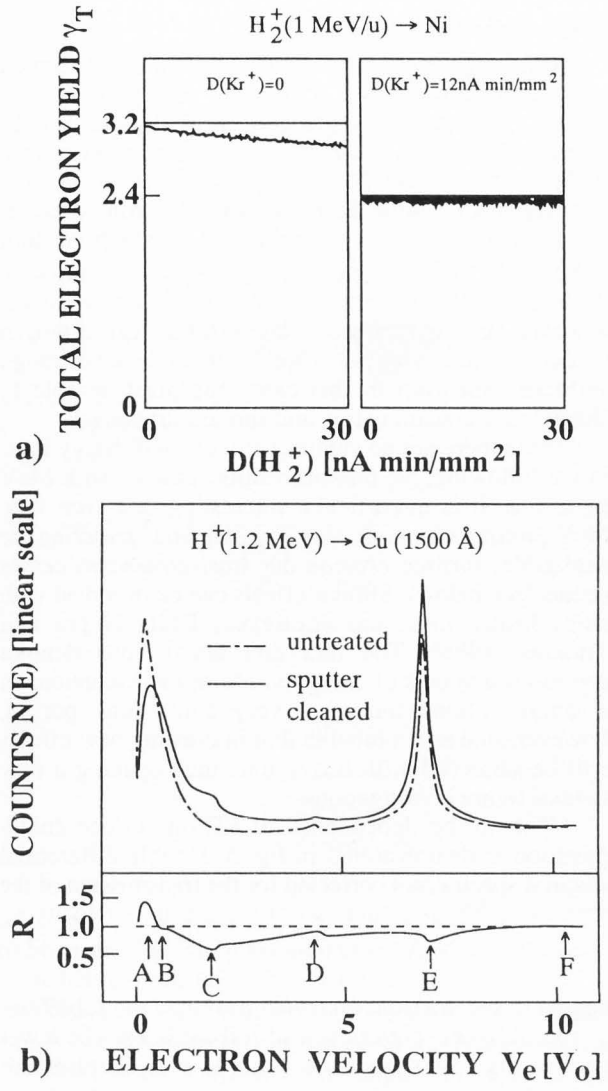

Fig. 5: The effect of surface cleaning on electron emission. **a.)** Electron yields γ_T from Ni foils induced by H_2^+ (1 MeV/u) as a function of the projectile fluence D. Left-hand side: a strong decrease of the electron yields as a consequence of H_2^+ bombardment is observed. Right-hand side: After sputter-cleaning with Kr^+ (20 keV/u), the yields remain constant, which can be taken as an indication for a clean surface (from Burkhard et al., 1988b). **b.)** Top: double differential electron spectra (not corrected for the transmission of the spectrometer) as a function of the electron velocity v_e from H^+ (1.2 MeV) penetration through a Cu foil (d = 1500 Å). The dash-dotted lines belong to spectra from untreated foils, and the dashed lines to spectra from sputter-cleaned foil surfaces. Bottom: ratio R = n(untreated surface)/n(sputter-cleaned surface) of the spectra. Intensity enhancements after cleaning can be observed as dips, intensity reductions as peaks. The distinct structures which can be observed in the spectra labeled (A-F) are discussed in the text (from Rothard et al., 1991).

Furthermore, the height of the low energy SE distribution (A) decreases, its full width at half maximum (FWHM) increases, and the energy of the SE maximum (peak A) is shifted to higher energies. Both yield and FWHM of the convoy electron peak (E) are significantly enhanced. This shows that a large fraction of CE are formed at the last layers of the solid. The dip labelled (B) in the ratio spectrum of fig. 5b may result from collective excitations (plasmons) of the metal. Electrons from the decay of plasmons can only be observed from sufficiently clean surfaces.

The effect of surface cleaning on the low energy cascade electrons (A) can also be seen by just measuring the electron yields: The left side of fig. 5a shows electron yields induced by H_2^+(1 MeV/u) as a function of the projectile fluence D. We clearly see the strong decrease of the electron yields as a consequence of even light MeV ion bombardment, where electronic sputtering pro-cesses dominate and sputtering due to nuclear stopping can be neglected. After sputter-cleaning with (slow) heavy ions, the yields remain constant, which can be taken as an indication for a clean surface (right-hand side of fig. 5a). In the present case, these observations have been explained by the following arguments (Rothard, Groeneveld, Kemmler, 1991):

(1) A layer of adsorbates on a clean metal surface can lead to a reduction of the electron workfunction and thus an enhanced surface transmission probability.

(2) Layers of adsorbates or oxides lead to larger electron escape depths and thus to a higher yield. We come back to this in V.a. Electron diffusion lengths, which are related to the concept of the escape depth, are treated in more detail in chap. III.

(3) The change of the composition (i.e. the target material Z_T) of the near-surface layers affects the stopping power and thus the production of electrons.

(4) It can be shown that a rough, uncleaned surface is associated with an enhanced electron escape probability compared to a smooth, planar surface (Borovsky, McComas and Barraclough, 1988). The sputtering process applied here has been shown to clean and flatten the surfaces by preferential sputtering (Rothard et al., 1989). In general, this is not the case (Hauffe, 1991).

Also, the arguments (1-4) mentioned above may not apply generally, in particular, adsorbates may also increase the workfunction. This is also the case if samples are exposed to atmosphere which results in oxidation and generally increases the workfunction. Different mechanisms have been discussed in a recent review by Baragiola (1993b). More information on the influence of surface contamination on electron emission can also be found in the reviews by Hofer (1990) and Hasselkamp (1991).

The influence of controlled deposition of adsorbates on electron spectra from thin foils has been studied by Sanchez, de Ferrariis and Suarez (1989) and Schosnig et al. (1992) with different techniques: In the first experiment, an ion source was used to deposit Na on the

surface of an Al foil, in the second, gases such as CO_2 and Xe, were condensed on the cold surfaces of sputter-cleaned targets. Recently, the dependence of forward- and backward electron yields on adsorption and desorption of different gases (N_2, O_2, H_2O) has been studied by Arrale et al. (1994).

Finally, let us note that, as a first approach, it is possible to study (target thickness dependent) electron emission with carbon foils in standard vacuum. It has been observed that electron yields obtained with carbon foils produced by the same manufacturer are reproducible within about 5% (Rothard et al., 1993a,b). In fact, the surface contamination during charged particle bombardment is determined by an equilibrium between induced desorption and adsorption from the residual gas. It is plausible that for particles which deposit large amounts of energy, this equilibrium is strongly shifted towards a "clean" surface. Also, concerning all effects which depend on Z_T, carbon targets represent a favorable choice, because Z_T of most of the residual gas particles is close to that of carbon. Furthermore, even very thin carbon foils are easy to produce. These facts, together with the possibility to study the evolution from primary ionization to cascade multiplication involving electron transport by varying the target thickness, explains why most of the studies on EE by swift heavy ions have been performed with thin carbon foils (Schneider, Schiwietz and DeWitt 1993, Rothard 1994, Rothard et al., 1995).

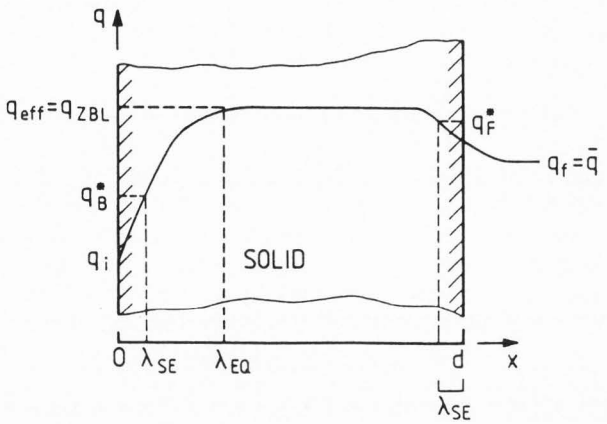

Fig. 6: The effective ion charge q(x) inside a thin solid foil of thickness d as a function of the penetration depth x according to experimental results by Zaikov et al (1986). The ions have an initial charge state of $q = q_i$, and their mean final charge after leaving the foil is $q_f = \langle q \rangle$. λ_{eq} denotes the charge equilibration depth: at $x = \lambda_{eq}$, the ionic charge is in equilibrium, the effective charge is $q_{eff} = q^*(x>\lambda_{eq}) = q_{ZBL}$ corresponding to the values used in stopping power tables (Ziegler, Biersack and Littmark, 1985). According to Rothard, Schou and Groeneveld (1992), electron yields are a function of the effective ion charges $q^*(x)$ very close to the surface within a depth comparable to the low energy electron escape depths λ_S, $\gamma \sim [q^*_{F,B}(x \approx \lambda_S)]^2$.

II. Theoretical Approaches

a. The Four-Step-Model: Preparation-Production-Transport-Transmission

The conventional theoretical approaches divide the processes leading to electron emission into the following consecutive stages :

(1.) the *production* of the electron at a certain point x inside the solid by (a.) a single ion-target interaction (*primary ion ization*, PI) and (b.) secondary ionization events (by recoil atoms, high energy electrons and possibly photons)

(2.) the *transport* of the liberated electron to the surface of the solid at x = 0 or x = d in the case of thin foils with thickness d. From another point of view it is also possible to include secondary ionization (secondary, tertiary, ..., ionization) by fast electrons in this step as part of the *transport* of the electrons through the solid (*cascade multiplication*). The final step is

(3.) the *transmission* through the surface.

(4.) In the case of heavy ions, also a fourth step, which in reality arises before or in connection with the first step, the *preparation* (Kemmler, 1990) of the electronic projectile state for the moment of electron production has to be considered.

The preparation step is related to the evolution of the ionic charge state due to electron capture and loss into the ground state or excited states and collisional projectile excitation (fig. 6). This becomes particularly important in order to understand the dependence of EE on the incoming charge state, or if we are dealing with foils too thin to allow charge state equilibration (*charge-state pre-equilibrium* (Rothard, Groeneveld and Kemmler, 1991, Rothard, Schou and Groeneveld,1992).

All basic features of the theoretical description of EE are comprehensively treated in the review by Sigmund and Tougaard (1981) which thus is an excellent starting point. Further information on theoretical approaches and the great progress that has been made during the last decade can be found in Sternglass (1957), Schou (1980, 1988), Devooght, Dubus and Dehaes (1987a,b), Koschar et al (1989), Rösler and Brauer (1991), Devooght et al. (1991) and Rösler (1993). Information on primary ionization in ion-atom collisions can be found in the reviews by Toburen (1990) and Schiwietz (1993). Recent theoretical and experimental studies on electron transport in and transmission through solids have been performed by Lencinas et al. (1990).

However, a general description of secondary electron spectra and yields based on the above-mentioned multi-step concept is complicated, because the measured spectra in energy and angle are always composed of contributions from PI (electrons carrying information about the preparation and direct production stage), and also from secondary or higher order electrons reflecting

the transport (characterized by slowing down and cascade processes). In principle, three different kinds of approaches have been used in order to describe EE:

(1.) The "simplest" are *semi-empirical models* similar to the one described in sect. II.c. The weakness of this kind of models is the use of averaged, "mean" quantities. For example, such models deal with "mean" energies, "mean" diffusion lengths or escape depths (averaged over all particle energies), "mean" escape probabilities, etc., as critically discussed by Hasselkamp (1991). However, their advantage lies in the fact that they are "easy to apply" and allow a first approach to an qualitative understanding of experimental observations. This holds also for the final results of the *transport theory* as formulated by Schou (1980, 1988). In fact, most of the publications on ion induced electron yields contain either an interpretation of the results in the framework of the semiempirical theory (similar to the approach described below in II.c, compare also the discussion in Hasselkamp, 1991) or in the framework of the transport theory as described by Schou (1980, 1988) and Sigmund and Tougaard (1981). A comparison of the results of both of these approaches with each other (and experimental results) has been done by Schou (1988) and Hasselkamp (1991).

(2.) "*Microscopic*" or "*analytical theories*" have reached a high degree of sophistication. This becomes clear from the papers by Rösler and Brauer (1991), Devooght et al. (1991) and Rösler (1993). The transport theory (Schou 1980) and the age-diffusion model (Devooght, Dubus and Dehaes, 1987a,b) also belong to this group.

Such models have to consider electron creation by a multitude of processes such as excitation of core and quasi free electrons, plasmon excitation and decay, Auger processes, ... both by the primary and the secondary particles. The corresponding excitation functions as well as elastic and inelastic electron scattering mean free paths can in some cases (nearly free metal targets) even be calculated from first principles (Rösler, 1993). The transport problem is treated in the framework of transport theory (Schou, 1980) solving the Boltzmann equation. However, these models are quite complex and have mainly been applied to the "model case" of proton impact on aluminium. In the following section, as an example, we describe a model which was applied to swift heavy ion collisions with thin foils by Schiwietz et al. (1990) (sect. II.b).

(3.) A third alternative are Monte Carlo methods (sect. II.d), which nowadays are widely used to simulate electron transport in solids: see Cailler and Ganachaud (1990), Kotera, Kishida and Suga (1990), Luo and Joy (1990) (all in the same volume by Schou, Kruit and Newbury, 1990), Ganachaud and Cailler (1979a,b), Dubus et al. (1993).

b. The SELAS Approximation and the Theory of Schiwietz

The most sophisticated theoretical description of EE from solids in fast heavy ion collisions has been worked out by Schiwietz et al. (1988,1990) and Schiwietz (1990, 1993). In particular, the review by Schiwietz (1993) and the paper by Schiwietz et al. (1990) contain a comprehensive description of the treatment of primary target- and projectile ionization and electron transport in thin foils. Therefore, in the following, we will only give a brief overview and refer the reader to the above-mentioned papers for details. As an example for results obtained with this theory, fig. 7 displays calculated electron spectra for the collisions system U^{68+} (8 MeV/u) $\rightarrow$ C (d = 44 $\mu g/cm^2$) at three different emission angles Θ.

Schiwietz et al. (1990) calculated double differential electron yields within the framework of classical transport theory. Let $F(E_0,\Theta_0)$ be the flux of electrons moving in direction Θ_0 with energy E_0 inside the solid from direct (PI) target ionization. In this model, it is assumed that angular scattering and energy loss of the electrons are independent (see below). The *angular scattering* of electrons is accounted for by the scattering probability $M(E,\Theta,E_0,\Theta_0)$, i.e. the probability for an electron of initial energy E_0 and direction Θ_0 to be scattered in a direction Θ with energy E. The *energy loss* of the electrons is described as a continuus slowing down described by an energy-dependent stopping power S(E), and energy straggling has been neglected. If electrons from *primary ionization* of a surface layer of thickness d are separately accounted for, because no energy straggling or angular scattering occurs for these electrons, the external electron flux for direct (PI) *target ionization* can be calculated from:

$$I_{PI}^{T} = d\,F(E,\Omega) + \left|\frac{\cos(\Theta)}{S(E)}\right| \times$$

$$\times \int dE_0 \int d\Theta_0 \, \sin(\Theta_0)\, F(E_0,\Theta_0)\, M(E,\Theta,E_0,\Theta_0) \qquad (9)$$

An example of the resulting PI electron emission is shown in the top of fig. 7. The surface transmission is accounted for by simply subtracting the corresponding energy of the surface potential barrier from the kinetic energy of electrons.

The electron flux $F(E_0,\Theta_0)$ of electrons moving in direction Θ_0 with energy E_0 is taken as the product of scaled semiempirical atomic ionization cross sections and target density. In the second term of eq. (9), we are dealing with electrons from deep inside the solid which can only escape if their initial energy E_0 is high enough ($E >> 100eV$). Thus, the multiple collisions during transport to the surface destroy the interdependence between angular scattering and energy loss. Therefore, Schiwietz et al. (1990) applied the *S*eparation of *E*nergy *L*oss and *A*ngular *S*cattering (SELAS) approximation. The energy loss is described by S(E) in eq. (9).

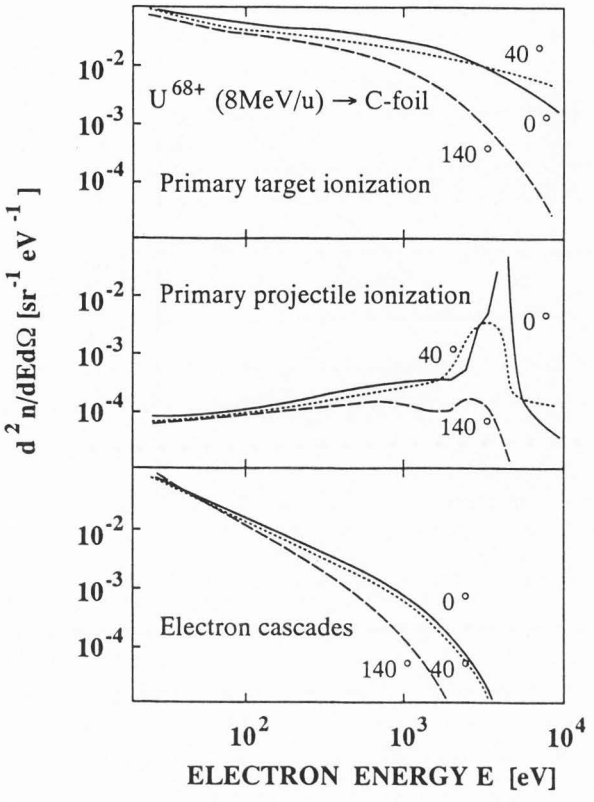

Fig. 7: Calculated double differential electron spectra for the collisions system U^{68+} (8 MeV/u) → C (d = 44 μg/cm^2) at three different observation angles Θ (from Schneider, Schiwietz and deWitt, 1993). The calculations have been made in the framework of classical transport theory and the SELAS approximation according to Schiwietz et al. (1988, 1990) and Schiwietz (1990, 1993) (see text). Top: direct primary *target ionization*. Middle: primary *projectile ionization*. Bottom: higher order target ionization (secondary, tertiary, ... electrons from *cascade multiplication*).

The *angular scattering* is included in the scattering probability $M(E,\Theta,E_0,\Theta_0)$. Analytic expressions for $S(E)$, $F(E_0,\Theta_0)$ and $M(E,\Theta,E_0,\Theta_0)$ have been given by Schiwietz et al. (1990). *Projectile ionization* is treated in a similar manner as target PI, i.e. its intensity I_{PI}^P is given by an expression similar to the second term in eq. (9), except that the ionization cross sections were transformed from the laboratory to the projectile frame of reference. An example is shown in the middle of fig. 7.

The treatment of *cascade multiplication* consists in iterating the transport equation for the double differential electron intensities $I_n(E,\Omega)$ from the 1st up to the nth generation I_n. The flux of cascade electrons is assumed to be isotropic inside the solid. The intensity of the first generation of electrons $I_1 = I_{PI}^T + I_{PI}^P$ is then the sum of the contributions of target PI, shown in the upper part in fig. 7 as given by eq. (9), and of primary projectile ionization (middle part of fig. 7). The 2nd generation I_2 contains the electrons produced by the 1st generation electrons, and so on, up to the nth generation. Thus, the 2nd to the nth generation represent the cascade multi-plication (CM) contribution as shown in the lower part of fig. 7. The final total spectra of emitted electrons are calculated by summing up over the contributions of all generations :

$$\frac{d^2n}{dEd\Omega}(E,\Theta) = \sum_{n=0}^{\infty} I_n(E,\Omega) \qquad (10)$$

For the calculation of PI, Schiwietz et al. (1990) used scaled atomic ionization cross sections in the form of analytical expressions including semiempirical corrections for e.g. screening by projectile electrons and plasmon screening of the projectile charge. According to Schiwietz (1993), the singly differential *ionization* cross section can be written as a sum of 4 contributions :

$$\frac{d\sigma}{dE} = \frac{d\sigma_S}{dE} + \frac{d\sigma_H}{dE} + \frac{d\sigma_C}{dE} + \frac{d\sigma_M}{dE} \qquad (11)$$

$\frac{d\sigma_M}{dE}$ represents electron emission from *quasi molecular ionization*. Important contributions can only be excepted if the projectile velocity is of the order or smaller compared to the orbital electron velocity. $\frac{d\sigma_C}{dE}$ comes from the *E*lectron *C*apture to the *C*ontinuum (ECC) contribution (Breinig et al 1982). $\frac{d\sigma_H}{dE}$ and $\frac{d\sigma_S}{dE}$ denote ionization occurring in hard (and soft) collisions with small (and large) impact parameters leading to large (and small) momentum transfer from the projectile to the electron. This concept is also used in the semiempirical model (compare also fig. 8).

Both the contributions from soft- and hard collisions may be calculated within the semiclassical approximation (SCA) and the quantum mechanical plane wave Born approximation (PWBA), whereas the binary encounter approximation (BEA) includes only hard collisions. However, these theoretical models (BEA, SCA and PWBA), which have been applied successfully to describe the emission of fast (δ-) electrons in collisions involving light projectiles (H, He), fail in the prediction of heavy ion induced δ-electron emission characteristics (Kelbch et al., 1992, Shinpaugh et al., 1993) as discussed in IV.b. The perturbation parameter q/v_p (where q denotes the projectile charge) is the key parameter for the description of the corresponding scaling laws. Further information on ionization and electron emission in fast ion collisions can e.g. be found in publications by Stolterfoth et al. (1987), Fainstein, Ponce and Rivarola (1988), Schneider et al. (1989, 1992), Toburen (1990) and Gerasimov (1993). Theoretical treatments of binary encounter

electron emission has been briefly reviewed by Bhalla, Shingal and Grabbe (1993). An introduction to phenomena arising with heavy relativistic projectiles (such as electron-positron pair creation, super heavy quasi molecules, etc.) can e.g. be found in Becker et al. (1987).

As discussed above, the Schiwietz model allows to calculate and compare the contributions of primary target and primary projectile ionization and the contribution from electron cascades. From fig. 7, it can be seen that target ionization dominates in the whole energy range (≈ 20 eV-10 keV) with two exceptions :

(1) Around $v_e \approx v_P$ projectile ionization to the continuum (ELC) can be observed. Together with electrons from capture of target electrons to projectile continuum states (ECC), which have been neglected in the calculations, these electrons form the *convoy electron* peak (Breinig et al 1982). It is interesting to note that convoy electron emission can be treated by models which are quite similar to the model described in this section, i.e. by using (scaled) atomic cross sections and assuming independence of elastic and inelastic scattering during transport (Koschar et al., 1987, Kemmler et al., 1988, Lencinas et al., 1990, Rothard, Groeneveld and Kemmler 1991). A further remarkable feature of the model is that the population probability P_n of the projectile states with a principal quantum number n can be kept as a free parameter, and its value can be determined from a fit of the theoretical expression to the experimental data as discussed in Schiwietz (1990). This procedure allows the determination of the fraction of excited projectile states *inside* the solid by means of electron spectroscopy.

(2.) At low electron energies, E < 100 eV, electron emission from cascade *multiplication* is (at least) of the same order of magnitude as direct target ionization.

c. The Semiempirical Model

In the following, we describe an extension of the semiempirical theory of EE as introduced by Sternglass (1957). It is based on the work by Koschar et al. (1989), Borovsky and Suszcynski (1991a,1991b) and Rothard, Schou and Groeneveld (1992). This model will serve for the interpretation of results on electron yields in chap. III. Fig. 8 illustrates the basics idea of the semiempirical model. Sternglass (1957) and Koschar et al. (1989) started from the assumption that electron yields are (roughly) proportional to the electronic energy loss per unit path length dE/dx. The projectile kinetic energy is lost in two different types of collision processes, i.e. *close collisions* with small projectile-target electron impact parameter, and *soft collisions* with large impact parameter. This concept is discussed in the classic paper by Bohr (1948).

Koschar et al. (1989) introduced the so-called "*partition factor*" β_δ describing the fraction of the projectile energy loss dE/dx leading to δ-electron emission from violent binary collisions with a small impact parameter. The fraction dissipated in soft collisions with large impact parameters leading to direct production of low energy electrons is given by $\beta_S = (1-\beta_\delta)$.

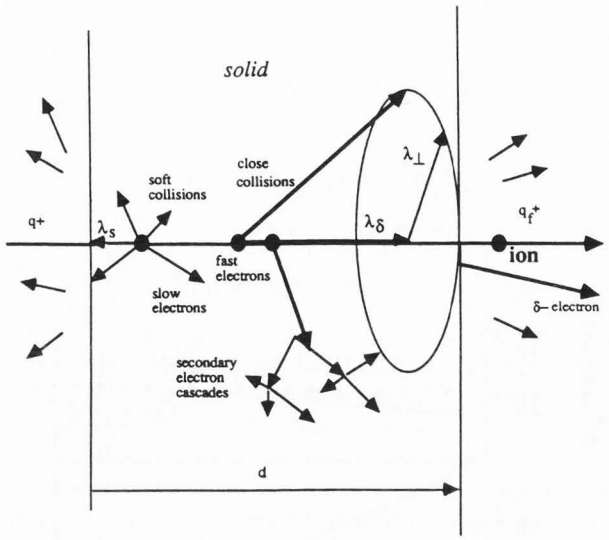

Fig. 8: Ionization of a solid by ions: basic concepts concerning the semiempirical model of electron emission involving electron transport lengths of high energy (E > 100 eV) δ–electrons parallel, λ_δ, and perpendicular, $\lambda_\perp$, to the ion trajectory, and also diffusion lengths λ_S of slow "secondary" electrons (E < 100 eV) (from Rothard et al., 1994, see also Rothard et al., 1995).

This concept is related to the so-called *equipartition rule* as discussed by Bohr (1948). In the literature on electron emission, one often finds the statement that the energy loss is equally divided among these two types of collision processes, i.e. $\beta_\delta = \beta_S = 0.5$ for fast projectiles of velocities $v_P > Z_P^{2/3}\, v_0$. This goes back to the classical paper of Sternglass (1957). In fact, it should be pointed out that the term "equipartition" denotes a sum rule for an integration of $1/\varepsilon(\omega,k)$ over the momentum k for fixed phase velocity ω/k. This integral appears in the calculation of the stopping number L in the well-known expression for the energy loss dE/dx

$$\frac{dE}{dx} = \frac{4\pi Z_P^2 e^4}{m_e v_P^2}\, n_e\, L \qquad (11)$$

for a swift heavy particle in an electron gas of density n_e described by means of a dielectric function $\varepsilon(\omega,k)$. "Equipartition" means that this integral receives exactly equal contributions from close collisions and plasmon resonances. Since in the calculation of L a further integration over velocity ω/k appears, this does not mean that $(dE/dx)_{close} = (dE/dx)_{distant}$, but rather that close collisions and plasmon resonance give rise to equal incremental contributions to stopping when the velocity is increased, $(dL/dv)_{distant} = (dL/dv)_{close}$. A thorough discussion has been given by Lindhard and Winther (1964).

Assuming from now on that dE/dx varies only slowly with penetration depth and target thickness, the number of slow electrons from primary ionization by soft collisions (s) in a layer dx at depth x is given by

$$dn_S(x) = \frac{(1-\beta_\delta)}{<E>} \frac{dE}{dx} dx \qquad (12)$$

where <E> denotes the mean energy dissipated in one PI event being in the order of some 10 to a few 100 eV. The high energy δ-electrons will also create low energy electrons due to secondary ionization processes during their migration through the solid. The number of these *secondary electrons* (SE) liberated by δ-electrons (δ) in a layer dx at x is

$$dn_\delta(x) = \frac{\beta_\delta}{<E>} \frac{dE}{dx} f(x,\lambda_\delta)\, dx \qquad (13)$$

Here, we have introduced a *dissipation/attenuation function* including a characteristic *transport length* λ_δ for the δ-electrons:

$$f(x,\lambda_\delta) = 1 - \exp(\frac{-x}{\lambda_\delta}) \qquad (14)$$

At this point, it is important to note that the meaning of eq. (14) is far from being as simple as the diffusion functions for slow electrons introduced below in eqs. (16,17). Indeed, one has to consider the effect of δ-electron creation in all layers dz at z on secondary electron creation in a layer dx at the depth x of the solid. This means that $f(x,\lambda_\delta)$ is of the form

$$f(x,\lambda_\delta) = \int_0^d g(x-z)\, dz \qquad (15)$$

where g(x-z) "cannot be readily obtained". However, as shown by Sternglass (1957) in an appendix to his paper, the simple form eq. (14) can be used for low atomic number materials under the assumption that g(x-z) is the solution of the diffusion equation for a plane source. The effect of layers dz at z > x on SE creation at x has been neglected, too.

Coming back to the three-step concept, we note that up to now, we treated the *production* of low energy SE by assuming that their number is proportional to the electronic energy loss per unit path length. The *transport* of high energy electrons is described by eq. 14, but we have also to consider the *transport* of SE from their point of creation to the surface. This can be done by introducing attenuation functions

$$P_B(x) = P \exp(\frac{-x}{\lambda_S}) \qquad (16)$$

$$P_F(x) = P \exp(\frac{-(d-x)}{\lambda_S}) \qquad (17)$$

for the beam entrance (B for "backward") and the beam exit side (F for "forward"). λ_S is the characteristic transport length for low energy SE, and P denotes the surface *transmission* probability. P depends on the internal energy- and angular distribution of SE and on the height of the surface potential barrier U_0 and is in the order of 0.5 as shown by Sternglass (1957). It should be noted that the surface transmission is usually treated by assuming a flat surface with a potential step $U_0=\Phi+E_F$ given by the sum of workfunction and Fermi energy by considering the laws of energy- and momentum conservation (see e.g. Rösler and Brauer, 1991). Quantum mechanical effects or a more complex surface structure have so far been neglected.

By summing up eqs. (12,13) multiplied by eqs. (16,17) and integrating over the target thickness d, we obtain the forward (F) and backward (B) yields of low energy SE:

$$\gamma_{F,B}(d) = \int_0^d [dn_S(x) + dn_\delta(x)]\, P_{F,B}(x) \qquad 18)$$

By assuming that $\lambda_\delta >> \lambda_S$ (and the results shown in III.2 confirm this), the integration results in simple equations for the target thickness dependence of forward and backward electron yields, γ_B and γ_F:

$$\gamma_B(d) = \gamma_B(\infty)\,[1 - \exp(-d/\lambda_S)] \qquad (19)$$

$$\gamma_F(d) = \gamma_F(\infty)\,[1 - \beta_S \exp(-d/\lambda_S) - \beta_\delta \exp(-d/\lambda_\delta)] \qquad (20)$$

The "*equilibrium yields*" for foils thicker than the range of high energy electrons ($d >> \lambda_\delta >> \lambda_S$) and sufficiently thick to assure charge equilibration of the ions (without changing the projectile energy substantially) can be written as

$$\gamma_B(\infty) = \Lambda\, \beta_S\, C_B\, dE/dx \qquad (21)$$

$$\gamma_F(\infty) = \Lambda\, C_F\, dE/dx \qquad (22)$$

with

$$\Lambda = P\, \lambda_S / <E> \qquad (23)$$

The dimensionless factors $C(Z_P,v_P)$ have been introduced to quantify deviations from eq. (4) observed with *heavy ions*. With protons, by definition, we have $C_{F,B}(Z_P) = 1$. Furthermore, over a wide range of energies, electron yields from *proton* impact have been found to be proportional to the electronic energy loss dE/dx. The energies cover a range from a few keV up to 10 MeV for carbon foils (Clouvas et al., 1989, Rothard

et al. 1993a,b) and up to 28 MeV for massive targets (Koyama et al., 1981, Borovsky, McComas and Baraclough, 1988). Thus we have $C_{F,B}(\text{protons},v_P) = 1$ also as a function of proton energy. In contrast, strong electron yield *reductions*, $C_{F,B}(Z_P>1,v_P) < 1$, have been observed with *heavy ions* at low and medium velocities (< 1 MeV/u) by Shi et al. (1985), Rothard et al. (1990c) and Clouvas et al. (1991, 1993). Surprisingly, similar findings have also been reported for energies as high as 5-6 MeV/u by Koyama et al. (1982a,b) and Borovsky and Suszynski (1991a). This can even be seen from fig. 1, since the mean value (averaged over a large range of Z_P and v_P) of $\gamma_T/(dE/dx) = 5.1$ μg/cm^2 is lower than the value obtained by Clouvas et al. (1989) and Rothard et al. (1993a, 1993b) with protons alone, $\gamma_T/(dE/dx) = 11.95$ μg/cm^2.

The results have been interpreted in terms of a *pre-equilibrium near surface stopping power in correlation to a penetration-depth dependent effective ion charge q** on one hand, and in terms of *electron trapping in the wake of the ions due to an attractive track potential* ϕ_{TR} on the other hand. According to Rothard, Schou and Groeneveld (1992), electron yields are a function of the effective ion charges q*(x) very close to the surface within a depth comparable to the low energy electron escape depths λ_S.

$$\gamma \sim \frac{dE}{dx}(x\approx\lambda_S) \sim [q^*_{F,B}(x\approx\lambda_S)]^2 \qquad (24)$$

This idea is illustrated in fig. 6, which shows schematically the dependence of the effective ion charge q(x) inside a thin solid foil of thickness d as a function of the penetration depth x according to experimental results by Zaikov et al. (1986). λ_{eq} denotes the charge equilibration depth. At $x = \lambda_{eq}$, the ionic charge is in equilibrium, the effective charge is $q_{eff} = q^*(x>\lambda_{eq}) = q_{ZBL}$ corresponding to the values used in stopping power tables (as, for example, Ziegler, Biersack and Littmark, 1985). It is clear that this near-surface value of the effective charge leads to a modification of the pre-equilibrium energy loss compared to the equilibrium (tabulated) ZBL-value

$$\frac{dE}{dx}(x\approx\lambda_S) = C_{F,B}\,\frac{dE}{dx}(ZBL) \qquad (25)$$

and thus in the case sketched in fig. 6 to reduced electron yields. Recent calculations of the dependence of the energy loss on the charge state of ions inside the solid performed by Arnau et al. (1990) and measurements of the target-thickness dependence of the energy loss of ions with different charge states by Ogawa et al. (1992) (shown in fig. 14) strongly support this approach. This correction ($C_{F,B}$) should be most important at medium velocities around and below the stopping power maximum where charge exchange is important.

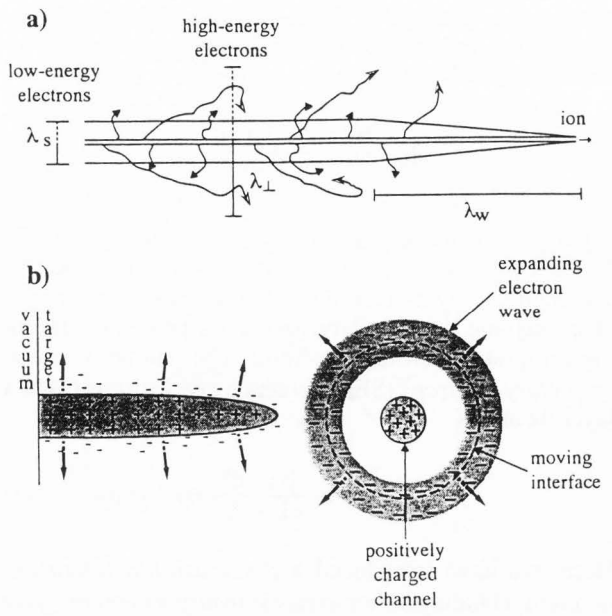

Fig. 9: The concept of the ions *wake*. **a.)** A swift ion in solids creates a dynamic response which consists of two contributions, a collective electron density fluctuation (dynamic creation and decay of plasmons) with a typical wavelength of $\lambda_w \approx 10$ Å, and a single particle wake (high energy δ- and low energy electrons). Ionization leads **b.)** to an expanding electron wave, and also, due to the high density of ionization, a positively charged track in the wake of the ion. **c.)** As a result, the track potential ϕ_{TR} causes an attractive force which retains a certain number of the electrons from moving away from the ion track (from Borovsky and Barraclough, 1989, and Borovsky and Suszcynsky, 1990b).

Borovsky and Suszynsky (1991b) proposed a theoretical model based on the concept of electron trapping in the wake of the ions. The concept of the ions *wake* (Bohr, 1948, Echenique, Ritchie and Brandt, 1979, Echenique, Flores and Ritchie, 1990) is further discussed in IV.c. The wake consists of two contributions, a *collective electron density fluctuation* (dynamic creation and decay of plasmons), and a *single particle wake* of ejected electrons (fig. 9). The idea of the existence of bound states of electrons in the wake of ions inside the solid and the possible trapping of electrons has been brought up in the pioneering work by Neelavathi, Ritchie and Brandt (1974). This lead to an experimental search for such "wake-riding" electrons (see, e.g., Strong and Lucas, 1977, and Laubert et al., 1978) in connection with experimental studies of the convoy electron peak. In recent years, this subject has regained interest, because the wake of negatively charged particles heavier than electrons may lead to an enhanced probability of single electron trapping in wake-bound states (Rivacoba and

Echenique, 1987, Burgdörfer, Wang, Müller, 1989, see below, IV.c).

Consider a completely stripped ion of high enough velocity to assure charge state conservation over a penetration distance much larger than typical low energy electron diffusion lengths, i.e., let the mean free path for electron capture be large compared to the escape depth of SE. Such an ion creates, due to the high density of ionization, a positively charged track in its wake, as illustrated by fig. 9. As a result, the track potential ϕ_{TR} causes an attractive force which retains a certain number of the electrons liberated and moving away from the ion track (fig. 9b). Consequently, electron yields will be reduced. This idea is somewhat different from the above-mentioned idea of single-electron trapping in wake-bound states. The main predictions of the model are : (1.) For given velocity v_p = const., the yield reduction increases with Z_P or q because of the increasing ionization density. (2.) The effect decreases with v_P and disappears in the high velocity limit E > 100 MeV/u (compare also Akkerman et al., 1993a, for more details and applications of the model)

If we combine the models proposed by Borovsky and Suszcynsky (1991a,1991b) and Rothard, Schou and Groeneveld (1992) the backward "reduction factor" becomes

$$C_B(Z_P,v_P) = \left(\frac{q^*(x)}{q_{ZBL}}\right)^2 \frac{(I + e\phi_{TR})^{-1} - E_{BE}^{-1}}{I^{-1} - E_{BE}^{-1}} \qquad (26)$$

with the maximum momentum transfer in a binary encounter collision corresponding to an electron energy of $E_{BE} = 2\, m_e\, v_P^2$. The C-factors become projectile and velocity dependent via the track potential ϕ_{TR} and the effective charges q^*. The track potential ϕ_{TR} can be calculated from electron yield data by means of eqs. (21,26), if the effective charge and the mean ionization potential I are known.

d. Monte Carlo Simulations

Monte Carlo codes have been used to describe electron emission from foils under heavy ion impact in the velocity range around 100 keV/u by Kozochkina, Leonas and Fine (1993) and around 1 MeV/u by Azuma et al. (1993) and Yamazaki et al. (1993). These codes treat the transport of individual electrons doing random collisions with atoms and electrons in the solid. Primary ionization can e.g. be calculated in Born approximation (as done by Gervais and Bouffard, 1994). Also, electron transport has been studied in connection with exposure of silicon based devices to cosmic rays by McGarrah, Williamson and Keeton (1992) and in relation to ion track formation. Examples and further references can e.g. be found in Krämer and Kraft (1993) and Gervais and Bouffard (1994).

Sparrow, Olson, and Schneider (1992) have applied the nCTMC (n-body Classical Trajectory Monte Carlo Method) as described in Olson, Ullrich and Schmidt-Böcking (1989) to calculate the multiple ionization of single atoms. Double differential electron spectra from 3.5 MeV/u U^{38+} ion impact on C foils have been obtained by transporting these electrons numerically until they exit the foil. An example of their results is shown in fig. 19 and will be discussed in chap. IV. It is interesting to note that this method has also been applied to (PI) δ-electron emission in ion-atom collisions (see e.g. Shinpaugh et al., 1993).

In the following, as an example of the simulation of electron emission by swift heavy ions, we show results from a Monte Carlo treatment of electron transport in solids based on the work of Gervais and Bouffard (1994). The projectiles are treated as point charges of constant kinetic energy with a straight trajectory and an effective charge $q^*(Z_P,v_P)$. Electron capture and loss as well as projectile excitation are not taken into account explicitly. The target material carbon is treated as homogenous and isotropic and is characterized by its atomic number and mass (Z_T = 6, A = 12), density (ρ = 1.65 g/cm^3), Fermi energy E_F = 17 eV and corresponding plasmon excitation frequency ($\hbar\omega_P$ = 21.2 eV), and finally the 1s ionization energy U1s = 284 eV. The density of electronic states is divided in two parts: atomic core levels and free electron gas of valence electrons. The band structure is not taken into account explicitly.

Primary ionization of core levels is calculated in first Born approximation using hydrogenic wave functions as given by Khandelwahl and Merzbacher (1966,1969). Valence electrons are treated in the framework of the dielectric theory (Lindhard, 1954). In particular, plasmon excitation and subsequent creation of secondary electrons due to plasmon decay in electron-hole pairs is taken into account. The lifetime of the plasmons was deduced from optical measurements by Taft and Philipp (1965) neglecting the wave number (k) dependence. The angle of ejection of a liberated electron is deduced from classical laws of momentum and energy conservation.

The electrons and all secondaries from cascade multiplication released by primary ionization are transported through the solid on classical trajectories. Considering the de Broglie wave length $\lambda \approx 12/\sqrt{E}$ of electrons (with E in eV and λ in Å), this is a good assumption for high energy electrons (E > 100 eV). Secondary ionization processes by these primary (but also secondary, tertiary...) electrons are treated in a similar way as primary ionization by the ions. Approximately $5*10^4$ ejected electrons from primary ionization events were passed through the carbon target in order to obtain good statistics. The primary, secondary, tertiary, ... electrons have been followed until they reached a kinetic energy of less than a cut-off value of E_{co} = 2 eV chosen arbitrarily. It can be expected that such low energy electrons do not further ionize and remain confined within a small volume with respect to the diffusion lengths of high-energy electrons. The energy levels are counted with respect to the Fermi level E_F.

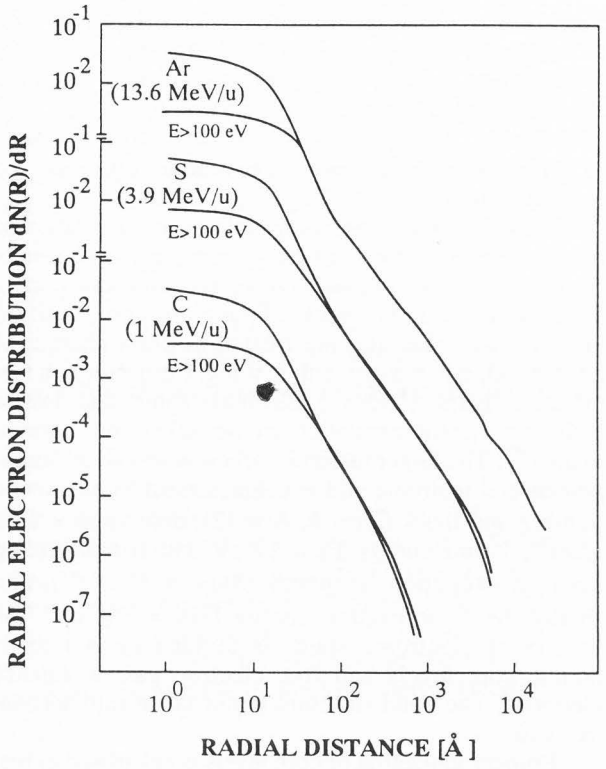

Fig. 10: Radial electron density distributions dN/dR [1/Å^3] (projectiles and energies as indicated) from numerical simulations (Gervais and Bouffard 1994) as a function of the distance R from the ion track. Two different cases are shown: electron creation by electrons of all energies E > 2 eV (upper curves) and electron creation by primary high energy δ-electrons E > 100 eV only (lower curves) (from Rothard et al. 1994, 1995).

If we are interested in internal distributions only, surface effects can be neglected. From this simulations, the density of electrons $d^3n(x,y,z)/(dxdydz)$ of a kinetic energy of less than a cut-off value of E_{co} at (x,y,z) can be obtained. The calculation is described in detail in Gervais and Bouffard (1994). As an example, fig. 10 shows radial distributions dN(R)/dR of the density per volume of all electrons which fall below E_{co} = 2 eV as a function of the radial distance R from the ion trajectory (from Rothard et al., 1994, 1995). Two cases have been investigated: (1.) electron liberation by all primary, secondary, tertiary, ... electrons of all energies E > E_{co} = 2 eV (upper curves) and (2.) electron liberation by primary high energy δ-electrons E > 100 eV only (lower curves). Above a certain distance R_0 from the ion track, both curves fall together. For R < R_0, much more low energy electrons are created if electron creation by all electrons is taken into account. This means that for R > R_0 low energy electrons are mainly created by high energy electrons, whereas electrons with energies below 100 eV deposit their energy within a radius of about R_0 ≈ 60 Å in the case of Ar. The calculations have been performed for different projectiles (C at 1 MeV/u, S at 3.9 MeV/u, and Ar at 13.6 MeV/u).

From fig. 10, it can be seen that more electrons are created at small radial distances with S than with Ar and C. This is in agreement with the experimental results: total yields for S are $\gamma_T \approx 120$, for Ar we find $\gamma_T \approx 70$, and $\gamma_T \approx 45$ for C ions. With the fastest projectile, Ar, the electron distribution extends over much larger distances, because Ar induces electrons of much higher energy and range than the other two projectiles: the maximum velocity of δ-electrons depends linearly on the projectile velocity. In the present case, $v_P(Ar):v_P(S):v_P(C) \approx 4:2:1$. Further results are discussed in sect. III.b.

III. Electron Yields

In order to shed light on the influence of ion charge pre-equilibrium and electron transport on electron emission from solids, in the following, we will discuss results of measurements of the target thickness dependence of electron yields obtained with swift heavy ions and thin carbon foils (III.a). The results will be interpreted in the framework of the semiempirical model (II.c) and compared to numerical simulations (fig. 10, II.d) in III.b. The relation of electron yields and stopping power (remember fig.1) is subject of sect. III.c.

a. Target Thickness Dependence: Primary Ionization Versus Cascade Multiplication

The dependence of total (T), forward (F) and backward electron yields (B) on target thickness obtained at GANIL in Caen by Rothard et al. (1994, 1995) are shown in fig. 11 for incident Ar^{16+} ions. For comparison, γ_T- data obtained with Ni^{26+} (15.2 MeV/u) at UNILAC in Darmstadt by Latz (1984) have been included (open squares, labeled Ni). Note that both of the projectiles carry 2 electrons. Also shown are the low energy electron yields $\gamma_{SE} = \gamma_B + \gamma_F$ (eq. 6) and least square fits of eqs. (19,20) to the experimental data. Furthermore, the high energy δ-electron yields $\gamma_\delta = \gamma_T - \gamma_{SE}$ (eq. 5) are included. Fig. 13 shows total electron yields γ_T measured by Koschar et al. (1989) with S^{q+}(3.9 MeV/u) of different incoming charge states q = 10-16. Also shown are fits of the sum of eqs. (19,20) to γ_T. The fraction belonging to high energy electrons $\gamma_\delta = \gamma_T - \gamma_{SE}$ is included in the experimental values, in contrast , eqs.(19,20) only refer to low energy electrons, and the direct yield of δ–electrons is *not* included. We shown in fig.12 (bottom) the ratios $R_{F,B}(d) = \gamma_{F,B}(q) / \gamma_{F,B}(q=18)$ of forward (and backward) yields obtained with incoming charge state q

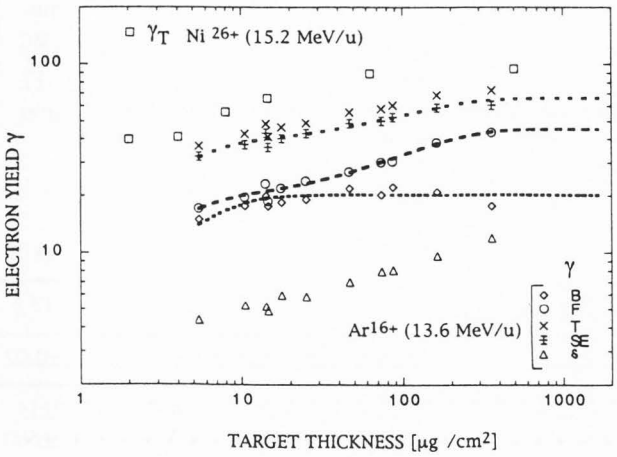

Fig. 11: Total (T), forward (F) and backward electron yields (B) as a function of target thickness (carbon foils) obtained with fast (v_P = 23 a.u., E = 13.6 MeV/u) heavy (Ar^{16+}) ions at GANIL in Caen by Rothard et al. (1994, 1995). Also included are $\gamma_\delta = \gamma_T - \gamma_{SE}$ (labeled δ) and $\gamma_{SE} = \gamma_B + \gamma_F$ (labeled SE), as well as γ_T data obtained with Ni^{26+} (15.2 MeV/u) by Latz (1984) (open squares, labeled Ni). Also shown are the results of least square fits of eqs. (19) and (20) to the experimental values and to the low energy electron yields, $\gamma_{SE} = \gamma_B + \gamma_F$.

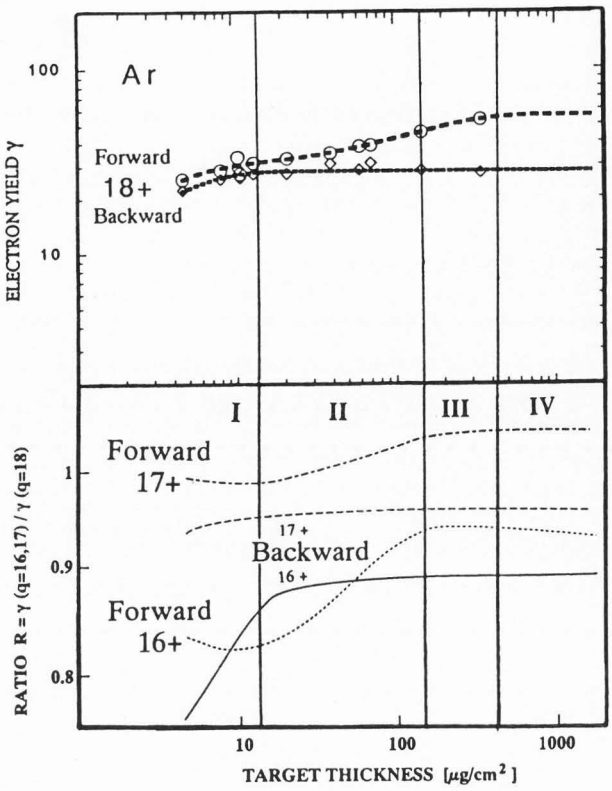

Fig. 12: Bottom: Ratios of forward (and backward) electron yields obtained with incoming charge state q = 16 and q = 17 to yields obtained with q=18, i.e. $R_{F,B}(d) = \gamma_{F,B}(q) / \gamma_{F,B}(18)$. Also shown are the backward- and forward yields obtained with Ar^{18+}(top) (from Rothard et al., 1994,1995). Experimental errors are estimated to be ±(6–8)% for yields and about ±12% for the ratios R.

= 16 (and q = 17) to yields obtained with q = 18. The mean charge <q> = 17.85 of Ar at 13.6 MeV/u is nearly equal to Z_P = 18. In fig. 12 (top), we also included the forward- and backward electron yields obtained with Ar^{18+}. The following discussion elucidates an important result of these studies: due to the high velocity of the heavy Ar ions used, by comparing bare and electron-carrying projectiles, it became for the first time possible to distinguish secondary electron production by high energy δ–electrons (cascade multiplication) from electron production by PI. Since electron production is roughly proportional to dE/dx and thus to the square of the effective charge $q^*(x)$, the dependence of the effective charge (due to electron capture and loss) on the penetration depth x also determines the electron production by PI.

From fig.11, we learn that γ_F are always higher than backward yields γ_B, for all target thicknesses and all charge states. The *forward yields* always increase within the target thickness range studied (4-360 μg/cm²). From the total yield data shown in fig. 11 for Ar^{16+} (5-700 μg/cm²) and also the Ni^{26+} data (2-500 μg/cm², at comparable velocity) we can presume that a saturation of γ_F is reached at about 400-500 μg/cm². In fig. 12, we can distinguish four regions (labeled I, II, III, and IV) of the yield evolution with increasing target thickness:

(I) Below ≈10-15 μg/cm², a plateau of R_F can be seen, whereas the yields γ_F always increase: we are close to single collision conditions and the targets are so thin that cascade multiplication (CM) just begins to start. The fastest (keV) δ-electrons leave the foils without being able to dissipate their energy. However, electrons of about some hundred eV will contribute to CM. Charge evolution does not yet play a role.

(II) Between ≈15 and 150 μg/cm², both γ_F and R_F evolve strongly: both charge changing and cascade multiplication account for this.

(III) Between 150 μg/cm² and 400 μg/cm², R_F are constant, but the yields still evolve: this region is dominated by the evolution of the low energy electron cascade, whereas the mean charge state is near the equilibrium value and changes only very slowly.

(IV) γ_F and R_F have reached constant values at d > 400-500 μg/cm^2: both charge equilibrium and full development of the secondary electron cascade induced by high energy δ-electrons are reached. We note that $R_F(\infty)$ should not depend on the initial charge state. The deviation from unity, $R_F(\infty,q=17) \approx 1.04$ and $R_F(\infty,q=16) \approx 0.92$ is compatible with the experimental error bar. However, for analysis within the semi-empirical model, it is rather the shape of the yield curve than its absolute value which is important.

From figs.11 and 12, we see that *backward yields* increase with d, but rapidly reach a saturation value $\gamma_B(\infty)$. At d < 15-20 μg/cm^2 (I), one observes an evolution of both γ_B and R_B with d until constant values are reached. This behaviour depends on the evolution of $q^*(x)$, the evolution of the secondary electron cascade multiplication, and also on the transition from nearly single collision conditions (d < 2 μg/cm^2) to multiple collisions. For d ≥ 20 μg/cm^2, (regions II-IV), the ratios R_B are constant and equal to $R_B(\infty) = \gamma_B(\infty,q)/\gamma_B(\infty,18)$.

The dependence of the *yield of high energy δ–electrons* γ_δ on d is similar to that of γ_F. A strong increase with d is observed, a saturation may be reached beyond ≈ 400 μg/cm^2 (IV). These δ-electrons represent a fraction of ≈ 15-20% of the total electron yields, and can thus not be neglected if electron yields are to be analyzed within the semiempirical model eqs.(19,20). Thus, forward and backward low energy electron yields have to be measured seperately (compare the set-up shown in fig. 4). No dependence on the charge state q has been observed, because these electrons result from close collisions where screening by the projectile electrons does not play an important role.

b. Electron Transport: Diffusion Lengths in Solids

From the fits of eqs.(19,20) to the experimental yield data, we can obtain the characteristic transport lengths for low energy electrons (λ_S) and high energy δ-electrons (λ_δ) as shown in II.c. The results of the analysis of the Ar and S data (figs.11-13) are summarized in the last column of tab.1. In order to obtain a first approach for a "characteristic transport length" $\lambda_\perp$ in the direction perpendicular to the ion trajectory, the most reasonable procedure seems to utilize the first moment of the calculated distribution dN(R)/dR (fig.10)

$$\lambda_\perp{}^{MC} = \frac{\int (dN(R)/dR)\, R\, dR}{\int (dN(R)/dR)\, dR} \qquad (27)$$

The integrations are to be performed from 0 to ∞. Longitudinal transport lengths in forward- or backward direction, $\lambda_\delta{}^{MC}$ and $\lambda'_\delta{}^{MC}$ (see below, eq. 18), can be obtained in complete analogy to the procedure descibed above from the first moments of longitudinal

Tab. 1: Electron transport lengths from analysis of the experimental data (λ_S, λ_δ) and from numerical simulations ($\lambda_\perp{}^{MC}$ radial, $\lambda_\delta{}^{MC}$ longitudinal forward, $\lambda'_\delta{}^{MC}$ longitudinal backward (see text, and compare fig. 1). Also, the partition factor β_δ is included. From Koschar et al. (1989) and Rothard et al. (1990c, 1994,1995).

Z_P	$_{10}$Ne	$_{6}$C	$_{16}$S	$_{18}$Ar
E_P/M_P [MeV/u]	0.1	1.0	3.9	13.6
β_δ	0.42±0.03	0.54±0.05	0.59±0.05	0.55±0.02
λ_S [Å]	—	17±3	14±2	180±15
λ_δ [Å]	⟨⟨ 200	300±26	1200±50	9800±680
$\lambda_\delta{}^{MC}$ [Å]	—	70	450	2600
$\lambda'_\delta{}^{MC}$[Å]	—	3	15	56
$\lambda_\perp{}^{MC}$[Å]	—	80	570	4000

distributions which can also be obtained from the MC code of Gervais and Bouffard (1994). In order to study the velocity-dependence of all the quantities characterizing electron transport in solids from heavy ion induced electron emission yields, we compiled tab.1, which shows λ_S, λ_δ, $\lambda_\perp{}^{MC}$ (radial), $\lambda_\delta{}^{MC}$ (longitudinal, forward), $\lambda'_\delta{}^{MC}$ (longitudinal, backward) for the indicated ions and carbon targets.

We can also extract the partition factor β_δ from eqs.(19,20), which we also included in tab.1. The reader should keep in mind the discussion on the term "equipartition" of II.c in this respect. In good agreement with a value of β_δ = 0.59±0.05 for S(3.9 MeV/u) and β_δ = 0.54±0.05 for C(1MeV/u), we get β_δ = 0.55±0.02 from our measurements with Ar^{q+} (13.6 MeV/u, q = 16-18). This means that although they represent only about 15% of the total electron yield, slightly more than 50% of the projectile kinetic energy lost.

The values of the characteristic transport lengths are found to be much larger in the case of Ar (13.6 MeV/u). The semiempirical model yields λ_S = (180±20) Å ≈ 3 μg/cm^2 (compared to λ_S ≈ 15 Å for S and C, and λ_δ = (9000±680)Å ≈ 150 μg/cm^2 (compared to λ_δ = 300 Å for C at 1MeV/u and λ_δ = 1200 Å for S at 3.9MeV/u). From the MC simulations, we get $\lambda_\delta{}^{MC}$ values being about 3 times smaller, but, more important, which show the same dependence on the projectile velocity. At this point, it must be noted that although both quantities, λ_δ and $\lambda_\delta{}^{MC}$, give us qualitatively an idea of the range and diffusion length of δ-electrons, they can not be compared directly in a quantitative manner. Remember that at x = λ_δ, about 67% of δ–electrons have deposited their energy in low energy SE cascades.

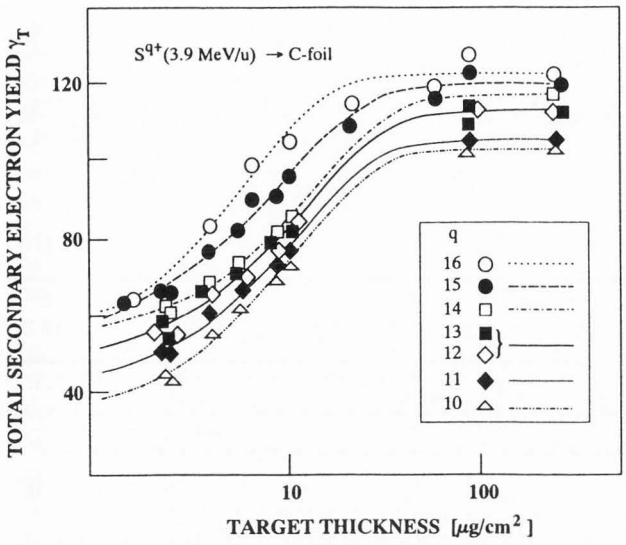

Fig. 13: Total electron yields γ_T measured by Koschar et al. (1989) with S^{q+}(3.9 MeV/u) of different incoming charge states q = 10-16 and carbon foils as a function of the target thickness. Also shown are fits of the sum of eqs. (19,20) to γ_T.

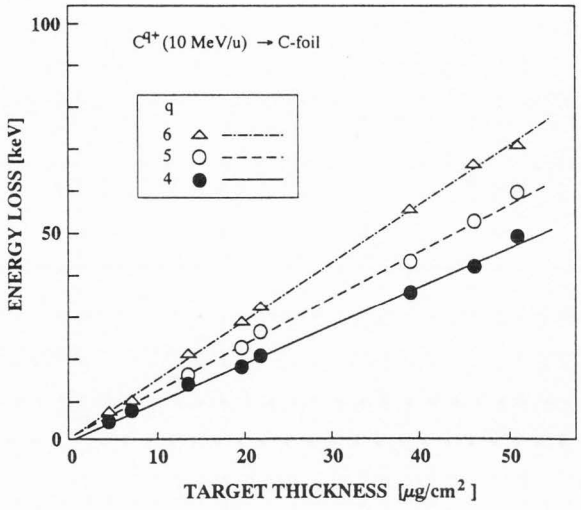

Fig. 14: Energy loss of C^{q+}(10 MeV/u) as a function of carbon foil thickness as measured by Ogawa et al., 1992). As a striking similarity with the data on electron yields shown in fig. 13, a clear dependence on the incoming charge state (q = 4-6) of the ions is observed.

The large value of λ_S = 180 Å found with Ar (13.6 MeV/u) is surprising, since the isotropic diffusion of low energy electrons should mainly depend on the target material and not on the projectile velocity. This is indeed what is found for C and S at lower projectile velocity. Probably, this large λ_S value could be explained if diffusion of δ–electrons in backward direction was taken into account. Following again Sternglass (1957), this can be done by using a more realistic δ–electron energy dissipation/diffusion function than eq. (13):

$$f(x,\lambda'_\delta,\lambda_\delta) = \frac{1}{(1+\frac{\lambda'_\delta}{\lambda_\delta})}\left[1-\exp(\frac{-x}{\lambda_\delta})+\frac{\lambda'_\delta}{\lambda_\delta}\right] \quad (28)$$

A derivation of this formula is given in the appendix of the paper by Sternglass (1957). When replacing eq. (14) by eq. (28), the integration of eq.(18), which is still feasible (Beck and Langkau, 1975) results in more complicate expressions for the electron yields as eqs. (19,20). λ'_δ has a similar meaning as λ_δ, but for energy dissipation in *backward* direction (opposite to λ_δ). Possibly, the relatively slow increase of γ_B(Ar) (figs. 11,12) is due to the fact that the slope of the non equilibrium backward yields are defined by λ'_δ and not by λs. A similar observation has been made by Koschar et al. (1989) for γ_B obtained with C (1 MeV/u). At high projectile velocity leading to high δ-electron energies, it is possible that a considerable fraction of these electrons undergo a few large-angle scattering events and finally propagate in backward direction with enough energy left to create secondaries. The results of the MC simulations for $\lambda'_\delta{}^{MC}$ strongly support this idea: a much larger value is found for Ar than for C or S.

In contrast to that, the result for λ_δ and $\lambda_\perp{}^{MC}$ is easy to understand: the maximum momentum transfer is increased. Hence, the mean electron energy and, consequently, the range of the fast electrons increase with projectile velocity v_P(Ar):v_P(S):v_P(C) ≈ 4:2:1. The values for the radial momenta $\lambda_\perp{}^{MC}$ give an estimate for the radial range of ion induced damage in materials, the so-called *ultra-track*. We see from tab. 1 that the fast Ar ions of 13.6 MeV/u can induce damage over radial distances as large as 400 nm, compared to less than 10 nm at 1MeV/u. It would be interesting to study the v_P-dependence of all the quantities summarized in tab.1 for one heavy ion, i.e. at fixed Z_P in a large velocity range (say, 0.1 to 100 MeV/u).

c. Relation between Electron Yields and StoppingPower

In contrast to the equilibrium forward- and the high energy electron yields, the total yields (fig.13) clearly increase with the charge state of the incoming ions. This is mainly due to the charge-state dependence of backward electron yields, as becomes clear from figs. (11-12). The incoming charge state (q) dependence is due to the fact that for fast projectiles, the initial charge state is conserved over distances λ_{eq} much larger than the characteristic low energy electron transport lengths λ_S.

Tab. 2: The factors $C(Z_P,v_P)$ as defined by eq. (29) and the quotients $\Lambda^*(Z_P,v_P)$ as defined by eq. (30) for total, forward, and backward electron yields (indicated by the indices T, F, B) as well as the track potential ϕ_{TR} as calculated from backward electron yields from eq. (26). Data from Rothard et al., 1993a (H), Rothard et al., 1990c (Ne, 0.1 MeV/u), Koschar et al., 1989 (S), Schiwietz et al., 1990 (Ne, 5 MeV/u), Schneider, Schiwietz and DeWitt , 1993 (U), Rothard et al. 1994, 1995 (Ar) and Latz, 1984 (Ni).

Z_P	$_1H$	$_{10}Ne$	$_6C$	$_{16}S$	$_{10}Ne$	$_{92}U$		$_{18}Ar$	$_{28}Ni$
q	1	1	6	16	10	38	68	18	26
E_P/M_P[MeV/u]	0.02-9.5	0.1	1.0	3.9	5	3.5	8.5	13.6	15.2
Λ_T [μg/(keVcm^2)]	11.95	5.1	8.3	8.8	5.6	13.3	12.6	9.1	5.5
Λ_F [μg/(keVcm^2)]	6.55	3.28	4.52	--	4.0	9.0	10.1	5.15	--
Λ_B [μg/(keVcm^2)]	5.45	1.82	3.14	--	1.2	4.3	2.5	2.44	--
C_T	1	0.43	0.69	0.73	0.47	1.11	1.05	0.76	0.46
C_F	1	0.5	0.69	--	0.67	1.37	1.65	0.78	--
C_B	1	0.33	0.58	--	0.22	0.79	0.46	0.45	--
ϕ_{TR} [V]	--	--	51	--	258	20	87	91	--

In the present case, about 50% of incoming Ar^{17+} ions have changed their charge state to q = 18 after ≈ 120 μg/cm^2 (to be compared to $\lambda_S \approx 3$ μg/cm^2). As an important result, even projectile shell effects have been observed by Koschar et al. (1989). These findings can be explained by the charge state dependence of the pre-equilibrium energy loss leading to a modified, *near-surface pre-equilibrium stopping power* as discussed in II.c. According to eq.(24), the backward yields scale approximately as $\gamma \sim q(d \approx \lambda_S)^2$. This idea is illustrated schematically in fig. 6. In accordance, we find $R_B(\infty)$ = 0.92 (0.84) versus $[<q>(q)/<q>(18)]^2$ = 0.91 (0.81) for q = 17 (16). Charge equilibrium is reached at about d_{eq} = 450 μg/cm^2. This concept is strongly supported by the results shown in fig. 14, which shows the energy loss of C^{q+} (10 MeV/u) as a function of carbon foil thickness (Ogawa et al., 1992). As a striking similarity with the data on electron yields shown in fig. 13, a clear dependence on the incoming charge state (q = 4-6) of the ions is observed.

However, even if the pre-equilibrium evolution of charge states and stopping power are taken into account, discrepancies between experimental results and conventional theories remain: Strong deviations from a simple scaling of electron yields with the electronic stopping power ($\gamma \sim dE/dx$) have been observed even with *fast, bare* ions (Z_P = 1-8) at high velocities (5 MeV/u), where the above-mentioned pre-equilibrium effects are negligible (Koyama et al., 1982a,b, Borovsky and Barraclough, 1989, Borovsky and Susczynski, 1991a). The reduction/suppression effect can be quantified by introducing the ratios

$$C(Z_P,v_P) = [\gamma(Z_P) / \gamma(H^+)] \, [\frac{dE}{dx}(H^+) / \frac{dE}{dx}(Z_P)]$$

$$= \Lambda^*(Z_P,v_P) / \Lambda^*(H^+,v_P) \qquad (29)$$

as it has been done in eqs. (21,22,26). The factors $C(Z_P)$ have the same physical meaning as the quotients

$$\Lambda^*(Z_P,v_P) = \gamma/(dE/dx) \qquad (30)$$

but are simply scaled and measured in units of $\Lambda^*(H^+)$. Following Sigmund (1993), we note that stopping power tables should be used with care if electron yields are to be compared to the stopping power by calculation the factors eqs.(29,30). A discussion on the target- and projectile dependence of the parameters Λ^*, eq.(30), can be found in Hasselkamp et al. (1990). Recently, electron yields from Al, Cu, Ag and Au have been measured simultaneously with the projectile energy loss of H^+ and He^{2+} by Benka, Steinbauer and Bauer (1994). For H^+, the expected proportionality was found within 2%. Strong deviations were observed with He^{2+}.

In sect II.c, we introduced the model proposed by Borovsky and Suszcynski (1991b): their prediction for the magnitude of the reduction effect is contained in eq. (26). In order to compare the available experimental results to these predictions, we compiled tab.2. We included the factors $C(Z_P,v_P)$ and $\Lambda^*(Z_P,v_P)$ as defined by eqs. (29-30) for total, forward, and backward electron yields (indicated, as usual, by the indices T, F, B). No strong increase of the reduction effect with Z_P for the

different ions at comparable velocities (Ne, S and U around 3.5 MeV/u) can be observed. At about 15 MeV/u, however, the effect is stronger for Ni than for Ar. For Z_P = 20, the model predicts much stronger reduction effects in an order of magnitude of C ≈ 0.1, in contrast to the experimental findings. The reduction effect is always stronger in backward than in forward direction. Furthermore, it seems that with increasing projectile velocity and increasing projectile charge or atomic number, the reduction effect disappears in forward direction: even an enhancement $C_F > 1$ is observed in one case. Probably, this is due to the increasing contribution of δ-electron induced secondary cascade multiplication in combination with increasing mean electron energy: compare the discussion given by Schiwietz (1993) and Schneider, Schiwietz and deWitt (1993) on this subject. The calculation of the track potential ϕ_{TR} with eqs. (21,26) from backward yields for 13.6 MeV/u Ar in C results in ϕ_{TR} values one order of magnitude lower than those given by Borovsky and Suszcynski (1991b) for Au. This may be an indication that this model should not be applied to metals. Because of the lack of systematic studies on the v_P-dependence of the "yield reduction effect" for fixed Z_P in a larger velocity range (say, 0.1 to 100 MeV/u), no clear conclusions on the validity of the model can be drawn. It is even possible that a saturation of $C(Z_P)$ may be found as a function of Z_P for given v_P, as it has been observed at lower velocities by Clouvas et al. (1991, 1993) and Rothard, Schou and Groeneveld (1992).

Further light on these findings can be shed by studying low energy electron spectra (fig. 21, IV.c). It is interesting to note that quite similar observations such as strong suppression of low energy electron emission (compared to the case of *protons, and always taking into account the different energy loss of different projectiles)* have also been made with molecular and cluster ions, even at MeV/u energies (see, e.g., Kroneberger et al., 1988, Rothard et al. 1990a, Suszcynski and Borovsky, 1991, Rothard et al., 1993a,b). It is a challenging question whether all of these results may be understood in an universal picture involving the same physical processes such as e.g., screening effects, long range plasmon excitation or wake effects (see IV.c).

IV. Energy Distributions

a. Electron Spectra as a Function of the Emission Angle

The measurement of electron yields permits the indirect determination of the characteristic diffusion lengths of high energy electrons. For more detailed information, further investigations by means of spectroscopy are necessary. Besides investigations on electron emission related to channelling phenomena (chap.V), to our knowledge, the only systematic measurements of energy and angular distributions have been performed at VICKSI in Berlin with Ne ions by Schiwietz et al. (1990) and at the Super HILAC in Berkeley with U ions (3.5 and 8.5 MeV/u) by Sparrow, Olson and Schneider (1992) and Schneider, Schiwietz and DeWitt (1993) with thin carbon foils (5-100 μg/cm^2). Examples of their work are shown in figs. 15, 16 and 19. Results from recent studies at GANIL (Caen/France) with Ar ions (13.6 MeV/u) by Rothard et al. (1994,1995) are shown in fig. 17. Betz et al. (1988) and Schramm and Betz (1992) studied electron spectra from heavy ion penetration of thin carbon foils at somewhat lower energies.

The angle-integrated forward (F) and backward (B) energy distributions dn(E)/dE = N(E) from 3.5 MeV/u U^{38+} (and 8 MeV/u U^{68+}) penetration through 20 and 44 μg/cm^2 carbon foils are shown in fig. 15. The corresponding double differential spectra $d^2n/dEd\Omega$ taken at different observation angles Θ for 8 MeV/u U^{68+} are displayed in fig. 16. We can identify similar structures as in the proton induced spectrum of fig. 2: Low energy electron emission (10 eV ≤ E < 100 eV) is dominating, although the maximum of the "true SE" peak cannot be seen, because its intensity maximum for carbon targets is lower than the minimum energy investigated (E = 10 eV). With MeV protons, it has been found at (2.1±0.3) eV (fig. 2). The target KLL Auger electron distribution at E = 260 eV is clearly visible in all of the spectra shown. The convoy electrons (CE) can be seen as a prominent peak in the Θ = 0 deg. spectra. The measurements with 8 MeV/u U ions do not cover all of the high energy binary encounter electron (BEE) distribution at twice the projectile velocity at extreme forward angles around Θ = 0 deg. The target thickness dependence of BEE emission has been studied at Θ = 40 deg. with 3.5 MeV/u U^{38+} (fig. 19). We note that in all of these spectra, the plasmon decay peak at ≈ 15-20 eV cannot be seen, probably because of the low energy and because electrons from the decay of plasmons are more pronounced from clean surfaces (Hasselkamp 1991, Burkhard, Rothard and Groeneveld 1988). Also, no prominent loss electron peak in backward direction, as it has e.g. been observed with MeV He^+ (or H_2^+ molecule) impact as broad structure around $v_e = -v_P$ in double differential spectra (see below, IV.d), can be seen.

Also included in the figures are the results of a calculation using the model described in II.b, which have also been shown in fig. 7. The calculations shown in the double differential spectra (fig. 16) correspond to the sum of the contributions by the primary target and projectile ionization and cascade multiplication. For sufficiently high electron energies (> 4 keV), the calculations agree well with the experimental data in forward direction. Emission of slower electrons, however, is underestimated by up to a factor of 5, and the reason for this is not fully understood. In backward direction, the angle-integrated spectra (fig. 15) are well reproduced, whereas deviations appear in the double differential spectra, in particular at high energies. High energy electrons in backward direction result from a few large-angle scattering events for which the SELAS approximation is not valid.

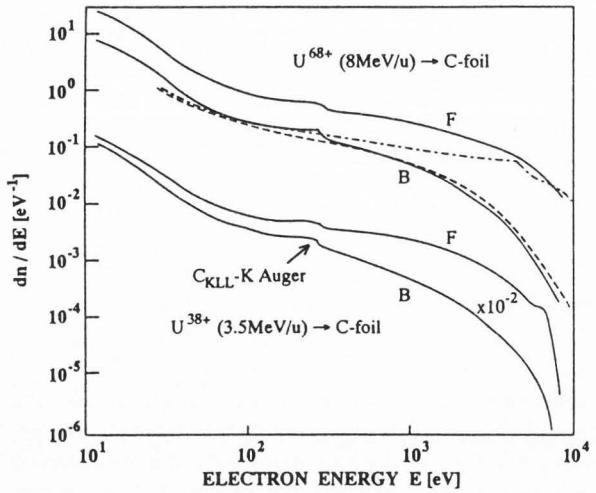

Fig. 15: Angle-integrated forward (F) and backward (B) energy distributions dn(E)/dE=N(E) from 3.5 MeV/u U^{38+} penetration through a C foil of d = 20 μg/cm² and 8 MeV/u U^{68+} penetration through a 44 μg/cm² C foil as measured by Schneider, Schiwietz and DeWitt (1993). Also included are the angle-integrated calculations (dashed lines) of fig.7.

Fig. 17 shows spectra obtained recently at GANIL (Caen) by Rothard et al. (1994, 1995). We measured the evolution of double differential electron spectra (E = 1-40 keV, Θ = 0-180 deg., d = 4.4-350 μg/cm²) with carbon target thickness for Ar^{17+} and Ar^{18+} at 13.6 MeV/u as complement to the electron yield measurements for the same collision system shown in figs. (11,12). As an example, we show in fig. 17 the angular dependence of δ-electron spectra for Ar^{17+} penetrating C(4.4μg/cm²) at observation angles Θ = 0–80 deg. The measured intensity is shown as a function of the electron velocity v_e. These spectra would, integrated over all angles, correspond to a fraction of about 15% of all emitted electrons (compare γ_δ in fig. 11). The spectra, taken with a magnetic spectrometer (Latz, 1984) show three main structures. At the low energy side, electrons from target ionization can be observed. At 0 deg., one can see the cusp-shaped CE-peak at v_P and a BEE peak at $2v_P$. The CEpeak vanishes slowly with increasing angle and can be seen up to θ = 20 deg..

With increasing angle Θ, the maximum of the BE peak shifts to lower energies. The angular dependence of the maximum should follow the law

$$v_{BE} = 2\, v_P \cos(\Theta) \qquad (30)$$

These theoretical values are indicated by arrows and shown as solid line in the inset of fig. 17. Surprisingly, we observe slight deviations from this law at large angles θ ≥ 40 deg. as it has been observed in ion-atom collisions at lower energies, too (fig. 21). We will come back to this in sect. IV.b.

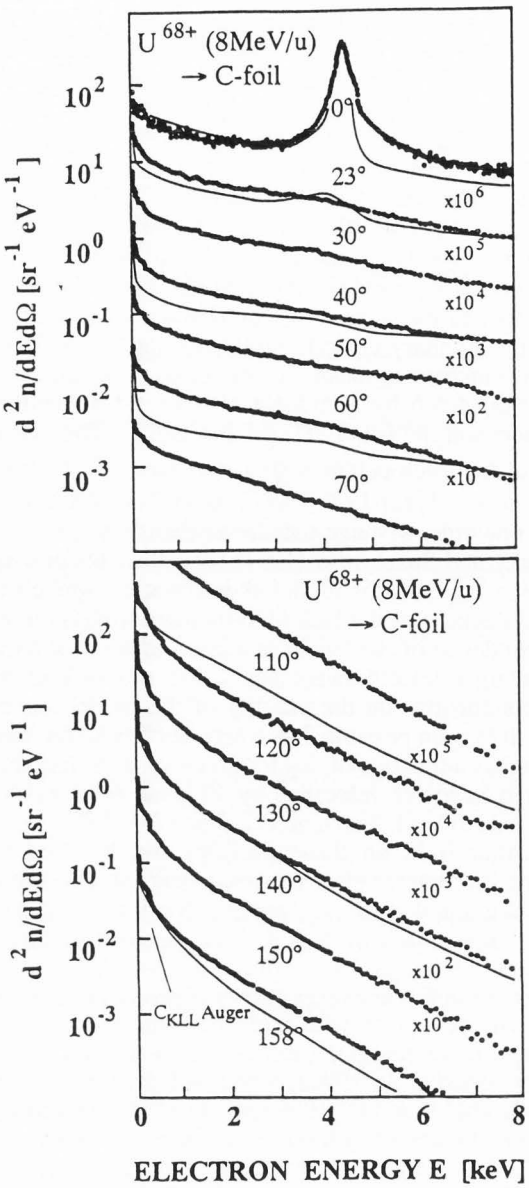

Fig. 16: Double differential spectra $d^2n/dEd\Omega$ taken at different observation angles Θ for 8 MeV/u U^{68+} (same collisions system as in figs. 7 and 15, from Schneider, Schiwietz and DeWitt, 1993). The results of the calculations (thin solid lines) correspond to the sum of the contributions by the primary target- and projectile ionization and cascade multiplication of fig. 7.

From simple geometrical arguments, assuming an almost isotropic internal distribution of the low energy electron flux, it can be expected that the low energy "true SE" from cascade processes should follow a $N(\Theta) \sim \cos(\Theta)$ law (Sigmund and Tougaard, 1981, Schou 1988). For thick samples in backward direction, this has been confirmed experimentally (Mischler et al., 1984).

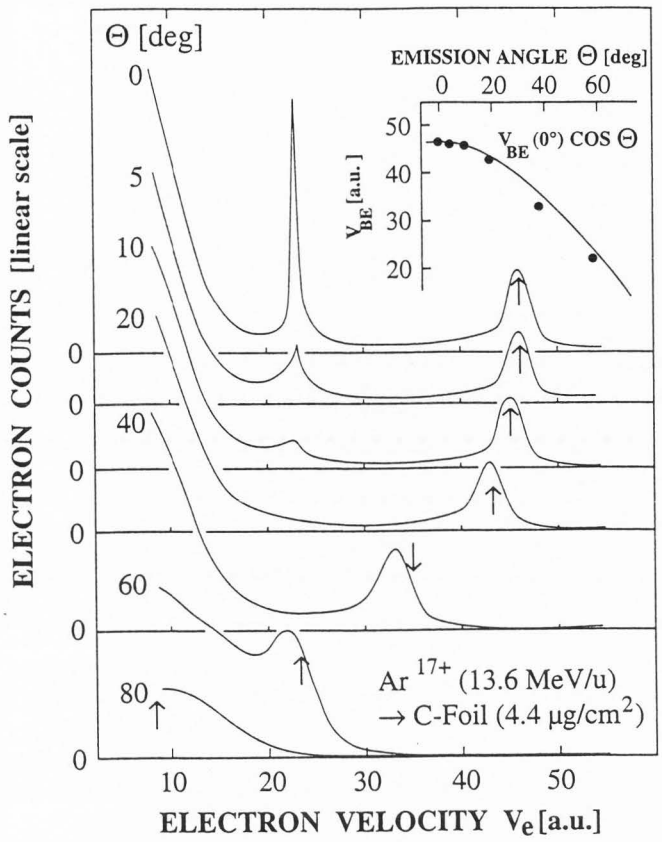

Fig. 17: Double differential electron spectra obtained with Ar^{17+} (13.6 MeV/u) at different observation angles 0 deg. $\leq \Theta \leq$ 80 deg. from a thin carbon foil (d = 4.4 $\mu g/cm^2$) as a function of the electron velocity v_e. The spectra were obtained at GANIL (Caen) by Rothard et al. (1994, 1995). The expected mean velocity $v_{BE} = 2\ v_P \cos(\Theta)$ of binary encounter (BE) electrons is indicated by arrows and shown as solid line in the inset in comparison to the experimental values obtained from the position of the BE peaks.

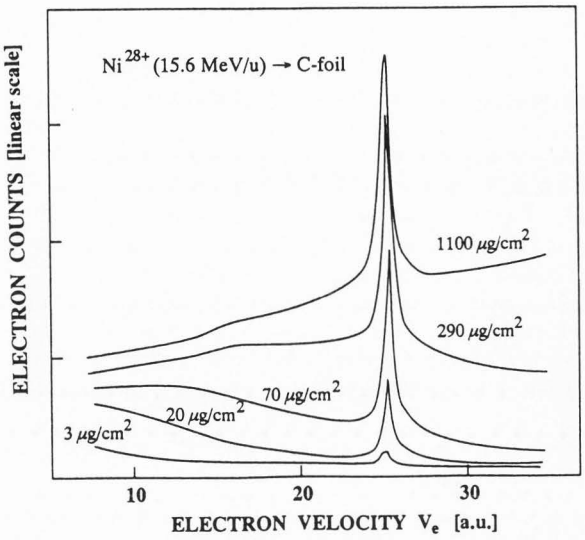

Fig. 18: Electron spectra taken unter Θ = 0 deg with Ni^{28+} ions (15.6 MeV/u) traversing carbon foils of different thickness obtained at GSI/Darmstadt by Kemmler et al. (1988), taken from Kemmler (1988). The intensity scale is the same for all spectra, but is not given in absolute units.

In forward direction, however, there may be deviations because of the anisotropic internal production (PI) of SE due to contributions from fast δ-electrons. Furthermore, it has recently been shown by Suarez et al. (1993) that even soft electron (low energy, E = 0-30 eV) emission in ion-atom collisions is non-isotropic and that those electrons are preferentially emitted in forward direction.

High charge effects on *Auger* electron emission with swift heavy ions have been discussed by Saemann-Ischenko and Schmidt (1983) and Koyama et al. (1986, 1988a, 1988b). Useful information can also be found in the review by Brusilovsky (1990). The yield of carbon Auger electrons is about 1% of the total yield of $\gamma_T \approx$ 2470 electrons per ion for uranium at 8 MeV/u and 4% of $\gamma_T \approx 22$ for neon at ≈ 8.5 MeV/u. An enhancement of Auger electron yields in forward direction from fast Ne ion impact compared to Auger electron yields in backward direction from thin foils has been attributed to additional ionisation by fast electrons (Schiwietz et al., 1988). The angular distribution of these Auger electrons roughly exhibits a $N(\Theta) \sim \cos(\Theta)$ dependence.

b. Target Thickness Dependence:

Convoy- and Binary encounter electrons

Until today, low energy electron spectra (E < 50 eV) have not been studied as a function of the target thickness. One reason for this are the general difficulties connected with low energy electron spectroscopy (instrumental efficiency, compensation of residual magnetic fields, preparation of clean surfaces). However, double differential electron velocity distributions at higher electron energies have been investigated in particular concerning *convoy electron* emission, but also for *binary encounter electron* emission (Betz et al., 1988). During ion penetration through solids, charge exchange and excitation processes form a dynamic charge cloud around the projectile. Some of the electrons are not lost into free states, and some are not captured into bound states, but are transferred into high Rydberg or projectile centred continuum states where they accompany the projectile ion with the same speed and direction. These electrons in a particular final state in the low energy projectile continuum, the so-called *convoy electrons* (CE), arise from either capture of a target electron into a continuum state of the projectile (ECC) or the loss of a projectile electron into the continuum (ELC) (Breinig et al., 1982).

Koschar et al. (1987) made a difference between *direct* and *indirect* (I) ELC and ECC if these processes take place with the projectile ion in its incident charge state ("direct") or if a charge exchange event has occurred before. For example, if the electron is first captured and then lost in a two step process, this is called IELC. Field-ionized Rydberg electrons (ionization occurs in the spectrometer) can also contribute to the CE peak. The relative importance of these *production* processes depends on the evolution of the electronic configuration of the projectile ion on its way through the solid. In chap. II, this step was called *preparation*, and it is characterized by the mean free paths (MFPs) for charge exchange and excitation, compare fig. 6, where λ_{eq} gives a rough estimate at which penetration distance the ion has reached its dynamic charge equilibrium. High-velocity experiments at GANIL/Caen by Gibbons et al. (1991) have shown that CE are very sensi-tive to pre-equilibrium so that in particular their angular (multipole) distribution shows an astonishingly rapid evolution in target thickness dependence measurements, compared to the MFPs of the elementary processes .

The *transport* of CE can be treated in the same way as for a free electron which suffers energy loss and angular deflection, but a more sophisticated treatment must take the influence of the accompanying projectile ion charge into account. Surface *transmission* effects can be neglected for high energy CE of interest here. Because of the complexity of the problem, Monte Carlo simulations have been used by Burgdörfer and Gibbons (1990). Further information can be found in the recent reviews bei Burgdörfer (1991a, 1991b). As an example, we show in fig. 18 electron spectra taken at $\Theta = 0$ deg with Ni^{28+} ions (15.6 MeV/u) traversing carbon foils of different thickness obtained at GSI in Darmstadt by Kemmler et al. (1988). Note the strong dependence of both CE yields and intensity of the ionization electron background on target thickness, and also that the shape of this background changes. With increasing target thickness, high energy electron emission at $v_e > v_P$ strongly increases. It should be mentioned that background subtraction is an important problem in CE emission studies. CE represent only a small fraction of all electrons emitted, in our example (Ni at 15.6 MeV/u), the equilibrium CE yield is $Y_{CE} \approx 0.002$ compared to a total yield of $\gamma_T \approx 120$ (Kemmler et al., 1988).

It is useful to connect the measured convoy electron yields (and velocity or angular distributions) to the corresponding outgoing projectile ion charge states by coincidence measurements. A comparison of the target-thickness dependent convoy electron yield Y_{CE} in coincidence with a specific charge state q and the charge state distribution F(q,x) itself can yield important information about the possible contributions of electron loss and/or capture. In our example of Ni^{28+} ions exiting from carbon foils at 15.6 MeV/u, the coincidentally measured convoy electrons originate both from ECC and ELC with nearly the same probability (Kemmler et al. 1988, Kemmler, 1988, 1990). ECC comes from Ni^{27+} states formed in the solid by capture of target electrons. The contribution of both processes strongly depends on the target thickness and the projectile velocity.

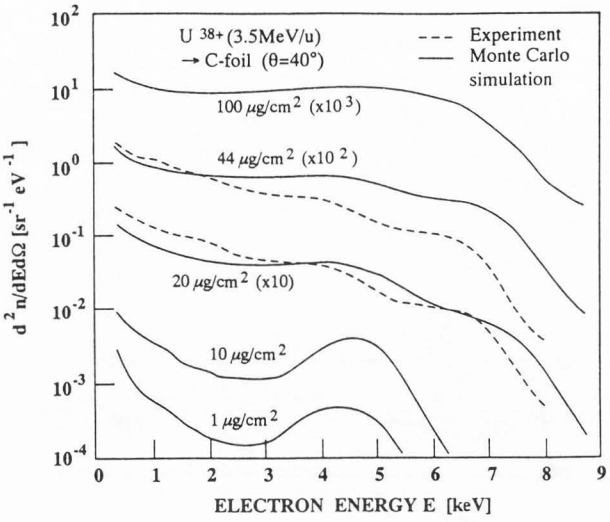

Fig. 19: Double differential spectra $d^2n/dEd\Omega$ at different observation angles Θ for 3.5 MeV/u U^{38+} calculated by Sparrow, Olson and Schneider (1992) (solid lines). In particular, the evolution of the *binary encounter electron* ($2v_P$) peak structure with target thickness from single collision conditions to multiple collisions including wide angle scattering of electrons can be observed. Also included are experimental data for intermediate target thickness (20 and 44 μg/cm^2, dashed lines).

Sparrow, Olson and Schneider (1992) performed a numerical simulation of electron transport in solids, where the primary ionization of target atoms was determined by the nCTMC method (II.d). An interesting result of these simulations is shown in fig. 19. The evolution of the *binary encounter electron* ($2v_P$) peak structure with target thickness from single collision conditions to multiple collisions including wide angle scattering of electrons can be observed. It is also interesting to compare ion-atom to ion-solid collisions (fig. 20).

In ion-atom collisions, quite unexpected observations in view of the theoretical models like SCA, PWBA, BEA (see II.b) have been made (Kelbsch et al., 1992, Shinpaugh et al., 1993). In particular, the position, shape and intensity of the BEE peak showed a surprising behaviour. The BEE peak was splitting up into a high energy and a low energy component for a certain range of observation angles, instead of being a broad distribution. Furthermore, the peak energies were not varying with the observation angle as predicted by the expected $E_{BE} \sim \cos^2(\Theta)$ law given by eq. (30), but the intensity of the two components appeared to shift from the high energy- to the low energy part. Also, the double differential cross section for binary encounter electron

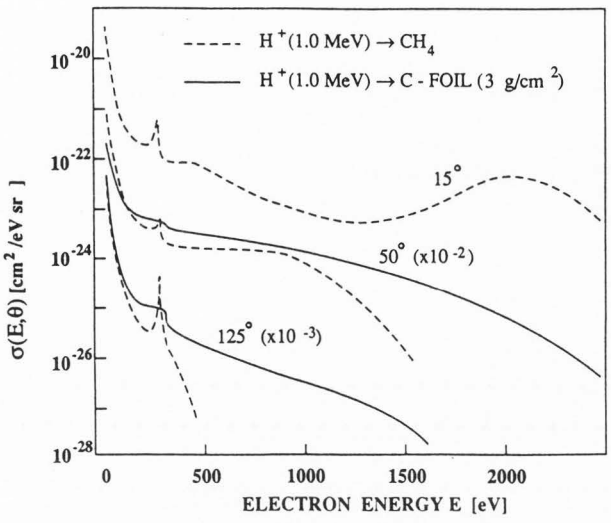

Fig. 20: Comparison of electron spectra from proton (1 MeV) impact on a hydrocarbon gas target (CH_4) and on a thin carbon foil (from Toburen, 1990) at three observation angles (as indicated, Θ = 15, 50 and 125 deg.).

emission in forward direction (0 deg) was observed to be much larger for partly ionized projectiles ($q < Z_P$) than for bare projectiles ($q = Z_P$).

As an example for this behaviour, we show double differential electron spectra $d^2\sigma/dEd\Omega$ for different emission angles Θ in fig. 21a. The collision systems are Xe^{21+}(1.4 MeV/u) → Ar (left) and Xe^{21+}(3.6 MeV/u) → He (right). We note that the unexpected behaviour of the BEE peak does not strongly depend on the target, but rather on the projectile charge state and velocity. Fig. 21b shows the experimental value for the energy E_{BE} of the maximum of the BEE peak as a function of the emission angle for different velocities in comparison to the "free electron" $E_{BE} \sim \cos^2(\Theta)$ law of eq.(30) as indicated by the solid lines. These results can be explained by the elastic scattering of quasifree target electrons in the screened projectile potential which causes strong diffraction structures (often called *Ramsauer-Townsend*-effect) in the angular distribution. However, in the high energy limit, these interference features disappear, no diffraction patterns in the BEE peak were observed at high energies (E_P = 6 MeV/u, fig. 21b).

Coming back to the ion-solid case, in fig. 19 (U^{38+}, Θ = 40 deg.), an interesting double peak structure can be observed for intermediate target thickness (20 and 44 $\mu g/cm^2$) both in the experimental data and the nCTMC calculations. For the thinnest foils, 1 and 10 $\mu g/cm^2$, a well pronounced single BEE peak at the "good" position E_{BE}(40 deg.) = 4.5 keV corresponding to $2v_P \cos$(40 deg.) can be seen. With increasing target thickness, a second structure at higher energies develops. It is due to BEE ejected near 0 deg. with E_{BE} (0 deg.) = 7.5 keV which have suffered large angle scattering with small

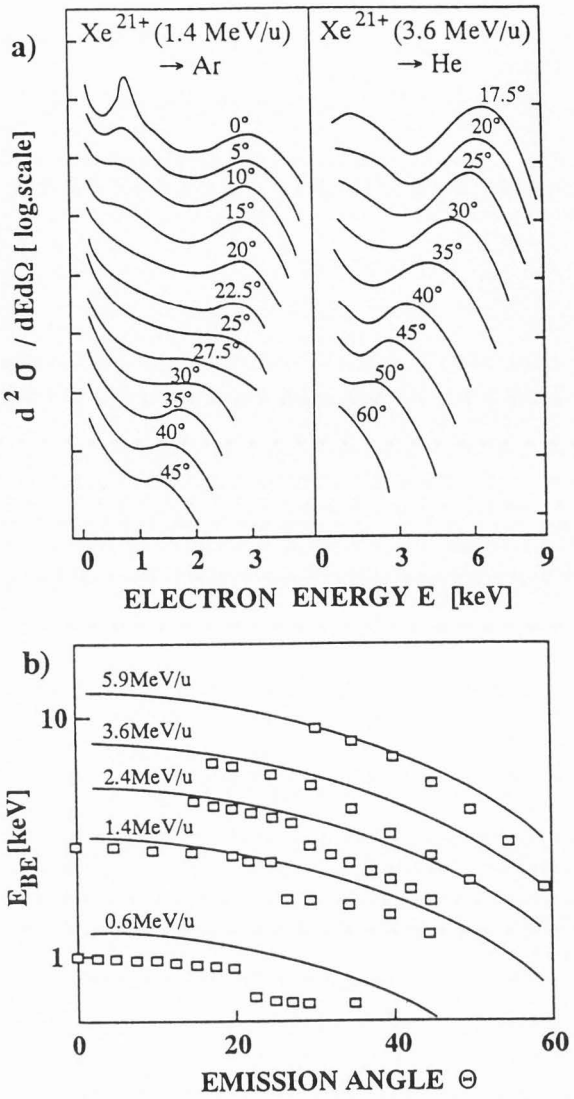

Fig. 21: a.) Electron spectra $d^2\sigma/dEd\Omega$ for different emission angles Θ obtained with gaseous targets. The collision systems are Xe^{21+}(1.4 MeV/u) → Ar (left) and Xe^{21+}(3.6 MeV/u) → He (right). **b.)** Experimental value for the energy E_{BE} of the maximum of the binary encounter electron peak as a function of the emission angle for different velocities in comparison to the "free electron" $E_{BE} \sim \cos^2(\Theta)$ law of eq. (30) as indicated by the solid lines (Shinpaugh et al., 1993).

energy loss. This is a clear hint that additional liberation of SE in backward direction may occur, if δ–electrons are scattered towards backward direction due to a few large angle scattering events, as discussed in III.b in connection with the finding of much too large slow electron diffusion lengths λ_S at 13.6 MeV/u. The double peak structure is smeared out with further increasing target thickness. The target thickness evolution shown in

fig. 19 is an example for the major advantage of thin foil experiments: the evolution from single collisions (PI only) to multiple collisions (including electron transport) is accessible.

In this context, it is elucidating to compare fig. 19 to fig. 20, which shows electron spectra from proton (1 MeV) impact on a hydrocarbon gas target (CH_4) and on a thin carbon foil (Toburen, 1990). With the gas target, a similar BEE peak angular dependence as shown in figs. 17 and 19 with fast heavy ions and very thin (1-10 $\mu g/cm^{2)}$ carbon foils is observed. With the foil target, however, the electron distribution extends to much higher energies at large angle (Θ = 50 and 125 deg.), because of wide-angle scattering of BEE created near 0 deg. This is remarkably similar to what is observed for thick targets in fig. 19. The cross sections for solid targets (estimated to be accurate within a factor of 2) seem to be lower at low electron energies. This can be understood if the attenuation and absorption of low energy electrons due to transport and surface transmission are taken into account. Note the different shape of the Auger lines: with solids, due to the contribution of deeper layers, one observes a long low energy tail (see also Burkhard et al., 1987a).

Finally, we mention that, recently, high energy "knock-on" electrons (E = 0.6-12 MeV) from direct collisions of 6.4 TeV sulphur ions (200 GeV/u) with target electrons in polypropylene targets have been studied by Vane et al. (1993) at CERN in Geneva. The experimental energy- and angular distributions agree with calculations of two body Coulomb scattering using relativistic Born approximation, except at E < 1 MeV, were electron emission is more forward-peaked than expected.

c. Dynamic Screening of the Projectile Charge

Differences between the solid- and gas target collisions arise also from *dynamic screening* effects (Echenique, Flores and Ritchie, 1990). One has to consider

(1.) the screening of the projectile charge by projectile electrons. As becomes clear from the above discussion concerning CE, this is a dynamic process including charge exchange and excitation of the projectiles leading to excited state population inside the solid (Burgdörfer 1991b, Betz et al., 1988). Also,

(2.) the target electrons and in particular, the gas of quasi free electrons in metals contribute to the dynamic screening of the projectile. This later phenomenon is often called the "*wake*" of a charged particle (Bohr 1948, Echenique, Brandt and Ritchie 1979). It includes plasmon excitation.

It should be pointed out that such screening effects of types (1.) and (2.) are closely related to the "*effective charge*" concept for heavy ion energy loss, and that in principle all of the above-mentioned processes together form the charge and excitation state of the ion in matter and determine the "*dynamic response*" of the target medium to the perturbation by the moving ion.

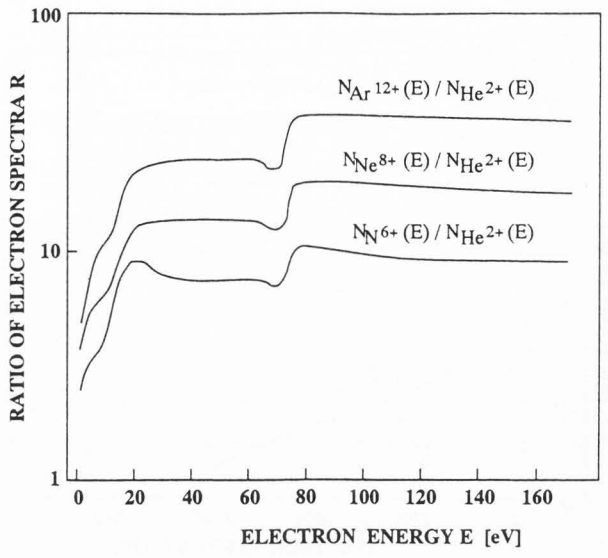

Fig. 22: Ratio of electron spectra induced by N^{6+}, Ne^{8+} and Ar^{12+} ions (E_P = 1.1 MeV/u) to the spectrum obtained with α-particles of the same velocity. The charge states of the ions are close to the equilibrium charge in the Al target. Taken from the work of Koyama et al. (1986, 1988a, 1988b).

Such screening effects have been invoked in order to explain the *suppression of low energy electron emission* both in heavy ion- solid and ion-atom collisions (as shown in figs. 22 and 23). In these figures, electron spectra obtained by Koyama et al. (1988) and Toburen (1990) from heavy ion and light ion impact are compared. Fig.22 shows the ratio of electron spectra induced by N^{6+}, Ne^{8+} and Ar^{12+} ions (E_P = 1.1 MeV/u) to the spectrum obtained with α-particles of the same velocity. The charge states of the ions are close to the equilibrium charge in the Al target used by Koyama et al. (1986, 1988a, 1988b). Similar plots have been given for carbon foil targets by Pferdekämper and Clerc (1975, 1977), and similar results were also obtained by Folkmann et al. (1975). One observes three regions: (1.) at high energies, E>80 eV, the intensities scale as the squares of the bare ionic charges, $N(E) \sim Z_P^2$. (2) Between 20 and 60 eV, the intensities scale as the corresponding electronic stopping powers, $N(E) \sim q^2_{ZBL}$. (3) Below 20 eV, a pronounced decrease (suppression) of low energy electrons is observed. It was explained by dynamic screening of the projectile charge by target electrons in soft (distant) collisions (Koyama et al., 1988a).

It is worth noting that similar observations have been made with molecular- and cluster ions (see, e.g., Hasselkamp, 1991, Rothard et al., 1993a,b, and also Rothard, 1994). They have been explained in terms of screening of the projectile charge by projectile electrons and collective (interference) effects on the projectile energy loss.

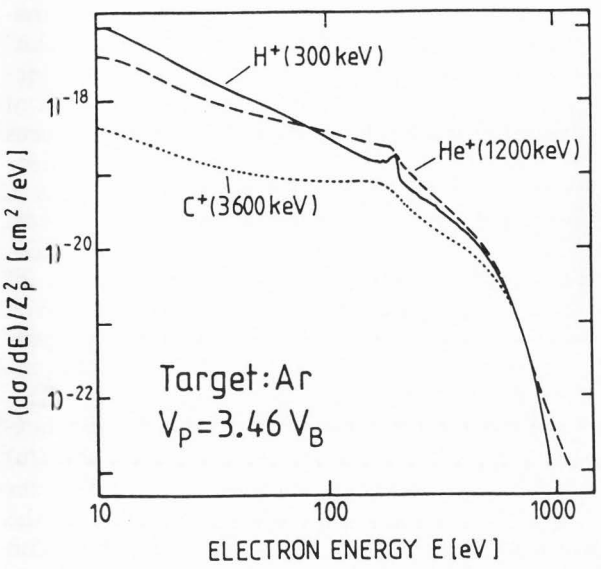

Fig. 23: Angle-integrated electron spectra $d\sigma(E)/dE$ for H^+, He^+ and C^+ collisions with Ar (10 eV $\leq E_e \leq$ 1000 eV) taken at the same ion velocity for the three ions (v_P = 3.5 v_0, E_P = 300 keV/u). The cross sections have been divided by the square of the projectile nuclear charge, Z^2_P (from Toburen, 1990).

Quite similar results are observed in ion-atom collisions, and in this case they cannot be attributed to solid-state dynamic screening. As an example, in fig.23, we show angle-integrated electron spectra $d\sigma(E)/dE$ for H^+, He^+ and C^+ colliding with Ar (10 eV $\leq E \leq$ 1000 eV) taken at the same ion velocity for the three ions (v_P = 3.5 v_0, E_P= 300 keV/u). The cross sections have been divided by the square of the projectile nuclear charge, Z_P^2. At high energies (E > 200 eV), for electrons resulting from collisions with small impact parameter, the primary spectrum is quite similar, and the absolute magnitude scales, as the energy loss of bare high-velocity ions would, with Z_P^2. At low electron energies and thus larger impact parameters, the Z_P^2 scaled spectra differ significantly and the cross sections depend on the projectile,

$$\frac{d\sigma(H^+)/dE}{1} > \frac{d\sigma(He^+)/dE}{4} > \frac{d\sigma(C^+)/dE}{36} \qquad (31)$$

In other words, the ratios of He^+ and C^+ spectra and proton spectra decrease with decreasing electron energy. Thus, they show the same behaviour as the ratios shown in fig. 22 obtained with solid Al.

In the ion-atom collision case, however, the depression of low energy electron emission has been explained by a screening of the projectile charge by the projectile electrons (Toburen 1990). This, and the screening of the projectile charge by target electrons in metals mentioned above (Koyama et al., 1988a, 1988b) are probably the most important mechanisms responsible for the effect. Note that concerning the screening by projectile electrons even projectile shell effects have been observed in electron emission by Koschar et al. (1989).

A variety of different mechanisms has been discussed in order to explain low energy electron reduction effects, but it is still unclear in which magnitude each of them contributes. We mention the quite related concepts of *changes of the surface barrier* height caused by a charging up near the ion track (Koyama et al., 1982a,b), *electron trapping in the wake* of the ions due to an attractive track potential (Borovsky and Susczynski, 1991b) and *interaction* of the ion's *wake* with the *surface potential* (Frischkorn and Groeneveld, 1983). Also, the depression of the ionization probability due to a high density of electron-hole pairs which then no longer remain uncorrelated has been invoked by Koyama et al. (1982a), as well as energy deposition by non-ionizing excitation of target atoms (Rothard, Schou and Groeneveld, 1992).

The collective response of the nearly free electron gas manifests also *directly* in electron emission:

(1.) As can be seen from fig.2, the energy of a *plasmon* can be transferred to a single electron. If the plasmon energy exceeds the workfunction ϕ, such electrons can be observed at an energy of $E < \hbar\omega_p - \phi$ in the electron spectra. The maximum energy which can be transferred to an electron inside the solid is $\hbar\omega_p$, and since there is a band of energies extending from this value to $\hbar\omega_p - E_B$ (with the valence band width E_B), the plasmon peak may even extend to zero kinetic energy in vacuum. The decay of plasmons from ion impact on Al, Mg, Si, Ti, Ni and Au (Hippler 1988, Hasselkamp 1988, 1991) and on C, Al and Cu foils (Burkhard, Rothard and Groeneveld, 1988) has been observed.

(2.) Peaks appearing at certain observation angles in electron angular distributions $N(\Theta)$ have been attributed to the directed emission of *shock electrons* perpendicular to the cone of the ion induced wake in the electron plasma of the solid. This phenomenon has been predicted by Schäfer et al. (1978, 1980) and Brice and Sigmund (1980). Experimental studies have been performed by Frischkorn et al. (1980, 1981), Burkhard et al. (1987b) and Rothard et al. (1989,1990b). Fig. 24a shows low energy spectra at different observation angles obtained by Frischkorn et al. (1981) with C (20 MeV) traversing carbon foil targets which were tilted with respect to the beam axis (δ = 45 deg.). The continuous "true secondary electron" background has been subtracted. At about 2-3 eV a peak appears at angles around a mean emission angle Θ_{em}.

In fig. 24b, this experimentally observed mean emission angle is plotted as a function of the projectile velocity v_P. The theoretical prediction (solid curve) that the mean emission angle of shock electrons should follow the Mach-relation

$$\Theta_{em} = \arccos (v_S / v_P) \qquad (32)$$

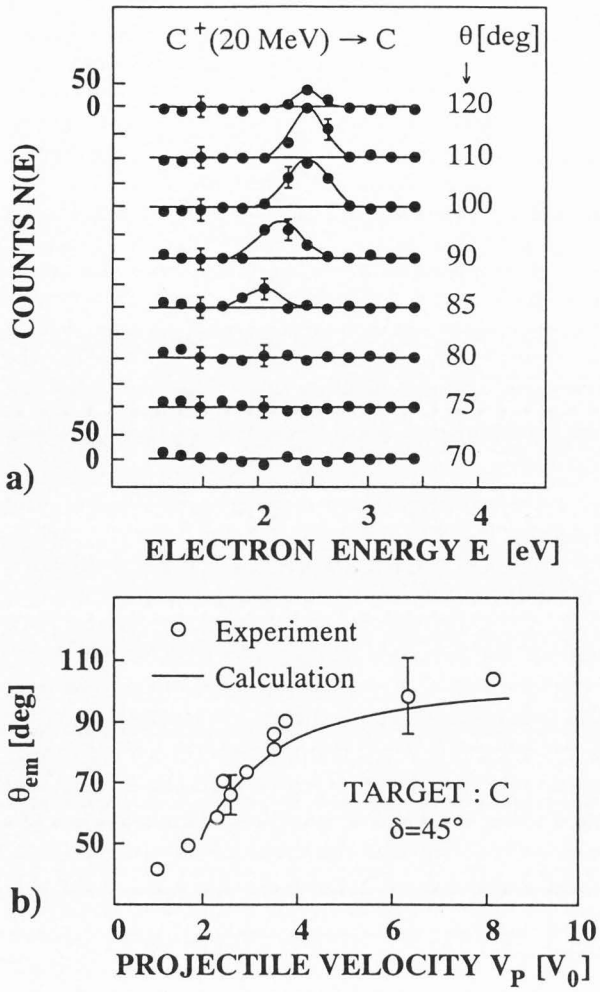

Fig. 24: a.) Low energy electron spectra after subtraction of the continuous "true secondary electron" background at different observation angles (Θ = 70-120 deg.) obtained with C (20 MeV) traversing C foil targets which were tilted with respect to the beam axis (δ = 45 deg., from Frischkorn et al., 1991). At about E = 2-3 eV a peak appears at angles around a mean emission angle Θ_{em}. These additional electrons have been attributed to the directed emission of *shock electrons* perpendicular to the cone of the ion induced wake in the electron plasma of the solid **b.)** Experimentally observed mean emission angle Θ_{em} as a function of the projectile velocity v_P. The theoretical prediction (solid curve, Mach-relation eq. 32) takes the refraction of low energy electrons at the solid surface into account (Rothard et al., 1989, 1990b).

---

reproduces the observed angular dependence if the refraction of low energy electrons at the solid surface is taken into account (Rothard et al., 1989, 1990b). v_S denotes the shock wave group velocity, mostly depending on the plasma frequency and thus the density of the free electron gas of the solid.

(3.) Both theoretical studies (Burgdörfer, Wang, Müller 1989) and experimental investigations (Yamazaki et al. 1990) show evidence for an additional "wake" related mechanism for electron emission: forward electron spectra (Θ = 0 deg.) induced by the penetration of antiprotons through thin carbon foils show structures which can be attributed to the emission of *wake riding electrons*. Such electrons originate from bound states in the wake potential of the antiproton and can be observed as bumps at electron velocities slightly below the projectile velocity (Yamazaki, 1991). In contrast to the case of positively charged particles, there is no convoy electron peak at $v_e \approx v_P$, and the "*anticusp*" caused by the repulsive interaction between the negatively charged antiproton and the electrons is filled up by scattered electrons.

(4.) Unexpected *correlation of forward- and backward electron emission* in collisions of Ar (1.8 MeV/u) with foils of $\approx$ 2-10 $\mu g/cm^2$ thickness, i.e. over distances of about 500 Å, has been observed by measuring the electron emission statistics (Yamazaki et al., 1993). With the help of a Monte Carlo simulation, this has been explained by cascade ionization including in particular plasmon decay taking place all over the target thickness.

Although all of the above-mentioned experiments have been performed at velocities below $\approx$ 2 MeV/u ($\approx$ 10 v_0), it can be expected that wake effects should also play a role for $\approx$ 10 MeV/u heavy ions. Indeed, experimental evidence for wake-effects on the population of excited capture states has been found with heavy ions of energies as high as 33 MeV/u by Rozet et al. (1987).

d. Projectile Excitation and Ionization

The dependence of the electron emission cross section on electron energy and emission angle, and also the evolution with target thickness have been calculated within different theoretical approaches, as mentioned above: The analytical model of Schiwietz et al. (1990) allows from a comparison of calculated projectile ionisation and experimental spectra to determine the population of excited projectile states ($n \geq 2$) and the ground state (n = 1) inside the solid. Details can be found in the publication by Schiwietz (1990). The Rydberg state population P_n can be treated as a free parameter thus allowing a fit of the theoretical curves to the experimental data. With Ne ions at 5 MeV/u or less, about 30% of all bound projectile electrons were found to be in excited states, whereas at the highest energies investigated (8.5 MeV/u), this number dropped to a few percent (Schiwietz, 1990). The density of Rydberg state population with the 8 MeV/u U ions was found to be $P_n \approx 50/n^3$ by Schneider, Schiwietz and DeWitt (1993). Projectile ionisation, as can be seen from fig.7, is in particular important around v_P at 0 deg. (the CE peak).

With heavy ions (or molecular ions) bringing electrons with them in the collision, enhanced electron emission in backward direction can be observed from collisional loss of projectile electrons. These electrons, observed at $v_e \approx -v_P$ in the laboratory frame, correspond to binary encounter electrons from the target in forward

direction observed at $\mathbf{v}_e \approx -\mathbf{v}_T$ in the projectile frame, with $\mathbf{v}_T = -\mathbf{v}_P$ being the target velocity in the projectile frame $\mathbf{v}_P = \mathbf{0}$. In other words, imagine the target approaching the electron-carrying projectile and undergoing a binary collision with a projectile electron. Experimentally, the electron loss distribution with a maximum at an electron energy E_L can be deduced by subtracting the ionization electron background approximated from bare ion impact. Experimental studies by Koyama et al. (1987), Rothard et al. (1990b) and Tobisch et al. (1994) have shown that both E_L and the FWHM of the loss electron distribution show a significant target material (Z_T) dependence. E_L is always smaller than the energy expected for a totally elastic reflection, $E_{eq} = m_e v_P^2/2$.

The target material dependence of E_L can be explained within a simple model introduced by Koyama et al. (1987). The projectile electrons are lost within a certain mean depth λ_L inside the solid. They suffer energy loss (dE/dx) during their transport to the surface. If as a first approach the energy loss per unit path length is considered to be constant, the maximum E_L of the loss electron distribution can be calculated by

$$E_L = E_{eq} - \lambda_L (dE/dx) \qquad (33)$$

in good agreement with experiments (Koyama et al. 1987, Rothard et al. 1990b, Rothard, Groeneveld and Kemmler, 1991, Tobisch et al., 1994). Finally, we mention that interference structures due to the *Ramsauer-Townsend effect* in electron-atom scattering similar to the ones observed for BE electrons (fig. 21) have also been observed for backward loss electron emission by Kuzel et al. (1993), see also Egelhoff (1993).

V. Non-Conducting and non-Random Targets

Hasselkamp (1991) points out that "*investigations of non-metal targets under controlled experimental conditions are rare*". A reason for this is that, in particular with good insulators, *charging up* of the target (Cazaux, 1993, Burkhard et al. 1987c) and *secondary ion emission* (LeBeyec, Della-Negra and Thomas, 1989) render experiments difficult. The only high energy experiments have been performed by Borovsky, McComas and Barraclough (1988), Borovsky and Barraclough (1989), and Borovsky and Suszcynsky (1991a) with aluminium oxide Al_2O_3 (but under standard vacuum conditions). For further information on electron emission from insulators and semiconductors, we refer the reader to the papers by Hasselkamp (1991) and Schou (1993).

Studies on electron creation by fast heavy particles in semiconductors are in particular interesting in the context of single event upset phenomena in electronic devices in spacecraft (see, e.g., McGarrah, Williamson and Keeton, 1992, Akkerman et al. 1993b). However, except for the channelling experiments described below, to the knowledge of the author, there are no systematic studies with swift heavy ions (see also Hasselkamp, 1991). Therefore, in the following we present selected important result concerning the direct measurement of the ion induced track potential and high energy channelling experiments.

a. Insulators

In the preceding chapters, we have been dealing with polycrystalline, conducting (metallic) solids. There is one exception: in sect. I.d., we discussed the influence of layers of adsorbates (hydrocarbons, H_2O, CO_2, N_2, oxides, ...) on electron spectra and yields. Such layers can be regarded as insulators, and we are dealing with a two layer system and a metal/insulator interface. From the arguments (1-4) given in II.d as explanation for low energy electron yield dependence on surface coverage, we can learn about the differences in EE from metals and insulators. As a main result, electron yields from insulators are higher than those obtained with metals of comparable atomic number, but the velocity dependence is similar to the case of metal targets, i.e. electron yields roughly follow the velocity dependence of the stopping power. The position of the SE peak is found at very low energies $E \approx 1$ eV. The arguments (1) and (2) given in I.d, i.e. reduced workfunction and enhanced electron escape depth (steps 2 and 3 in the three step model of EE) may explain these findings. However, it should be noted that they may not apply generally, and that other mechanisms, as discussed by Baragiola (1993b), may have to be considered. Production (step 1) is smaller, because in order to ionize, the binding energy (or the band gap E_g) has to be overcome, in contrast to metals with quasi free electrons. Indeed, for alkali halides, electron yields are roughly related to E_g as

$$\gamma \sim 1 / E_g \qquad (34)$$

(see Hasselkamp, 1991 and König et al., 1975). A more thorough discussion on EE from insulators has been given by Schou (1993), see also the papers by Akkerman et al. (1993b) and Grosjean and Baragiola (1993).

A remarkable result is the observation of an energy shift of Carbon KLL Auger electrons to low energies emitted from polypropylene (PP) foils with respect to Auger emission from carbon foils, which can be attributed to the influence of the heavy ion nuclear track potential (Schiwietz et al. 1992, Schiwietz 1993). Fig. 25 shows electron spectra taken at $\Theta = 120$ deg. from C and PP foils bombarded with 5 MeV/u Ne^{9+} ions. One can see the carbon KLL Auger peak, wich appears at $E \approx 250$ eV for the C-target, at about $E \approx 230$ eV for PP foils after having been bombarded with a fluence of $D \approx 10^{15}$ ions/cm^2, and at $E \approx 180$ eV with lower fluence of $D < 4 \times 10^{13}$ ions/cm^2. Great care was taken in the experiments to prevent charging up or heating up of the samples. They were coated by a thin aluminium layer on one side of the foil, the spectra were taken from the other side. It was checked that the spectra did not depend

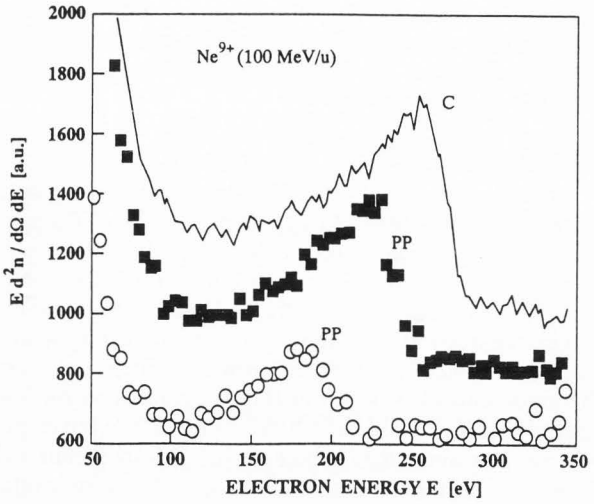

Fig. 25: Electron spectra taken at Θ = 120 deg. from carbon (C) and polypropylene (PP) foils bombarded with 5 MeV/u Ne^{9+} ions. On can see the carbon KLL Auger peak, wich appears at E ≈ 250 eV for the C-target, at about for E ≈ 230 eV for PP foils after having been bombarded with a fluence of D ≈ 10^{15} ions/cm^2, and at E ≈ 180 eV with low fluence of D < $4x10^{13}$ ions/cm^2. This energy shift of C_{KLL} Auger electrons can be attributed to the influence of the heavy ion nuclear track potential (from Schiwietz et al. 1992, Schiwietz 1993).

on the ion beam current. Charging up can clearly be observed by this method (Burkhard et al., 1987c). Chemical changes (*carbonization*) rapidly occurs under ion bombardment, as can also be seen from fig. 25: with increasing ion fluence, the Auger peak from PP shifts towards the energy of the carbon foil peak. Schiwietz et al. (1992) conclude that this is caused by a transition from an insulator to a conductor (PP → C). Using a Monte Carlo procedure, Schiwietz et al. (1992) show further that the largest contribution (about 50 eV) of the shift of about 70 eV observed must be due to the ion induced track potential. They also found that about 85% of all Auger electrons are created within the ion track. Taking into account the range of the track potential of ≈ 20 Å, the average electric field strength is estimated to ≈ 5 V/Å inside the solid. The remaining shift is attributed to the fact that recombination is strongly reduced in insulators, whereas in conductors Auger decay can occur after recombination leading to different initial states.

As discussed in chaps. II and III, electron yield measurement could yield an indirect information on the track potential if analyzed within the model proposed by Borovsky and Susczynski (1991b). The data shown in fig. 25 present a direct measure of ion induced track potential. In this context, it should be noted that Akkerman et al (1993a) applied the Borovsky and Suszynski (1991b) model in order to explain deviations of charge collected in Si based devices from predictions using a simple Linear Energy Transfer (LET) concept. As mentioned by these authors, electron yield measurements or Auger spectroscopy with Si targets could be relevant for the verification of this model. Also, using Si or amorphous SiO_2 or similar targets would exclude uncertainties due to chemical changes of the target.

b. Single Crystals: Channelling

While the dependence of electron production on the *projectile-target electron* collision impact parameter is included in the semi-empirical theory (by the rough distinction between soft- and close collisions (see eqs. 11-13), channelling studies yield the interesting possibility to study the dependence of target ionization on the *projectile- target nucleus* collision impact parameter distribution. Under channelling conditions, when the ion trajectory is confined within a channel (or a plane) of a crystal lattice, collisions with small impact parameter are largely suppressed. This means that the ions encounter mostly outer shell electrons ("*nearly free electron target*") when channelled. Thus, by comparing electron emission under random impact and channelling conditions, one cannot only study the dependence of electron production on the electron density encountered by the projectile, but also distinguish ionization of inner- and outer shells of the target atoms.

This is demonstrated in fig.26, which shows forward (Θ = 0 deg.) electron spectra obtained with Xe^{37+} (27 MeV/u, v_P = 33 a.u.) incident on a silicon crystal (d = 21 μm) in random orientation and <110> axial alignment (as indicated) at GANIL/Caen by Andriamonje et al. (1991) and Quéré et al. (1991). The most striking difference is the strong reduction of *convoy electron* emission for channelled ions: the convoy electron yield Y_{CE} is reduced by a factor of 13! This result is related to the suppression of convoy electron production either by capture of target electrons to the continuum (ECC) or loss of projectile electrons to low-lying projectile continuum states (ELC). In particu-lar, electron loss is largely suppressed (incoming charge state: q = 37, most probable final charge state: q_f^r = 50 for random incidence and q_f^c = 44 under channelling conditions).

The *binary encounter electron* yield (around 2 v_P = 66 a.u.) is reduced by a factor of 3.2, because it is directly proportional to the electron density encountered by the projectile which is strongly reduced if the projectile trajectories remain confined within at crystal channel. A closer inspection of the high-energy side of the binary electron peak, E > E_{BE} as given by eq.(30) (inset of fig.26) shows that the momentum distribution of these electrons is much smaller when channelled, because the contribution of Si K-shell electrons to the *Compton-profile* is suppressed (Bell and Böckl, 1984). In random incidence, the broad initial momentum distribution of these strongly bound inner-shell electrons leads to wings at the high- (and low-) energy side of the binary peak.

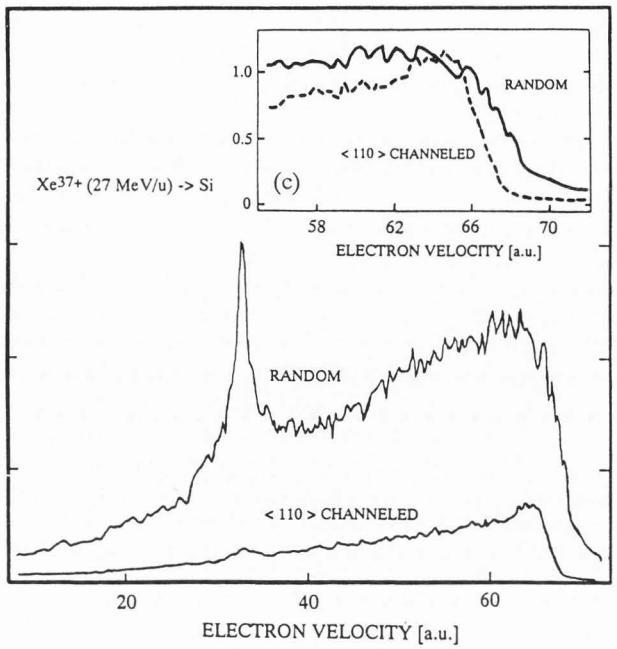

Fig. 26: Forward (θ = deg.) electron spectra obtained with Xe^{37+} (27 MeV/u, v_P = 33 a.u.) incident on a silicon crystal (d = 21 μm) in random orientation and <110> axial alignement at GANIL by Andriamonje et al. (1991) and Quéré et al. (1991). **Inset:** Enlargement of the high-energy side of the binary encounter electron peak, normalized to the same maximum peak height.

Similar results have been obtained by Kudo et al. (1991a,b), who studied electron emission from thick Si and GaAs single crystals bombarded with MeV/u ions. An example of their work is shown in fig. 27, which shows spectra obtained with 3.5 MeV/u bare O ions impinging on Si and GaAs single crystals under random- and <100> channelling conditions. In contrast to the results shown in fig.27, these spectra have been obtained in *backward* direction, the experimental set-up is shown in fig.3c. Also in this case, a strong reduction of electron emission beyond E_{BE} is observed. As a further result, Kudo et al. (1991a,b) obtained the effective ion charges as a function of the projectile atomic number Z_P and various channelling conditions. Similar studies have also been performed with MeV light H or He ions by Schneider, Kudo and Kanter (1985) and Hasegawa et al. (1991).

The dependence of electron emission on the projectile's minimum distance of approach to the target atoms $b_{min}(\varphi)$ can be studied by varying the angle of incidence φ from random incidence to channelling conditions ($\varphi < \varphi_{crit}$). The ion trajectories remain confined in a region outside the minimum impact parameter $b_{min}(\varphi)$.

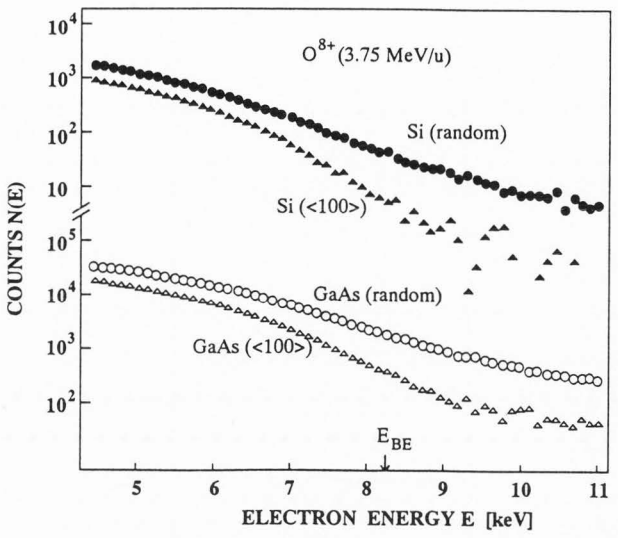

Fig. 27: Electron spectra obtained by Kudo et al. (1991a, 1991b) with 3.5 MeV/u bare O ions impinging on Si and GaAs single crystals under random- and <100> channelling conditions. In contrast to the results shown in fig. 26, these spectra have been obtained in *backward* direction (the experimental set-up is shown in fig. 3c).

The angle φ corresponds to the tilt angle δ of fig. 3, but with the crystal orientation taken into account. As an example, fig. 28 shows the dependence of convoy electron yields $Y_{CE}(\varphi)/Y_{CE}(\text{random})$ from protons (E_P = 0.17-1.9 MeV) on the angle of incidence φ as measured by Koschar et al. (1992). The angle φ is measured in units of Lindhards critical angle of channelling (for protons and gold, $\varphi_{crit} = 0.59 / \sqrt{E_P[\text{MeV}]}$) with respect to the (111) plane of an Au single crystal (d = 1200Å). One observes a strong dependence of convoy electron yields on the crystal orientation. The effect is not so strong as in the case of *axial* channelling discussed above, because here we are dealing with *planar* channelling.

$Y_{CE}(\varphi)/Y_{CE}(\text{random})$ decreases with increasing velocity and follows the velocity dependence of the emerging neutral charge state fraction $F_0(H)$. This may be a hint that in this case convoy electrons are produced by indirect electron loss to the continuum (IELC), i.e. electron capture from the target with subsequent ELC (Koschar et al., 1987, 1992).

VI. Conclusion: Open Questions

As the preceding chapters show, important steps towards an understanding of ionization and electron emission in high velocity heavy ion- (condensed) matter collisions have been made. However, this is a new field and more questions remain than answers have been given. In the following, we give an incomplete (and very personal) list of open questions and possible future investigations.

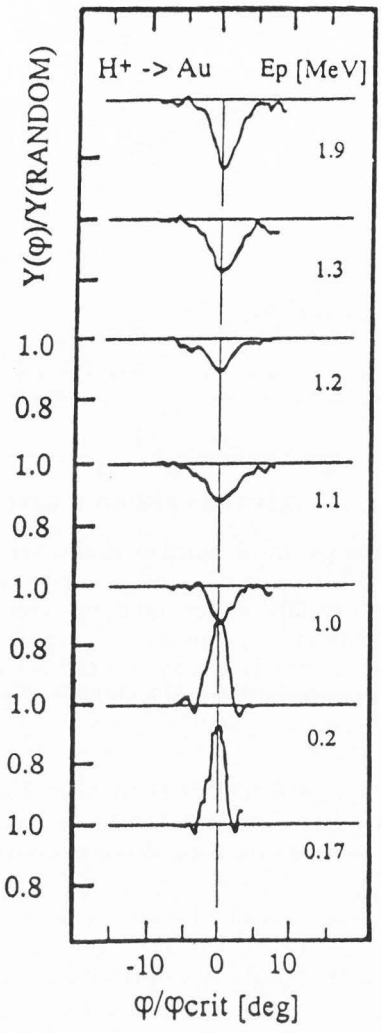

Fig. 28: Dependence of convoy electron yields (induced by protons, E_P = 0.17-1.9 MeV) Y(φ)/Y(random) on the angle of incidence φ with respect to the (111) plane of an Au single crystal (d = 1200Å) as measured by Koschar et al. (1992). φ is measured in units of Lindhards critical angle of channelling $\varphi_{crit} = 0.59 / \sqrt{E_P[MeV]}$.

(1.) Baragiola et al. (1992, 1993) found exponentially decreasing high energy tails in electron spectra induced by low energy (1-6 keV He and Ar) ion bombardment of metals. This low-level tail extended up to several keV and thus corresponds to electrons which are much faster than it can be expected from binary collisions only, even if the initial electron momentum distribution, the Compton profile (Bell and Böckl, 1984), is taken into account. Sigmund (1993) suggested that these tails could be due to electrons which are accelerated in multiple collision sequences between projectile and target atoms. This Fermi-acceleration scheme has been discussed in connection with cluster-induced fusion, too (see e.g. Burgdörfer, Wang, Ritchie, 1991 and Hautala, Pan, Sigmund, 1991). It should be possible to detect *projectile electrons* which have first been scattered by a target atom and subsequently by the projectile as enhanced electron emission compared to bare ion impact around and below $E_{FA} = 9\ (m_e/m_P)\ E_P$ (corresponding to $v_{FA} \approx 3v_P$). Attempts have been made to detect such fast electrons from multiple collision sequences between projectile and target atoms with ≈ 0.4-0.8 MeV/u H_n^+ (n = 1-3), but without success (see Rothard, 1994 and Suarez et al., 1994). However, Suarez et al. (1994) found theoretical and experimental evidence that fast *target electron* emission at $v_{FA} \approx -2v_P$ in backward direction may be caused by multiple collision sequences.

(2.) Surprisingly, even with fast heavy (MeV/u) ions, backward electron yields are suppressed, quite similar to what was observed with molecules and clusters. Further insight into differences and similarities of collective effects observed with clusters and heavy ions will be obtained by measurements with heavier particles and by extending studies to higher energy. In particular, the recent development of high energy beams of *heavy ion clusters* (such as C_n^+ and Au_n^+) at tandem accelerators in Orsay and Erlangen opens a promising new field of investigations.

(3.) A complete understanding of EE in ion-solid collisions requires experimental data on the primary ionization (PI) process in order to allow a refinement of theoretical description. Thus, measurements of EE in ion-atom collisions are necessary, which then have to be extended to complex gas targets (molecules, clusters), and finally, to solid targets. This allows to investigate differences between single free atoms and atoms confined in condensed matter ("collective" effects) concerning PI. The concept of the collective excitation of solids manifesting as a dynamic screening, the *wake*, may play an important role also at high projectile velocities beyond 10 MeV/u (Rozet et al., 1987, Borovsky and Susczynski, 1991b). Furthermore, electron transport can be studied as a function of target foil thickness.

(4.) EE should be studied in coincidence with emerging projectile charge states as it has largely been done for convoy electron emission (Breinig et al., 1982, Kemmler et al., 1988). Furthermore, it appears interesting to measure electron spectra in coincidence with recoil ions (Wang et al. 1993, Gaither et al. 1993, Moshammer et al., 1994).

(5.) The experiments have to be extended to higher energies (say, ten to some hundred MeV/u), in particular in view of the *application of heavy ion beams for cancer treatment* (Kraft and Gademann, 1993) and concerning *track formation* and *nanotechnologies* (Angert, Armbruster and Jousset, 1993). As another practical application that has been important up to now and will also be important in the future, we mention that electron emission from foils or converter plates in connection with single particle detectors such as channeltrons and

microchannel plates (Schütze and Bernhard, 1956) are widely used for beam current measurements at heavy ion accelerators such as SIS/GSI in Darmstadt (Brohm et al., 1991, Albert et al., 1992) and GANIL in Caen (Bouffard et al., 1989).

(6.) In connection with single particle counting, it is interesting to understand the statistics of electron emission (I.b) in order to know the probability that no electron is liberated from either a converter plate or the single particle detector. A Poisson distribution for P_n, eq. (8), has widely been used as reference standard and results have been discussed in terms of deviations from Poisson distribution. Sigmund (1993) proposes to measure EE statistics with a high energy beam (100 MeV/u) and e.g. an Al target. In such a case, electron yields are very small, in the order of $\gamma = 0.01$, and most of the impinging ions do not produce an electron at all. Such an experiment could "once and for all bury the Poisson distribution as a reference standard: You need not ask why a measured distribution *deviates* from Poisson, you need to ask for the reason why a given distribution *coincides* with Poisson, if it does." (cited from Sigmund, 1993).

(7.) It is not until very recently that first attempts have been made to study electron emission from atomic collision processes with *ultra-relativistic* projectiles by Vane et al. (1993). Also, the formation of "*quasi molecules*" in fast heavy ion collisions leading to extremely *strong (supercritical) fields* and in particular, electron-positron pair creation has been discussed in connection with δ-electron emission. These problems are treated in the framework of the two-center Dirac equation (Becker et al., 1987, Kankeleit, 1980). It has been evoked that pair creation can also occur as resonant process in heavy ion channelling (Becker et al., 1987) and that emission of δ–electrons can serve as a "clock" for nuclear contact times (Senger et al., 1987). Atomic processes such as screening, formation of quasi-molecules, and δ-electron emission have to be considered in nuclear physics experiments such as the study of Mott scattering as a tool for testing long-range color Van-der-Waals forces (Villari et al. 1993). Also, the interplay between nuclear interactions and atomic physics has not yet been investigated in connection with electron emission, but e.g. for charge exchange reactions (Gonzales, Giese and Horsdal-Pedersen, 1993). Such an interplay may also occur due to coherent resonant excitation (Okorokov-effect) in channelling experiments (Andriamonje et al., 1994).

(8.) In future experiments, well defined solid surfaces are necessary and thus, elaborated surface controlling and preparation technology is indispensable. It seems in particular interesting to me to study electron emission from insulators, or to study the influence of controlled deposition of adsorbates on solid surfaces on electron emission. This has been done recently with protons by Sanchez, de Ferrariis and Suarez (1989) and Schosnig et al. (1992). As a first step, measurements of electron yields (or energy distributions) as a function of the residual gas pressure, the ion flux and fluence, and the time of exposure of a surface to a contaminant gas and thus as a function of the equilibrium between adsorption and desorption of gases (N_2, O_2, H_2O) could be envisaged (Arrale et al., 1994, see also DuBois and Drexler, 1994). Since heavy ions deposit large amounts of energy in electronic excitations in a small volume during a very short time period, interesting new effects are likely to be observed with heavy ions.

Acknowledgements

I am indebted to my collaborators of CIRIL in Caen (C. Caraby, A. Cassimi, B. Gervais, J.-P. Grandin, P. Jardin, M. Jung), IPNL in Lyon (A. Billebaud, M. Chevallier), IKF in Frankfurt am Main (K.O. Groeneveld, P. Koschar, J. Kemmler, R. Maier) and Thessaloniki (A. Clouvas) who all contributed to parts of the work presented here. It is a pleasure to thank B. Gervais, K.O. Groeneveld and M. Jung for their comments on the manuscript and important discussions. I would like to thank the referees for their helpful comments. In particular, thanks to R. Baragiola, R.H. Ritchie, M. Rösler and J. Schou for their very careful reading of the manuscript. I also acknowledge helpful discussions with G. Schiwietz. Hearty thanks to S. Lamotte, who typed large parts of the manuscript, and to F. Levesque for editing the figures. It is a pleasure to thank all those who made the experiments possible and to those who inspired this work by discussions, comments and publications. Concerning the experiments done in Caen at GANIL, I would in particular like to thank D. Lelièvre, V. Mouton and J.-M. Ramillon (CIRIL) for their technical assistance. Thanks also to GPS / PIIM (Univ. Paris VII et VI, group leader J.-P. Rozet) and in particular D. Vernhet, for their friendly support and to L. Vidal (INPL, Lyon) who prepared the high quality target foils.

References

Akkerman A, Levinson J, Ilberg D, Lifshitz Y. (1993a). Track effects and their influence on heavy ion energy losses in semiconductor devices. In: Ionization of Solids by Heavy Particles (Baragiola RA, ed.). Plenum Publishing Corporation, NATO ASI Series **B**:Vol. **306**, 431-438.

Akkerman A, Breskin A., Chechik R., Gibrekhterman A. (1993b). Secondary electron emission from akali halides induced by X-rays and electrons. In: Ionization of Solids by Heavy Particles (Baragiola RA, ed.). Plenum Publishing Corporation, NATO ASI Series **B**:Vol. **306**, 359-380.

Albert A, Kroneberger K, Heil O, Groeneveld KO, Geissel H. (1992). A heavy ion beam current monitor with a wide dynamic range. Nucl. Instrum. Meth. **A317**, 397-398.

Andriamonje S, Chevallier M, Cohen C, Dural J, Genre R, Girard Y, Groeneveld KO, Kemmler J, Kirsch R, L'Hoir A, Maier R, Poizat JC, Quéré Y, Remillieux J, Schmaus D, Toulemonde M. (1991). Charge exchange processes of high energy heavy ions channeled in crystals. In: High-Energy Ion-Atom Collisions, Proceedings of the 4th Workshop on High-Energy Ion-Atom Collision Processes held in Debrecen, Hungary, 17-19 September 1990 (Berényi D, Hock G, eds.). Springer Lecture Notes in Physics **LNP376**, 221-234.

Andriamonje S, Blank B, Chevallier M, Cohen C, Cue N, Dauvergne D, Del Moral R, Dufour JP, Dural J, Faux L, Fleury A, Kirsch R, L'Hoir A, Poizat JC, Pravikoff MS, Remillieux J, Schmaus D, Toulemonde M. (1994). Search for the observation of resonant coherent nuclear excitation of channeled isomeres. Nouvelles du GANIL **49**, 15-19.

Angert N, Armbruster P, Jousset JC. (1993). Proceedings of the Second International Symposium on Swift Heavy Ions in Matter SHIM-92. Radiation Effects and Defects in Solids **126**, 1-412.

Arnau A, Penalba M and Echenique PM, Flores F, Ritchie RH. (1990). Stopping power for helium in aluminium. Phys. Rev. Lett. **65**, 1024-1027.

Arrale AM, Zhao ZY, Kirchhoff JF, Marble DK, Weathers DL, McDaniel FD, Matteson S. (1994). Model of the contamination effect in ion-induced electron emission. Nucl. Instrum. Meth. **B89**, 437-442.

Azuma T, Yamazaki Y, Komaki K, Watanabe H, Sekiguchi M, Hasegawa T, Hattori T, Kuroki K (1993). Incident and exit charge state dependence of secondary electron emission from a carbon foil by the passage of swift oxygen and carbon ions. In: Ionization of Solids by Heavy Particles (Baragiola RA, ed.). Plenum Publishing Corporation, NATO ASI Series **B**:Vol. **306**, 239-251.

Baragiola RA, Alonso EV, Oliva A, Bonnano A, Xu F. (1992). Fast electrons from slow atomic collisions. Phys. Rev. **A45**, 5286-5288.

Baragiola RA, Alonso EV, Oliva A, Bonnano A, Xu F. (1993). Reply to "Origin of 'fast electrons' from slow atomic collisions". Phys. Rev. **A48,** 1714-1713.

Baragiola RA. (1993a). Ionization of Solids by Heavy Particles. Plenum Publishing Corporation, NATO ASI Series **B**:Vol. **306**.

Baragiola RA. (1993b). Principles and Mechanisms of Ion Induced Electron Emission. Nucl. Instrum. Meth. **B78**, 223-238.

Beck HP, Langkau R. (1975). Die Sekundärelektronen-Ausbeute verschiedener Materialien bei Beschuss mit leichten Ionen hoher Energie, Zeitschrift f. Naturforschung **30a**, 981-985.

Becker U, Grün N, Monberger K, Scheid W (1987). Atomic processes in relativistic heavy ion collisions. In: Physics of Strong Fields (Greiner W, ed.). Plenum Publishing Corporation. NATO ASI Series **B**:Vol. **153**, 609-627.

Bell F, Böckl H. (1984). Solid State Compton Prfiles by Inelastic Ion-Electron Scattering. Nucl. Instrum. Meth. **B2**, 311-315.

Benka O, Steinbauer E, Bauer P. (1994). Kinetic electron emission yield induced by H^+ and He^{2+} ions versus stopping power for Al, Cu, Ag and Au. Nucl. Instrum. Meth. **B90**, 64-66.

Betz HD, Höppler R, Schramm R, Oswald W. (1988). Charge and Excitation of Swift Heavy Ions in Solids. Nucl. Instrum. Meth. **B33** (1988) 185.

Bhalla CP, Shingal R, Grabbe S (1993). Binary encounter electrons in ion-atom collisions. Nucl. Instrum. Meth. **B79**, 170-172.

Bohr N. (1948). The penetration of atomic particles through matter, K. Dan. Vidensk. Selsk. Mat. Fys. Medd. **18** No. 8.

Borovsky JE, McComas DJ, Barraclough BL. (1988). The Secondary-Electron Yield Measured for 5-24 MeV Protons on Aluminum-Oxide and Gold Targets. Nucl. Instrum Meth. **B30**, 191-195.

Borovsky JE, Barraclough BL. (1989). High-Velocity Ionic Projectiles Interacting with Metals: Models and Measurements of Secondary-Electron Yields from Gold and Aluminum Targets struck by 13.5-31.5 MeV ^{7}Li and 9-63 MeV ^{12}C. Nucl. Instrum Meth. **B36**, 377-394.

Borovsky JE, Suszcynsky DM. (1991a). Experimental investigation of the Z^2 scaling law of fast-ion produced secondary-electron emission. Phys. Rev. **A43**, 1416-1432.

Borovsky JE, Suszcynsky DM. (1991b). Reduction of secondary-electron yields by collective electric fields within metals. Phys. Rev. **A 43**, 1433-1440.

Bouffard S, Dural J, Levesque F, Ramillion JM. (1989). Les équipements d'irradiation du CIRIL, Annales de Physique, Coll. N^{o} 2, Suppl. au N^{o} 2 Vol. **14**, 395-398.

Brice D.K., Sigmund P. (1980). Secondary electron spectra from dielectric theory. K. Dan. Vidensk. Selsk. Mat. Fys. Medd. **40** No. 8.

Breinig M, Elston SB, Huldt S, Liljeby L, Vane CR, Berry SD, Glass GA, Schauer M, Sellin IA, Alton GD, Datz S, Overbury S, Laubert R, Suter M. (1982). Experiments concerning electron capture and loss to the continuum and convoy electron production by highly ionized projectiles in the 0.7-8.5 MeV/u range traversing the rare gases, polycrystalline solids, and axial channels in gold. Phys. Rev. **A25**, 3015-3048.

Brohm T, Clerc HG, Voss B, Ziegler C, Geissel H, Kildir M, Schmidt KH, Sümmerer K, Viera DJ. (1991). Sekundärelektronen Emissions Transmissions Monitor SEETRAM, Verhandl. DPG **26** (VI) 414.

Brusilovsky BA. (1990). Kinetic Ion-Induced Electron Emission from the Surface of Random Solids, Appl. Phys. **A50**, 111-129.

Burgdörfer J. (1991a). Convoy Electrons. In: Interaction of Charged Particles with Solids and Surfaces (Gras-Marti A, Urbassek HM, Arista NR, Flores F, eds.). Plenum Publishing Cooperation, NATO ASI Series **B**:Vol. **271**, 459-486.

Burgdörfer J. (1991b). Electronic Excitations in fast Ion-Solid Collisions. In: High-Energy Ion-Atom Collisions, Proceedings of the 4th Workshop on High-Energy Ion-Atom Collision Processes held in Debrecen, Hungary, 17-19 September 1990 (Berényi D, Hock G, eds.). Springer Lecture Notes in Physics **LNP376**, 198-220.

Burgdörfer J, Gibbons J. (1990). Electron Transport in the Presence of a Coulomb Field. Phys. Rev. **A42**, 1206-1221.

Burgdörfer J, Wang J, Müller J. (1989). Forward electron production in antimatter-solid collisions. Phys. Rev. Lett. **62**, 1599-1602.

Burgdörfer J, Wang J, Ritchie RH. (1991). Estimates for cluster-impact fusion yields using the Fermi acceleration map. Phys. Scr. **44**, 391-394.

Burkhard M, Koschar P, Heil O, Kemmler J, Kövér A, Szabo G, Berényi D, Groeneveld KO. (1987a). Molecular effects observed in Auger transitions form H^+ and H_2^+ collisions with solid, molecular and atomic targets. Nucl. Instrum. Meth. **B24/25**, 189-192.

Burkhard M, Rothard H, Biedermann C, Kemmler J, Kroneberger K, Koschar P, Heil O, Groeneveld KO. (1987b). Heavy-Ion-Induced Shock Electrons from Sputter-Cleaned Solid Surfaces. Phys. Rev. Lett. **58**, 1773-1775.

Burkhard M, Rothard H, Biedermann C, Kemmler J, Koschar P, Groeneveld KO. (1987c). Strong convoy electron yield dependence on surface properties. Nucl. Instrum. Meth. **B24/25**, 143-146.

Burkhard M, Rothard H, Groeneveld KO. (1988a). Single-Electron Deexcitation of Volume Plasmons Induced by Heavy Ions in Thin Solid Foils. Phys. Stat. Sol. (**b**) **147**, 589-592.

Burkhard M, Rothard H, Kemmler J, Kroneberger K, Groeneveld KO. (1988b). Surface characterisation of thin solid foil targets by ion impact. J. Phys. **D**: Appl. Phys. **21**, 472-477.

Cailler M, Ganachaud JP. (1990). Secondary electron emission from solids II. Theoretical descriptions, Scanning Microsc. Supplm. **4**, 81-110.

Cazaux J. (1993). Some physical descriptions of the charging effects in insulators under irradiation. In: Ionization of Solids by Heavy Particles (Baragiola RA, ed.). Plenum Publishing Corporation, NATO ASI Series **B**:Vol. **306**, 325-350.

Clerc HG, Gehrhardt HJ, Richter L, Schmidt KH. (1973). Heavy-Ion Induced Secondary Electron Emission - A possible Method for Z-Identification. Nucl. Instrum. Meth. **113**, 325-331.

Clouvas A, Rothard H, Burkhard M, Kroneberger K, Biedermann C, Kemmler J, Groeneveld KO, Kirsch R, Misaelides P, Katsanos A. (1989). Secondary electron emission from thin foils under fast-ion bombardment. Phys. Rev. **B39**, 6316-6320.

Clouvas A, Katsanos A, Farizon-Mazuy B, Farizon A, Gaillard MJ. (1991). Heavy-ion-induced electron emission from thin carbon foils. Phys. Rev. **B43**, 2496-2500.

Clouvas A, Katsanos A, Farizon-Mazuy B, Farizon A, Gaillard MJ. (1993). Projectile Dependence of ion-induced electron emission from thin carbon foils. Phys. Rev. **B48**, 6832-6838.

Devooght J, Dubus A, Dehaes JC. (1987a). Improved age-diffusion model for low-energy electron transport in solids I. Theory. Phys. Rev. **B36**, 5093-5109.

Devooght J, Dubus A, Dehaes JC. (1987b) Improved age-diffusion model for low-energy electron transport in solids II. Application to secondary emission from aluminium. Phys. Rev. **B36**, 5110-5119.

Devooght J, Dehaes JC, Dubus A, Cailler M, Ganachaud JP. (1991). Theoretical Description of Secondary Electron Emission induced by Electron or Ion Beams impinging on Solids. In: Particle Induced Electron Emission I (Höhler G, Niekisch EA, eds.). Springer Tracts in Modern Physics **122**, 67-128.

DuBois RD, Drexler CG. (1994). Electron Emission from Fast Ion Impact on Thin Metal Foils: Implications of these Data for Development of Track Structure Models. In: Computational Approaches in Molecular Radiation Biology (Varma MN, Chatterjee A, eds.). Plenum Press New York, 49-63.

Dubus A, Dehaes JC, Ganachaud JP, Hafni A, Cailler M. (1993). Monte Carlo evaluation of the interaction cross sections on the secondary electron emission yields from polycrystalline aluminum targets. Phys. Rev. **B47**, 11056-11073.

Echenique PM, Ritchie RH, Brandt W. (1979). Spatial excitation patterns induced by swift ions in condensed matter. Phys. Rev. **B20**, 2567-2580.

Echenique PM, Flores F, Ritchie RH. (1990). Dynamic screening of ions in condensed matter, Solid State Phys. **43,** 229-308.

Egelhoff WF Jr. (1993). Semiclassical explanation of the generalized Ramsauer Townsend minima in electron-atom scattering. Phys. Rev. Lett. **71**, 2883-2886.

Fainstein PD, Ponce VH, Rivarola RD. (1988). A theoretical model for ionisation in ion-atom collisions. Application for the impact of multicharged projectiles on helium. J. Phys. **B**: At. Mol. Opt. Phys. **21**, 287-299.

Folkmann F, Groeneveld KO, Mann R, Nolte G, Schumann S, Spohr R. (1975). Continuous Electron Energy Spectra Ejected from Solid Carbon Targets Bombarded with Light and Heavy Ions, Z. Phys. **A275**, 229-233.

Frischkorn H, Groeneveld KO, Schumann S, Latz R, Reichhardt G, Schader J, Kronast W, Mann R. (1980). Possible evidence for heavy-ion induced collective electron emission from solids. Phys. Lett. **76A**, 155-156.

Frischkorn H, Groeneveld KO, Schumann S, Schader J, Astner G, Hultberg S, Lundin L, Ramanujam R, Didriksson R, Hakansson P, Sundquist B, Mann R. (1981). In search of collective electron emission from heavy ion solid collisions. In: Inner shell and X-Ray Physics of ions and atoms (Fabian DJ, Kleinpoppen H, Watsun LM, eds.). Plenum Publishing Corporation, 193-196.

Frischkorn H, Groeneveld KO. (1983). Heavy ion induced electron emission from solid surfaces. Phys. Scr. **T6**, 89-93.

Füchtbauer C. (1906). Über eine von Kanalstrahlen erzeugte Sekundär-Strahlung und über eine Reflexion der Kanalstrahlen. Physikalische Zeitschrift Vol. **7** No. 5, 153-157.

Füchtbauer C. (1906). Über die Geschwindigkeit der von Kanalstrahlen und von Kathodenstrahlen beim Auftreffen auf Metalle erzeugten negativen Strahlen. Physikalische Zeitschrift Vol. **7** No. 21, 748-750.

Füchtbauer C. (1907). Über Sekundärstrahlung. Ann. d. Physik **23**, 301-307.

Ganachaud JP, Cailler M. (1979a). A Monte-Carlo Calculation of the Secondary Electron Emission of Normal Metals I: The Model. Surf. Science **83**, 498-518.

Ganachaud JP, Cailler M. (1979b). A Monte-Carlo Calculation of the Secondary Electron Emission of Normal Metals II: Results for Aluminium. Surf. Science **83**, 419-530.

Gaither CC III, Breinig M, Berryman JW, Hasson BF, Richards JD, Price K. (1993). Coincident detection of electrons ejected at large angles and target recoil ions produced in multiply ionizing collisions for the 1-MeV/u O^{q+} + Ar collision system. Phys. Rev. **A47**, 3878-3887.

Gerasimov SA.(1993). Electron emission from multielectron atoms in impulse and semiclassical approximation. Phys. Scr. **47**, 182-185.

Gervais B, Bouffard S. (1994). Simulation of the primary stage of the interaction of swift heavy ions with condensed matter. Nucl. Instrum. Meth. **B88** (1994) 355-364.

Gibbons J, Elston SB, Kimura K, DeSerio R, Sellin IA, Burgdörfer J, Grandin JP, Cassimi A, Husson X, Liljeby L, Druetta M. (1991). Observation of rapid evolution of convoy electron angular distributions. Phys. Rev. Lett. **67**, 481-484.

Gonzales AD, Giese JP, Horsdal-Pedersen E. (1993). Atomic-Electron capture in the presence of a narrow nuclear resonance: $^{40}Ar(p,p)^{40}Ar$ reaction. Phys. Rev. **A48**, 3663-3669.

Groeneveld KO. (1988). Nuclear track formation related electron production and transport from ion penetration through solids. Nucl. Tracks. Radiat. Meas. **15,** 51-60.

Groeneveld KO. (1991). Electronic energy deposition mechanisms. Nucl. Tracks. Radiat. Meas. **19**, 79-84.

Grosjean DE, Baragiola RA. (1993). Electron emission from ion bombarded solid argon. In: Ionization of Solids by Heavy Particles (Baragiola RA, ed.). Plenum Publishing Corporation, NATO ASI Series **B**:Vol. **306**, 381-393.

Hauffe W. (1991). Production of Microstructures by Ion Beam Sputtering. In: Sputtering by Particle Bombardment III (Behrisch R, Wittmaack K, eds.). Springer Topics in Applied Physics Vol. **64**, 305-338.

Hasegawa M, Kimura K, Fujii Y, Suzuki M, Susuki Y, Mannami M. (1988). Secondary electron emission due to MeV He ions at glancing incidence angles on clean single crystal surfaces. Nucl. Instrum. Meth. **B33**, 334-337.

Hasegawa M, Fukichi T, Susuki Y, Fukui S, Kimura K, Mannami M. (1991). Yield of ion-induced secondary electrons from single crystal. Japan. J. of Appl. Phys. **30**, 2074-2081.

Hasselkamp D. (1988). Secondary emission of electrons by ion impact on surfaces. Comments At. Mol. Phys. **21**, 241-255.

Hasselkamp D. (1991). Kinetic Electron Emission from Solid Surfaces under Ion Bombardment. In: Particle Induced Electron Emission II (Höhler G, Niekisch EA, eds.). Springer Tracts in Modern Physics **123**, 1-95.

Hasselkamp D, Hippler S, Scharmann A, Schmehl T. (1990). Electron emission from clean solid surfaces by fast ions, Ann. d. Physik **47** (7. Folge), 555-567.

Hautala M, Pan Z, Sigmund P. (1991). Accelerated deuterons in cluster-fusion experiments. Phys. Rev. **A44**, 7428-7437.

Hippler S. (1988). Spezielle Aspekte der ioneninduzierten Elektronenemission aus Festkörperoberflächen: Eine Untersuchung von Strukturen im niederenergetischen Emissionsspektrum und zur Z_2-Abhängigkeit des Sekundärelektronenemissionskoeffizienten. Inaugural-Dissertation, Justus-Liebig-Universität, Giessen, Germany.

Hofer WO. (1990). Ion-induced electron emission from solids, Scanning Microsc. Supplm. **4**, 265-310.

Höhler G, Niekisch EA. (1991a). Particle Induced Electron Emission I, Springer Tracts in Modern Physics Vol. **122**.

Höhler G, Niekisch EA. (1991b). Particle Induced Electron Emission II, Springer Tracts in Modern Physics Vol. **123**.

Johnson RE. (1993). Ionization tracks. In: Ionization of Solids by Heavy Particles (Baragiola RA., ed.). Plenum Publishing Corporation, NATO ASI Series **B**:Vol. **306**, 419-430.

Kankeleit E. (1980). Collisional Quasiatoms, Facts and Speculations. Nucleonika **25**, 253-275.

Kelbch C, Koch R, Hagmann S, Ullmann K, Schmidt-Böcking H, Reinhold CO, Schultz DR, Olson RE, Kraft G. (1992). Delta-electron emission in fast heavy ion-atom collisions: observations of new phenomena and breakdown of common scaling laws. Z. Phys. **D22**, 713-721.

Kemmler J. (1988). Produktion und Transport von Konvoielektronen-Molekulare und schwere atomare Projektilionen in dünnen Festkörpern, Inaugural-Dissertation, Johann-Wolfgang-Goethe-Universität, Frankfurt am Main, Germany

Kemmler J. (1990). Heavy ion convoy electron production and transport in solids. Nucl. Instrum. Meth. **B48,** 612-615.

Kemmler J, Heil O, Biedermann C, Koschar P, Rothard H, Kroneberger K, Groeneveld KO, Kövér A, Szabo G, Gulyàs L, Bérényi D, Focke P, Meckbach W. (1988). Non equilibrium convoy electron production in coincidence with outgoing projectile charge states. In:

High-Energy Ion-Atom Collisions-Proceedings of the 3rd Workshop on High-Energy Ion-Atom Collision Processes (Berényi D, Hock G, eds.). Springer Lecture Notes in Physics **LNP294**, 362-376.

Khandelwal GS, Merzbacher E. (1966). Characteristic X-ray Production in Atomic L and M Subshells. Phys. Rev. **151**, 12-13.

Khandelwal GS, Merzbacher E. (1969). Tables for Born Aproximation Calculations of K- and L-Shell Ionization by Protons and other charged Particles, Atomic Data **1**, 103-120.

König W, Krebs KH, Rogaschewski S. (1975). Untersuchungen zur Ionen-Elektronen-Emission einkristalliner Alkalihalogenide beim Beschuss mit postiven Edelgasionen im Energiebereich 1.5-25 keV, Int. J. of Mass Spectrometry and Ion Physics **16,** 243-256.

Koschar P, Szabo G, Clouvas A, Kemmler J, Heil O, Biedermann C, Rothard H, Kroneberger K, Lencinas S, Groeneveld KO. (1987). Production and transport of convoy electrons in the charge preequilibrium of ions in solids. J. de Phys. (Paris) **48**, Coll. C9, Supplm. au Nº 12, 275-278.

Koschar P, Kroneberger K, Clouvas A, Burkhard M, Meckbach W, Heil O, Kemmler J, Rothard H, Groeneveld KO. (1989). Secondary-electron yield as a probe of preequilibrium stopping power of heavy ions colliding with solids. Phys. Rev. **A40**, 3632-3636.

Koschar PG, Kemmler J, Rothard H, Groeneveld KO, Cue N, Kirsch R, Poizat JC, Remillieux J. (1992). Konvoielektronen aus der Wechselwirkung planar strahlgeführter Protonen in dünnen, monokristallinen Goldfolien, Verhandl. DPG (VI). **27** (A18.3) 1243.

Kotera M, Kishida T, Suga H. (1990). Monte Carlo simulation of secondary electrons in solids and its application for scanning electron microscopy. Scanning Microsc. Supplm. **4,** 111-126.

Koyama A, Shikata T, Sakairi H. (1981). Secondary electron emission from Al, Cu, Ag and Au metal targets under proton bombardment. Japan. J. of Appl. Phys. **20**, 65-70.

Koyama A, Shikata T, Sakairi H, Yagi E. (1982a). Secondary electron emission form metal targets under heavy ion bombardment. Japan. J. of Appl. Phys. **21**, 586-590.

Koyama A, Shikata T, Sakairi H, Yagii E. (1982b). Dependence of Secondary electron emission coefficients on Z_1 in metal targets under bombardment with bare projectiles. Japan. J. of Appl. Phys. **21**, 1216-1221.

Koyama A, Benka O, Sasa Y, Uda M.(1986). Energy spectra of secondary electrons from Al induced by heavy-ion impact. Phys. Rev. **B34**, 8150-8152.

Koyama A, Benka O, Sasa Y, Ishikawa H, Uda M. (1987). Z_2 dependence of peak energies of loss electrons backscattered from metal targets for He^+ impact. Phys. Rev. **A36**, 4535-4538

Koyama A, Ishikawa H, Sasa Y, Benka O, Uda M. (1988a). Depression of yields of low energy secondary electrons induced by impact of heavy ions with high electric charges. Nucl. Instrum. Meth. **B33**, 338-340.

Koyama A, Ishikawa H, Sasa Y, Benka O, Uda M. (1988b). High charge effects on electron excitations in metal targets for Ar^{12+} impact compared with those for He^{2+} impact. Nucl. Instrum. Meth. **B33**, 341-344.

Kozochina AA, Leonas VB, Fine VE. (1993). Statistics of heavy particle-induced electron emission from a foil. In: Ionization of Solids by Heavy Particles (Baragiola RA, ed.). Plenum Publishing Corporation, NATO ASI Series **B**:Vol. **306**, 223-237.

Kraft G., Gademann G. (1993). Einrichtung einer experimentellen Strahlentherapie bei der Gesellschaft für Schwerionenforrschung Darmstadt. GSI-Report **93**-23.

Krämer M., Kraft G. (1993). Heavy ion track structure calculations. Rad. Eff. and Defects in Solids **126**, 49-52.

Kroneberger K, Clouvas A, Schlüssler G, Koschar P, Kemmler J, Rothard H, Biedermann C, Heil O, Burkhard M, Groeneveld KO. (1988). Secondary electron yields from the entrance and exit surfaces of thin carbon foils induced by penetration of H^+, H^0 and H_2^+ projectiles (1.2 MeV/u). Nucl. Instrum. Meth. **B29**, 621-626.

Kudo H, Shima K, Masuda K, Seki S. (1991a). Secondary electrons induced by fast ions under channelling conditions I: Production and emission of secondary electrons. Phys. Rev. **B43**, 12729-12735.

Kudo H, Shima K, Seki S, Ishihara T. (1991b). Secondary electrons induced by fast ions under channelling conditions II: Screening of fast heavy ions in solids. Phys. Rev. **B43**, 12736-12743.

Kuzel M, Maier R, Heil O, Jakubassa-Amundsen DH, Lucas MW, Groeneveld KO. (1993). Ramsauer-Townsend effect in the electron loss from H^0 colliding with heavy atoms. Phys. Rev. Lett. **71**, 2879-2882.

Latz R. (1984). Spektrometrie von Elektronen aus Kollisionen atomarer und molekularer Projektile mit Festkörpern, Inaugural-Dissertation, Johann-Wolfgang-Goethe-Universität, Frankfurt am Main, Germany.

Laubert R, Sellin IA, Vane CR, Suter M, Elston SB, Alton AD, Thoe RS. (1978). Z, Velocity, and Target-Material Dependence of Convoy Electrons from Solids. Phys. Rev. Lett. **41**, 712-715.

Lencinas S, Burgdörfer J, Kemmler J, Heil O, Kroneberger K, Keller N, Rothard H, Groeneveld KO. (1990). Transport of fast electrons through thin foils. Phys. Rev. **A41**, 1435-1443.

LeBeyec Y, Della Negra S, Thomas JP. (1989). Proceedings of the Second International Workshop on MeV and keV Ions and Cluster Interactions with Surfaces and Materials, J. de Phys. (Paris) **50**, Coll. C2, Supplm. au Nº 2.

Lindhard J. (1954). On the Properties of a Gas of charged Particles. K. Dan. Vidensk. Selsk. Mat. Fys. Medd. **28** No. 1.

Lindhard J, Winther A. (1964). Stopping Power of an Electron Gas and Equipartition Rule. K. Dan. Vidensk. Selsk. Mat. Fys. Medd. **34** No. 4.

Luo S, Joy DC. (1990). Monte Carlo calculations of secondary electron emission. Scanning Microsc. Supplm. **4**, 127-146.

McGarrah DB, Williamson W, Keeton SC. (1992). Simulation of the effect of energetic ion radiation on silicon. Trans. on Nucl. Science **39**, 1401-1406.

Mischler J, Benazeth N, Nègre M, Benazeth C. (1984). Angular distribution of secondary electrons emitted in Ar^+ polycrystalline Al collisions. Surf. Science **136**, 532-544.

Moshammer R, Ullrich J, Unverzagt M, Schmidt W, Jardin P, Olson RE, Mann R, Dörner R, Mergel V, Buck U, Schmidt-Böcking H. (1994). Low-Energy Electrons and Their Dynamical Correlation with Recoil Ions for Single Ionization of Helium by Fast Heavy Ion Impact. Phys. Rev. Lett. **73**, 3371-3374.

Neelavathi VN, Ritchie RH, Brandt W. (1974). Bound Electron States in the Wake of Swift Ions in Solids. Phys. Rev. Lett. **33**, 302-305.

Ogawa H, Katayama I, Sugai I, Haruyama Y, Tosaki M, Aoki A,Yoshida K, Ikegami H. (1992). Charge state dependent energy loss of high velocity carbon ions in the charge state non-equilibrium region. Phys. Lett. **A167**, 487-492.

Olson R, Ullrich J, Schmidt-Böcking H. (1989). Multiple ionization collision dynamics. Phys. Rev. **A39**, 5572-5583.

Pferdekämper KE, Clerc HG. (1975). Energy distribution of electrons ejected from a thin carbon foil by alpha particles and fission products. Z. Phys. **A275**, 223-228.

Pferdekämper KE, Clerc HG. (1977). Energy spectra of secondary electrons ejected by ions from foils. Z. Phys. **A280**, 155-164.

Quéré Y, Andriamonje S, Chevallier M, Cohen C, Dural J, Genre,R, Girard Y, Groeneveld KO, Kemmler J, Kirsch R, L'Hoir A, Poizat JC, Remillieux J, Schmaus D, Schosnig M, Toulemonde M. (1991). GeV xenon ions channeled through a silicon crystal. Rad. Eff. and Defects in Solids **117**, 63-67.

Rivacoba A, Echenique PM. (1987). Electrons Trapped in the Wake of a Negative Muon. Phys. Rev. **B36**, 2277-2279.

Rösler M. (1993). Theory of ion induced kinetic electron emission from solids. In: Ionization of Solids by Heavy Particles (Baragiola RA., ed.). Plenum Publishing Corporation, NATO ASI Series **B**:Vol. **306**, 27-58.

Rösler M, Brauer W. (1991). Theory of Electron Emission from Nearly-Free-Electron Metals by Proton and Electron Bombardment. In: Particle Induced Electron Emission I (Höhler G, Niekisch EA, eds.). Springer Tracts in Modern Physics **122**, 1-66.

Rothard H. (1994). Interaction of swift heavy particles with solids: Electron Emission. Nucl. Instrum. Meth. **B87**, 149-155.

Rothard H, Kroneberger K, Burkhard M, Biedermann C, Kemmler J, Heil O, Groeneveld KO. (1989). Refraction of directed shock electrons at planar solid surfaces. J. de Phys. (Paris) **50**, Coll. C2, Supplm. au Nº 2, 105-110.

Rothard H, Kroneberger K, Veje E, Clouvas A, Kemmler J, Koschar P, Keller N, Lencinas S, Lorenzen P, Heil O, Hofmann D, Groeneveld KO. (1990a). Experimental study of molecular and cluster effects in secondary electron emission. Phys. Rev. **B41,** 3959-3967.

Rothard H, Kroneberger K, Schosnig M, Lorenzen P, Veje E, Keller N, Maier R, Kemmler J, Biedermann C, Albert A, Heil O, Groeneveld KO. (1990b). Secondary-electron velocity spectra and angular distributions from ions penetrating thin solids. Nucl. Instrum Meth. **B48**, 616-620.

Rothard H, Kroneberger K, Clouvas A, Veje E, Lorenzen' P, Keller N, Kemmler J, Meckbach W, Groeneveld KO. (1990c). Secondary-electron yields from thin foils: a possible probe for the electronic stopping power of heavy ions. Phys. Rev. **A41**, 2521-2535.

Rothard H, Schosnig M, Kroneberger K, Groeneveld KO. (1991). Electron spectra from ion bombardment of cleaned surfaces covered with frozen gases at low sample temperatures. In: Interaction of Charged Particles with Solids and Surfaces (Gras-Marti A, Urbassek HM, Arista NR, Flores F, eds.). Plenum Publishing Cooperation, NATO ASI Series **B**:Vol. **271**, 615-624.

Rothard H, Schou J, Koschar P, Groeneveld KO. (1992). Electron yields from solids: a probe for the stopping power of swift charged particles? Nucl. Instrum. Meth. **B69**, 154-157.

Rothard H, Groeneveld KO, Kemmler J. (1991). Kinetic Electron Emission from Ion Penetration of Thin Foils in Relation to the Pre-Equilibrium of Charge Distributions. In: Particle Induced Electron Emission II (Höhler G, Niekisch EA, eds.). Springer Tracts in Modern Physics **123**, 97-147.

Rothard H, Schou J, Groeneveld KO. (1992). Projectile- and Charge State Dependent Electron Yields from Ion Penetration of Solids as a Probe of Preequilibrium Stopping Power. Phys. Rev. **A45** (1992) 1701-1710.

Rothard H, Dauvergne D, Fallavier M, Groeneveld KO, Kirsch R, Poizat JC, Remillieux J, Thomas JP (1993a). Interaction of Swift Clusters with Solids: Relation between Electron Emission Yield and Energy Loss. Rad. Eff. and Defects in Solids **126**, 373-381.

Rothard H, Thomas JP, Remillieux J, Poizat JC, Kirsch R, Groeneveld KO, Fallavier M, Dauvergne D. (1993b). Electron emission from swift hydrogen cluster interaction with thin carbon foils. In: Ionization of Solids by Heavy Particles (Baragiola RA, ed.). Plenum Publishing Corporation, NATO ASI Series **B**:Vol. **306**, 215-222.

Rothard H, Billebaud A, Jung M, Caraby C, Gervais B, Cassimi A, Jardin P, Maier R, Chevallier M, Grandin JP, Groeneveld KO. (1994). Target Thickness Dependent Electron Emission from Carbon Foils Induced by Argon Ion Penetration. Nouvelles du GANIL **49,** 23-33.

Rothard H, Caraby C, Cassimi A, Gervais B, Grandin JP, Jardin P, Jung M, Billebaud A, Chevallier M, Groeneveld KO, Maier R. (1995). Target Thickness Dependent Electron Emission from Carbon Foils Bombarded with Swift Highly Charged Heavy Ions. Phys. Rev. **A51**, 3066-3079.

Rozet JP, Chetioui A, Bouisset P, Vernhet D, Wohrer K, Touati A, Stephan C, Grandin JP. (1987). Anomalous population of deep capture states of fast ions emerging from solid foils. Phys. Rev. Lett. **58,** 337-340.

Rutherford E. (1905). Charge carried by the α and β Rays of Radium. Phil. Mag. **10** No. 56, 193-209.

Saemann-Ischenko G, Schmidt W. (1983). Auger electron emission from solids during bombardment with MeV ions. Nucl. Instrum. Meth. 218, 757-763.

Sanchez EA, deFerraris LF, Suarez S. (1989). Convoy electron yield dependence on controlled surface properties by Na deposition. Nucl. Instrum. Meth. **B43**, 29-33.

Schader J, Kolb B, Sevier KD, Groeneveld KO. (1978). Electron ejection from beam tilted foil experiments. Nucl. Instrum. Meth. **151**, 563-565.

Schäfer W, Stöcker H, Müller B, Greiner W. (1978). Mach cones induced by fast heavy ions in electron plasma. Z. Phys. **A288**, 349-352.

Schäfer W, Stöcker H, Müller B, Greiner W. (1980). Mach shock electron distributions from solids. Z. Phys. **B36**, 319-322.

Schiwietz G. (1990). Population of projectile-ion states during the passage of high energy Ne-ions through thin carbon foils. Rad. Eff. and Defects in Solids **112**, 195-200.

Schiwietz G. (1993). Electron ejection induced by fast projectiles. In: Ionization of Solids by Heavy Particles (Baragiola RA, ed.). Plenum Publishing Corporation, NATO ASI Series **B**:Vol. **306**, 197-214.

Schiwietz G, Schneider D, Biersack JP, Stolterfoht N, Fink D, Mattis A, Skogvall B, Altevogt H, Montemayor V, Stettner U. (1988). Cascade induced asymmetry in Auger electron emission following fast ion solid interactions. Phys. Rev. Lett. **61**, 2677-2680.

Schiwietz G, Biersack JP, Schneider D, Stolterfoht N, Fink D, Montemayor V, Skogvall B. (1990). Investigation of δ-electron emission in collisions of highly charged fast Ne projectiles with carbon-foil targets. Phys. Rev. **B41**, 6262-6271.

Schiwietz G, Grande P, Skogvall B, Biersack JP, Köhrbrück R, Sommer K, Schmoldt A, Goppelt P, Kadar I, Ricz S, Stettner U. (1992). Influence of nuclear track potentials in insulators on the emission of target Auger electrons. Phys. Rev. Lett. **69**, 628-631.

Schneider D, Kudo H, Kanter E. (1985). Electron emission following fast ion impact on thin solid targets. Nucl. Instrum. Meth. **B10/11**, 113-115.

Schneider D, DeWitt D, Schlachter AS, Olson RE, Graham WG, Mowat JR, Dubois RD, Loyd DH, Montemayor V, Schiwietz G. (1989). Strong continuum-continuum couplings in the direct ionization of Ar and He atoms by 6 MeV/u U^{38+} and Th^{38+} projectiles. Phys. Rev. **A40**, 2971-2975.

Schneider D, DeWitt D, Bauer RW, Mowat JR, Graham WG, Schlachter AS, Skogvall B, Fainstein P, Rivarola RD. (1992). Absolute doubly differential cross sections for electron emission in collisions of 3.5 MeV/u Fe^{17+} and Fe^{22+} ions with He and Ar gas targets. Phys. Rev. **A46**, 1296-1302.

Schneider D, Schiwietz G, DeWitt D. (1993). Doubly differential secondary-electron yields following 8 MeV/u U^{68+} and 3.5 MeV/u U^{38+} ion impact on a thin carbon foil target. Phys. Rev. **A47**, 3945-3950.

Schosnig M, Rothard H, Kroneberger K, Schlösser D, Groeneveld KO. (1992). Electron emission and desorption from frozen gases under fast (MeV) ion bombardment. Nucl. Instrum. Meth. **B68**, 394-397.

Schou J. (1980). Transport theory for kinetic emission of secondary electrons from solids. Phys. Rev. **B22**, 2141-2174.

Schou J. (1988). Secondary electron emission from solids by electron and proton bombardment, Scanning Microsc. **2**, 607-632.

Schou J. (1993). Secondary electron emission from insulators. In: Ionization of Solids by Heavy Particles (Baragiola RA, ed.). Plenum Publishing Corporation, NATO ASI Series **B**:Vol. **306**, 351-358.

Schou J, Kruit P, Newbury DE. (1990). Fundamental Electron and Ion Beam Interactions with Solids for Microscopy, Microanalysis and Microlithography, Scanning Microsc. Supplm. **4.**

Schramm R, Betz HD. (1992). Problems concerning the effective charge of swift heavy ions traversing gaseous and solid targets. Nucl. Instrum. Meth. **B69**, 123-126.

Schütze W, Bernhard F. (1956). Eine neue Methode zur Messung extrem kleiner Ionenströme im Hochvakuum. Z. Phys. **145**, 44-47.

Senger P, Backe H, Begemann-Blaich M, Bokemeyer H, Glässel P, Harrach Dv, Klüver M, Konen W, Poppensieker K, Stiebing K, Stroth J, Wallenwein K. (1987). Nuclear contact times in dissipative heavy ion collisions measured via δ-ray spectroscopy. In: Physics of Strong Fields (Greiner W, ed.). Plenum Publishing Cooperation, NATO ASI Series **B**: Vol. **153** , 423-439.

Shi CR, Toh HS, Lo D, Livi RP, Mendenhall MH, Zhang DZ, Tombrello TA. (1985). Secondary electron emission from the entrance and exit surfaces of thin carbon foils under fast ion bombardment. Nucl. Instrum. Meth. **B9**, 263-269.

Shinpaugh JL, Wolff W, Wolff HE, Ramm U, Jagutzki O, Schmidt-Böcking H, Wang J, Olson RE. (1993). Transition from quantum to quasi classical behaviour of the binary encounter peak in collisions of 0.6 to 3.6 MeV amu^{-1} I^{23+} and Xe^{21+} with He and Ar. J. Phys. B: At. Mol. Opt. Phys. 26, 2869-2878.

Sigmund P. (1993). Particle-induced electron emission : open questions, pitfalls, and a few attempts at answers. In: Ionization of Solids by Heavy Particles

(Baragiola RA, ed.). Plenum Publishing Corporation, NATO ASI Series **B**:Vol. **306**, 1-20.

Sigmund P, Tougaard S. (1981). Electron emission from solids during ion bombardment: theoretical aspects. Springer Series in Chemical Physics **17**, 2-37.

Sparrow RA, Olson RE, Schneider D. (1992). Electron emission from foils induced by energetic heavy-ion impact, J. Phys. **B**: At. Mol. Opt. Phys. **25**, 295-230.

Sternglass EJ. (1957). Theory of secondary electron emission by high-speed ions. Phys. Rev. **108**, 1-12.

Stolterfoht N, Schneider D, Tanis J, Altevogt H, Salin A, Fainstein PD, Rivarola R, Grandin JP, Scheurer JN, Andriamonje S, Bertault D, Chemin JF. (1987). Evidence for two centre effects in the electron emission from 25 MeV/u Mo^{40+}+He collisions: Theory and experiment, Europhys. Lett. **4** (8), 899-904.

Strong R, Lucas M. (1977). Search for Wake-Bound Electron States. Phys. Rev. Lett. **39**, 1349-1352.

Suarez S, Garibotti C, Meckbach W, Bernardi G. (1993). Experimental evidence of the asymmetry of the soft electron peak in ion-atom ionization. Phys. Rev. Lett. **70**, 418-421.

Suarez S, Bernardi G, Focke P., Meckbach W, Tobisch M, Jung M, Rothard H, Schosnig M, Maier R, Clouvas A, Groeneveld KO. (1994). Search for Fermi Shuttle Mechanisms in Electron Emission from Atomic Collision Sequences. Nucl. Instrum. Meth. **B86**, 197-200.

Suszcynsky DM, Borovsky JE. (1991). Secondary-electron emission from metals impacted by high-velocity particles: molecular-effect deviations from a single-particle picture. Nucl. Instrum. Meth. **B53**, 255-266.

Taft EA, Philipp RA. (1965). Optical properties of graphite. Phys. Rev. **138A**, 197-202.

Thomson JJ. (1904). On the positive electrification of α rays and the emission of slowly moving cathode rays by radio-active substances. Proc. of the Cambridge Philosophical Soc. **13,** 49-54.

Tobisch M, Schosnig M, Kroneberger K, Kuzel M, Maier R, Jung M, Fiedler C, Rothard H, Clouvas A, Suarez S, Hofmann D, Groeneveld KO. (1994). Back-scattering of Projectile-Bound Electrons from Solid Surfaces. Nucl. Instrum. Meth. **B86,** 143-146.

Toburen LH. (1990). Angular and energy distributions of electrons emitted from gases and thin foils during light ion bombardment. Scanning Microsc. Supplm. **4**, 239-256.

Tombrello TA. (1993). The role played by fast electrons in heavy ion induced desorption and track formation. Int. J. Mass Spectrom. Ion Process **126,** 11-16.

Vane CR, Datz S, Dittner PF, Krause HF, Schuch R, Gao H, Hutton R (1993). Knock-on electrons produced in collisions of 6.4 TeV sulfur ions with fixed targets. Nucl. Instrum. Meth. **B79**, 26-29.

Varga P, Winter H. (1991). Slow Particle-Induced Electron Emission from Solid Surfaces. In: Particle Induced Electron Emission II (Höhler G, Niekisch EA, eds.). Springer Tracts in Modern Physics **123**, 149-213.

Villard MP (1899). Sur les rayons cathodiques, J. Phys. Theor. Appl. **8**, 5-16.

Villari ACC, Mittig W, Lépine-Szily A, Lichtenthäler Filho R, Auger G, Bianchi L, Beunard R, Casandjian JM, Ciffre JL, Cunsolo A, Foti A, Gaudard L, Lima CL, Plagnol E, Schutz Y, Siemssen RH, Wielczko JP. (1993). Search for Color van der Waals Force in ^{208}Pb+^{208}Pb Mott Scattering. Phys. Rev. Lett. **71**, 2551-2552

Wang J, Olson RE, Wolff H, Shinpaugh J, Wolff W, Schmidt-Böcking H (1993). Dependence of binary encounter electron production on the charge state of the recoil ion. J. Phys. B: At. Mol. Opt. Phys. **26**, L457-L463.

Winter H, Dierkes G, Hegmann A, Leuker J, Ortjohann HW, Zimny R. (1993). Electron emission phenomena in grazing collisions of fast ions with surfaces. In: Ionization of Solids by Heavy Particles (Baragiola RA, ed.). Plenum Publishing Corporation, NATO ASI Series **B**:Vol. **306**, 253-271.

Yamazaki Y , Kuroki K, Komaki KJ, Andersen LH, Horsdal-Pedersen E, Hvelplund P, Knudsen H, Moller SP, Uggerhoj E, Elsener K (1990). Measurements of electron spectra in the forward direction in slow antiproton-carbon foil collisions, J. Phys. Soc. of Japan **59**, 2643-2646.

Yamazaki Y. (1991). Wakes, Dynamic Screening. In: Interaction of Charged Particles with Solids and Surfaces (Gras-Marti A, Urbassek HM, Arista NR, Flores F, eds.). Plenum Publishing Cooperation, NATO ASI Series **B**:Vol. **271**, 423-441.

Yamazaki Y, Kuroki K, Azuma T, Komaki K, Watanabe H, Kakutani N, Hasegawa T, Sekiguchi M, Hattori T. (1993). Correlated electron emission from thin carbon foils bombarded by 1.8 MeV/u Ar ions. Phys. Rev. Lett. **70**, 2702-2705.

Zaikov VP, Kralkina EA, Nikolaev VS, Fainberg Yu A, Vorobiev NF. (1986). Passage of nitrogen and oxygen ions through carbon and celluloid films. Nucl. Instrum. Meth. **B17**, 97-107.

Ziegler JF, Biersack JP, Littmark U. (1985). The Stopping and Ranges of Ions in Solids. Volume 1 of: The Stopping and Ranges of Ions in Matter. Pergamon Press, New York.

Discussion with Reviewers

R. Baragiola: In many places through the text, the author mentions dependencies of different physical quantities with the square of the projectile charge, Z_P^2. Such dependencies are only expected when the Born approximation is valid, that is, when the perturbation is small. This occurs when Z_P/v_P is small ($Z_P/v_P << 1$ in atomic units). The neglect of this constraint is a common error in the literature.

Author: This should be pointed out clearly. In this context and in connection with the subject of this review,

it may be interesting to note that for multicharged heavy ions, velocities high enough so that this limit of small perturbation is fulfilled can be reached with (tandem) Van-de-Graaff accelerators for "light" heavy ions ($Z_P \leq 10$), for medium heavy ions (up to $Z_P \approx 50$) we have to go to some tens of MeV/u (this is for example possible with GANIL), and for heavier ions up to U, this limit can only be explored with the largest existing accelerators such as GSI-SIS. As can be seen from figs. 16 and 17, in some cases, a Z_P^2 scaling may even be observed if the above condition ($Z_P/v_P << 1$ or $q/v_P << 1$) is not completely fulfilled. Both figures deal with the impact parameter dependence of ionization: at high electron energies corresponding to close collisions, a Z_P^2 scaling of electron emission is observed.

J. Schou: The increase of the yield as a function of thickness is frequently described by a term with an exponential function so that the yield increases up to a saturation value. This simple description goes back to the early days of secondary electron emission, but has been used, for example, also by Sternglass (1957). However, Sigmund (1993) showed that a diffusion-like behavior is much better described by an complementary error function erfc(x) than by an exponential. The second point is that the energy of the delta-electrons may exceed several keV. In that case a typical electron trajectory does not resemble a diffusing particle except for the low-energy end, since the cross section for scattering decreases strongly with rising energy. The overall behavior for electrons of several keV has probably very few features common with the classical diffusion picture, but is much better described by a straight-line behavior.
Author: It is astonishing how well the target thickness dependence of the forward electron yields can be described by eq. (20), where exponential functions for electron transport have been used (figs. 11-13). I agree that more realistic approaches to electron transport as e.g., replacing the exponential by the proposed complementary error function (in eqs. 13-20) or by taking into account backscattering of fast electrons (eq.28) should be included in the semiempirical model. With both C at 1 MeV/u (Koschar et al., 1989) and Ar at 13.6 MeV/u (Rothard et al., 1994, 1995), a very slow increase of backward yields has been observed. This may be due to fast electrons which contribute to the backward cascade multiplication after a few large angle scattering events. Schneider, Schiwietz and DeWitt (1993) showed that the motion of fast electrons in forward direction can be well described by a straight line behaviour and the SELAS (Separation of Energy Loss and Angular Scattering) approximation, whereas this is no longer possible for backscattered fast electrons, where experimental data on electron emission intensity are underestimated by a factor of 2-5.

R. Baragiola: The discussion made by Borovsky and Suszcynski (1991a,b) should not be reproduced uncritically. I disagree with the physics of fig. 9 in the case of metals, where the huge electric fields they describe do not exist. The electrons that flow to screen the excess charge cause a repulsive force on ejected electrons which compensates the attractive force from the ions.
Author: One should indeed be cautious in applying the model of Borovsky and Suszcynski (1991a,b) to the case of metals. In particular, the experimental results presented in tab.2 seem to be in contradiction with this model, as discussed in III.c. The application to the case of semiconductors could be more fruitful as shown by Akkerman et al. (1993a).

R. Baragiola: The discussion about "semi-empirical" vs. "transport" or vs. "microscopic or analytical" theories may be misleading to readers. All theories come down to some semi-empirical approach, and it is in this form that they are used to explain observations. For instance, no theory discusses transport from first principles, taking into account the surface, but rather use an infinite medium and then fudge-in the surface. Practically all the theories treat electron transport with a semi-empirical exponentially attenuation function, which only holds in the absence of elastic scattering. None, including the "microscopic" describe in any detail the diffraction and **k**-conservation in transmission through the surface nor consider quantum effects in the scattering of low energy electrons in the solid. The main difference between theories, the so-called semi-empirical, those by Schou (1980), Sigmund & Tougaard (1981), and Rösler (1993) is really in the excitation function.
Author: I agree in that surface transmission and electron transport are not yet being treated with the same refinement as it is possible for the excitation functions connected to different electron production mechanisms. Personally, I feel however that the models which I called "microscopic" or "analytical" treat the electron excitation and the scattering mean free paths related to different excitation modes in a more sophisticated way than the semi-empirical models based on Sternglass' (1957) work, where a variety of "mean" quantities and not well defined parameters (which finally can only be deduced from experiment) have to be introduced.

M. Rösler: In your Monte Carlo simulations for the target material carbon the band structure is not taken into account. However, it is well-known that band structure effects are responsible for the plasmon damping in real metals. Can you give a comment about your model of plasmon creation and subsequent excitation of electrons by the decay of plasmons. What is the relation to the model used by Cailler and Ganachaud (1990) and Dubus et al. (1993)?
Author: In the present MC code (Gervais and Bouffard, 1994, see also Rothard et al., 1995), the band structure leading to plasmon damping is not taken into account explicitly, but implicitly: the plasmon lifetime is estimated from the plasmon peak width in the curve of energy loss versus energy obtained by optical reflectivity

measurements by Taft and Philipp (1965). The half width is found to be 5eV, the wave-number dependence of the lifetime being neglected. It is assumed that the plasmon energy $\hbar\omega_P$ is transferred as a whole to a single electron which is excited with isotropic angular distribution at the point of plasmon decay. This point is obtained from the plasmon lifetime and the plasmon group velocity. Detailed information can be found in the paper by Gervais and Bouffard (1994). Ganachaud and Cailler (1979a,b) not only consider this one-electron decay, but also two electron decay (where the plasmon energy is shared between two electrons) and multipair creation from bulk plasmons. Furthermore, they consider one electron decay and multipair creation in the damping of surface plasmons. In Cailler and Ganachaud (1990) and Dubus et al. (1993) a review on simulations of electron emission including different modes of plasmon damping can be found. In the paper by Dubus et al. (1993), it is assumed that one electron is created by bulk plasmon damping. The probability is assumed to be proportional to the density of states of electrons in the conduction band (this is the same approach as used by Ganachaud and Cailler, 1979a,b). A small spatially limited surface zone where only surface plasmon damping takes places is also taken into account.

A. Dubus: What do you expect from a comparison between electron emission in ion-atom collisions and electron emission from solid targets ?
Author: The answer to this question has recently been discussed in detail by Baragiola (1993b), and an interesting comparison of ionization in ion-gas and ion-solid collisions can be found in Toburen's (1990) paper. It is clear that collision and ionization processes will be different in the gas phase, for ion-surface collisions, and in the bulk of the solid, "due to differences in the initial and final electronic states. However, some of these differences are small and so one can draw general analogies as a heuristic approach to understand EE in solids. From there, one can then discuss specific condensed matter effects and evaluate their importance" (cited from Baragiola, 1993b). For example, it is often possible to use scaled atomic cross sections as input for the calculation of electron spectra from solids (Schiwietz et al., 1990) and then transport and surface effects are added. This is also the idea of the experiments on the target thickness dependence of EE with thin foils: start with something which to a certain degree resembles atomic collisions, and then increase transport effects (figs. 11-13 and 18-19). Specific differences in EE from gas and solid targets can nicely be seen from fig. 20 (Toburen, 1990), the main effects are: A strong difference in the energy distribution at low energies due to surface transmission and transport effects, and a strong difference in the angular distribution at large angles due to large-angle scattering of fast electrons.

J. Schou: The expression indicated by Hasselkamp that the yields for insulating materials is inversely proportional to the energy gap is intuitively tempting, but the experimental basis for the statement is rather weak. Hasselkamp supports his statement on measurements performed by König et al. (1975). Although these experiments were performed carefully and in UHV, only four targets of alkali halides, KCl, KBr, NaCl and LiF were studied. The energy gap increases from KBr up to LiF, but the yield depends very much on the projectile. For heavy ion incidence the yield is actually inversely proportional with the energy gap. However, for He-ions the yield is almost the same for all three targets and for Ne-ions the dependence is different. It is also true that one would expect an $1/E_g$ dependence from Eq. (74) in Schou (1980), but this expression is derived for electron emission from ionization cascades rather that from primary ionization only, and for electrons generated close to the surface. In general one would not expect a simple $1/E_g$ dependence.
Author: It is interesting that the electron energy distributions measured by König et al. (1975) show a similar dependence for all ions (He, Ne, Ar, Kr): their width increases and their height decreases from KCl to LiF, i.e. with increasing E_g. This means that the relative importance of low energy electrons decreases. The interpretation of König et al. (1975) is that for approximately constant escape probability of electrons excited into the conduction band, with increasing E_g, the flatter high energy part of the internal energy distribution determines the external one. However, in general, one cannot clearly separate the influence of the electronic structure of the target from that of the projectile. Also in the present case, the interplay of both must be taken into account in the interpretation of the experimental results.